THE WHIRL INSTABILITY OF A RIGID ROTOR IN A FLEXIBLY SUPPORTED GAS LUBRICATED JOURNAL BEARING

DAVID A. BOFFEY

Thesis submitted for the degree of

Doctor of Philosophy

University of Edinburgh

May 1972

ACKNOWLEDGEMENTS

The work reported in this thesis was supported by a grant from the Science Research Council.

The author wishes to express his gratitude to his Supervisor, Dr. A.D.S. Barr, for specifying the research project and for his guidance and encouragement throughout. The author wishes to acknowledge the help and advice of Dr. G.T.S. Done, notably with the computer programmes associated with the work reported in Appendix II of the thesis. The manufacture and assembly of the bearing test rig was carried out by Mr. D. Pringle and the technical staff of the Mechanical Engineering Department Workshop, without whose skill and patience the experimental programme could not have been successfully concluded. Finally, thanks are due to Miss Avril Myles for typing the thesis.

SYNOPSIS

Gas lubricated journal bearings are prone to a destructive self-excited whirl, which imposes an upper boundary to the safe operational speed of the bearing. The objective of the research reported in this thesis has been to study, both theoretically and experimentally, the effects of the introduction of a flexible damped bearing support as a means of inhibiting self-excited whirl.

The early part of the research, reported in Appendix II, relates to an analytical study of the stability problem with a hydrodynamic bearing. The analysis employs Ausman's "Linearized ph" solution to the time dependant Reynolds Equation in order to evaluate the frequency dependant gas film dynamic stiffness and damping coefficients. The coefficients are used in the equations of motion of the system to obtain the characteristic equation which is then solved on a digital computer to investigate the stability.

The major part of the thesis is concerned with the study of the stability problem with an externally pressurized bearing of finite length. The gas film dynamic coefficients are evaluated numerically on the computer using Lund's "Linearised ph" solution. The determination of stability is restricted to the threshold condition. An experimental test rig, with rubber O-rings to provide a flexible damped bearing support, has been designed and tested in order to check the theoretical predictions of threshold speed.

From the results of both analyses it is found that with a sufficiently high ratio of support damping/stiffness a gas bearing system can be achieved which is stable at all speeds.

Experimental confirmation of the results of the externally pressurised bearing has been achieved and the threshold speed of self-excited whirl is predicted to within 10 percent.

CONTENTS

CHAPTER 1

1.0 INTRODUCTION

Gas lubricated bearings offer the advantages of low friction and silent operation and allow operating speeds considerably higher than those attainable with rolling element or oil lubricated bearings. In recent years they have been used for a wide variety of applications which includes gyroscopes, dental drills, grinding wheel spindles, precision instruments and cryogenic systems.

The journal bearing is however prone to a self-excited whirl, in which the rotating journal shaft centre performs an orbital motion in the vicinity of its steady state operating position. This occurs when the effective damping capacity of the gas film vanishes. Once this whirl is initiated any further increase in speed will usually cause contact of the bearing surfaces, thus imposing an upper limit of safe operation. In the self-acting or hydrodynamic type of bearing, in which the pressure (load carrying capacity) is generated by the relative motion between the bearing surfaces, the frequency of whirl is approximately half that of the journal rotation. The conditions affecting the onset, or threshold of this so-called half-speed whirl have been widely studied theoretically [1 to 8].[1] The various stability analyses are primarily concerned with obtaining solutions of the classical Reynolds' Equation in order to estimate the dynamic stiffness and damping coefficients of the gas film. These solutions are discussed in a later chapter. Several experimental investigations have also been made [9 to 12] and there is close agreement with theory [13].

The load carrying capacity and stability of the hydrodynamic bearing can be improved by supplying the film with pressurized gas through small feeder holes.

[1] Numbers in brackets designate references.

With external pressurization alone the bearing is termed "hydrostatic" and if rotation is also present it is referred to as a hybrid bearing. The tendency to self-excited whirl, in this case called hybrid instability, still exists, and as a general rule it occurs at about twice the rigid body critical speed based on the hydrostatic bearing stiffness [14, 15, 16]. The threshold speed can thus be simply raised by increasing the supply pressure, though this may not always be feasible. Lund [17], employing the "linearized ph" method of solution to the Reynolds Equation due to Ng [4], has developed an analysis for the threshold of hybrid instability.

As the radial clearances in the above types of bearing are extremely small, there is a practical advantage in having the stationary part of the bearing on a flexible support, to facilitate ease of alignment. If, in addition, the support contains sufficient damping, then it is theoretically possible to alter the stability boundaries and obtain a higher threshold speed [18, 19, 20]. Powell [21] has successfully stabilized a hybrid air bearing using rubber O-rings and Kerr [22], in some experiments with a hydrodynamic air bearing also using rubber O-rings, showed that it was possible to operate in a stable region above the initial threshold speed.

In 1967 the firm of Joseph Lucas Ltd. were proposing to use air lubricated journal bearings in their high speed exhaust gas turbo-chargers. The system which they had in mind employed bearings of the hybrid type, flexibly supported in rubber O-rings. At that time there was no authoritative information upon which to design such a bearing system to be dynamically stable. This resulted in the undertaking of the present research programme, which has been supported by a grant from the Science Research Council. The objectives of the research have been twofold,

Firstly, to make a theoretical study of the effect on the threshold of hybrid instability of a flexible damped bearing support and secondly, to conduct a series of experiments to check the theoretical findings. As a preliminary step it was decided to make a theoretical study of the problem with a plain cylindrical hydrodynamic bearing. The analysis employed Ausmans "linearized ph" solution [3] to the Reynolds' equation, and is perhaps interesting because bearing mass was included as a parameter. The results were encouraging, since it was shown to be possible, given the necessary values of damping and stiffness of the bearing support, to have a bearing system that was stable at all speeds. A reproduction of the publication containing the results is given as an appendix to the thesis.

In the present analysis the gas film coefficients have been estimated using Lund's analysis [17] and it is thus applicable to bearings of finite length. Since the inception of the research programme there have been some further theoretical developments. Lund has produced some hybrid stability curves in which the bearing mass is set to zero [23] and Tondl [24] and Mori [25] have both made qualitative studies of the same problem. A comprehensive study employing numerical methods has recently been published by Elrod and Glanfield [26].

CHAPTER 2

2.0 THEORY OF GAS FILM LUBRICATION

2.1 The Reynolds Equations for an Isothermal, Compressible Film

The governing equation for all bearing design is the Reynolds equation, which contains the simplified equations of momentum together with those of continuity and state. A comprehensive derivation of the Reynolds Equation is given by DiPrima [27] and only an outline will be made here.

In their application to most bearing problems, the Navier-Stokes equations of flow for a viscous fluid can be considerably simplified. For a fluid being drastically sheared between two closely spaced surfaces, the viscous shearing forces predominate, and the inertia and gravitational forces can be neglected. On the fixed Cartesian co-ordinate system of Fig. 2.1.1 the momentum equations reduce to :

$$\frac{\partial p}{\partial x} = \mu \nabla^2 u$$
$$\frac{\partial p}{\partial y} = \mu \nabla^2 v \qquad 2.1.1$$
$$\frac{\partial p}{\partial z} = \mu \nabla^2 w$$

where $\nabla^2 = \frac{\partial^2}{\partial x} + \frac{\partial^2}{\partial y} + \frac{\partial^2}{\partial z}$

In one direction, namely y normal to the film, the flow is very small compared to the other two directions and p can be regarded as independant of y. Also the variation of u and w in the x and z directions are small compared with their variations in the y direction.

Equations 2.1.1 can thus be further reduced to

$$\frac{\partial p}{\partial x} = \frac{\partial}{\partial y}\left(\mu \frac{\partial u}{\partial y}\right)$$

$$\frac{\partial p}{\partial y} = 0 \qquad 2.1.2$$

$$\frac{\partial p}{\partial z} = \frac{\partial}{\partial y}\left(\mu \frac{\partial w}{\partial y}\right)$$

Integrating the first and third of equations 2.1.2 ω.r.t. y, with the boundary conditions $u = U_o$ at $y = 0$ and $u = U_h$ at $y = h$ etc., gives the following velocity profile for u and w

$$u = -\frac{1}{2}\frac{\partial p}{\partial x}(hy - y^2) + (U_h - U_o)\frac{y}{h} + U_o$$

$$w = -\frac{1}{2}\frac{\partial p}{\partial z}(hy - y^2) + (W_h - W_o)\frac{y}{h} + W_o \qquad 2.1.3$$

When gas is the lubricant the high thermal conductivity of the film boundaries relative to the film itself allows any heat generated to be readily dissipated, so that the fluid flow is assumed to be isothermal

$$p = \rho R T \qquad 2.1.4$$

The viscosity of an isothermal gas is not significantly affected by the range of pressures usually encountered in bearing design so that it is assumed to be constant.

For continuity of flow,

$$\frac{\partial \rho}{\partial t} + \frac{\partial}{\partial x}(\rho u) + \frac{\partial}{\partial y}(\rho v) + \frac{\partial}{\partial z}(\rho w) = 0 \qquad 2.1.5$$

From equation 2.1.4 p may be substituted for ρ in the above equation.

Substituting for u and w from equations 2.1.3 and integrating across the film from y = 0 to y = h, equation 2.1.5 becomes:

$$\frac{\partial}{\partial x}\left(h^3 p \frac{\partial p}{\partial x}\right) + \frac{\partial}{\partial z}\left(h^3 p \frac{\partial p}{\partial z}\right) = 12\mu \frac{\partial (ph)}{\partial t} + 6\mu \frac{\partial}{\partial x}\left[ph(U_h + U_o)\right] + 6\mu \frac{\partial}{\partial z}\left[ph(W_h + W_o)\right] \qquad 2.1.6$$

which is the time dependent Reynolds' equations for isothermal compressible flow. On account of the terms $p\frac{\partial p}{\partial x}$ and $p\frac{\partial p}{\partial z}$ the equation is nonlinear in p for a compressible gas. The first term on the right hand side of the equation is the so-called squeeze-film contribution to the film pressure, caused by the normal relative motion of the two bearing surfaces. It is essential to retain this time dependent term when analysing the dynamic behaviour of a gas bearing. The two remaining terms on the right are the hydrodynamic contributions to the film pressure.

Equation 2.1.6 may be applied directly to a cylindrical journal bearing, since the clearance ratio $\frac{C}{R}$ is very small and the curvature of the film may then be ignored. In dynamic studies it can be an advantage to use a system of polar co-ordinates, as shown in Fig. 2.1.2 referred to the instantaneous line of centres $O_b\ O_j'$. The local film thickness h can then be expressed by the relationship:

$$h = C(1 + \epsilon \cos\theta) \qquad 2.1.7$$

The independent variables can be made dimensionless by putting:

$$x = R\alpha$$

$$z = R\zeta \qquad 2.1.8$$

$$t = \tau/\nu'$$

where $\alpha = \theta + \phi_1(t)$ 2.1.9

Equation 2.1.9 is used to transform the Reynolds equation into a system of co-ordinates which rotate with the line of centres. The transformation is given by Marsh [7]. The dependant variables p and h can also be expressed in dimensionless form by writing:

$$p = \bar{P} P_a$$
$$h = \bar{h} C \qquad 2.1.10$$

For the case under consideration the surface velocities W_h, W_o and U_o are all zero. Substitution of equations 2.1.7 to 2.1.10 into equation 2.1.6 gives the required dimensionless form of time dependant Reynolds' equation for a cylindrical journal bearing:

$$\frac{\partial}{\partial\theta}\left(\bar{h}^3\bar{P}\frac{\partial\bar{P}}{\partial\theta}\right)+\frac{\partial}{\partial\zeta}\left(\bar{h}^3\bar{P}\frac{\partial\bar{P}}{\partial\zeta}\right) = \Lambda\left(1-2\nu'\frac{\partial\phi_1}{\partial\tau}\right)\frac{\partial(\bar{P}\bar{h})}{\partial\theta} + 2\nu'\Lambda\frac{\partial(\bar{P}\bar{h})}{\partial\tau} \qquad 2.1.11$$

where the non dimensional number $\Lambda = \frac{6\mu\omega R^2}{P_a C^2}$ is usually called the compressability number and $\nu' = \frac{\nu'}{\omega}$

2.2 Survey of Various Methods of Solution of the Reynolds' Equation

The general gas bearing problem can be stated as the determination of the gas film pressure profiles corresponding to

(a) Steady running conditions, for example when equilibrium design charts are required for a particular bearing.

(b) Small amplitude harmonic variations, which are externally imposed, to study instability in the small and the steady response to synchronous excitation. The determination of (a) is necessary as an input to (b).

(c) Transient running conditions, when the bearing may be subject to shock and vibration and large amplitude excursions due to instability.

The various methods of solution to the Reynolds equation, for the purpose of determining the gas film pressure profile, fall into three classes: (1) Analytical, (2) Direct-Numerical and (3) Analytical-Numerical. These classes will now be discussed in relation to the general gas bearing problem as stated above.

2.2.1 Analytical

These solutions must be regarded as approximate, since they necessitate the linearization of the Reynolds' equation and the use of a first-order perturbation of the dependent variable in order to separate the constant and time dependant parts. Such methods are limited to cases (a) and (b) and are suited to parametric studies.

The first successful solution was made by Ausman [1], for a hydrodynamic bearing, by a linear expansion of pressure in terms of eccentricity ratio (known as the "linearized p" solution). The bearing was assumed to be infinitely long, by neglecting axial flow $(\frac{\partial p}{\partial \zeta} = 0)$, and the analysis is further restricted to the stability of an unloaded bearing $(\epsilon \to 0)$. Ausman later used the product $\bar{p}\bar{h}$ as the dependant variable and simplified the Reynolds' equation by replacing the variable coefficients by appropriate constants and neglecting altogether nonlinear combination of the derivatives of $\bar{p}\bar{h}$ and $\bar{h}$ [3]. The "linearized ph" equilibrium solution partially retains the nonlinear influence of eccentricity ratio and is valid for the stability of a loaded bearing ($\epsilon \neq 0.4$ say) over the entire range of Λ. Using the same approach Ng [4], by assuming a harmonic form for the pressure profiles in the θ direction, has obtained a closed form solution for a bearing of finite length.

2.2.2 Direct--Numerical

A review of various numerical methods is given by Castelli and Pirvics [28]. The advantage of these methods lies in their solution to the "exact" Reynolds equation and they therefore include case (c). Against this must be set the disadvantages of expensive computing time and the difficulty of ascertaining parametric trends.

For the purposes of numerical approximation of Reynolds' equation, the dependant variable distribution is represented at a finite number of points N located at intersections of a grid mesh. Castelli and Elrod [6] using ph as the dependant variable express the derivatives in finite difference form for each point on the space-time grid. They employ the explicit method of integration, which reduces the finite difference problem to a set of N linear algebraic equations. By assuming the required initial conditions the finite difference form of the equations of motion and Reynolds equation can be repeatedly updated in order to trace out the orbit of the journal centre. Shapiro [29] has extended this method to the dynamic analysis of a hybrid journal bearing.

2.2.3 Analytical-Numerical

In this class some approximations are made in order to ~~partially~~ partially solve the problem by analytical means. Numerical techniques, which are less demanding in computer time, are then used, thus combining the advantages of classes (1) and (2).

Marsh [7] and Castelli and Elrod [6] have used first order perturbation methods to reduce the "exact" Reynolds equation to finite difference form. The perturbation amounts to a local linearization of the dynamic pressure profiles. Both solutions are confined to the case of a hydrodynamic journal bearing.

Cheng and Pan [5] have applied the method of Galerkin to the stability of a hydrodynamic journal bearing. The basis of the method is to express the dependent variable ph in the θ and ζ directions by sets of trigonometric functions. The Reynolds' equation is thereby reduced from its partial differential form to a set of ordinary differential equations. The equilibrium part reduces to a set of nonlinear algebraic equations and the stability is examined by a small perturbed displacement.

In the "Step-Jump" stability analysis of Elrod et al [8] a transient solution is used to very accurately generate the force responses of the bearing to stimulations of the dynamic degrees of freedom. The responses are stored in the computer in the form of La-Guerre polynomials. The orbit of the journal centre is computed numerically from the equations of motion which contain linearized force responses of the bearing. After the initial investment of computer time "linearized orbits" can be run relatively cheaply for different inertial conditions.

Based on the analytical solution due to Ng [4], Lund [17] has extended the "linearized ph" method to include external pressurization. Although it is an approximate method, the numerical calculation of the gas film coefficients is considerably simplified. This makes it suitable for the present parametric study, particularly when the problem is complicated by additional elements of flexibility. An outline of this analysis is given in the next section.

2.3 The "Linearized ph" Method of Solution of the Time Dependent Reynolds' Equation for a Hybrid Journal Bearing [17]

2.3.1 Analysis

Assuming the axes of the bearing and journal to remain parallel, equation 2.1.11 can be rewritten:

$$\frac{\partial}{\partial\theta}\left[\bar{h}\frac{\partial(\bar{p}\bar{h})}{\partial\theta}^2 - 2\frac{\partial\bar{h}}{\partial\theta}(\bar{p}\bar{h})^2\right] + \frac{\partial}{\partial\xi}\left[\bar{h}\frac{\partial(\bar{p}\bar{h})}{\partial\xi}^2\right]$$

$$= 2\Lambda\left(1-2\nu'\frac{\partial\phi}{\partial\tau}\right)\frac{\partial(\bar{p}\bar{h})}{\partial\theta} + 4\nu'\Lambda\frac{\partial(\bar{p}\bar{h})}{\partial\tau} \qquad 2.3.1$$

where $\bar{h} = 1 + \epsilon\cos\theta$ 2.3.2

$$\nu' = v'/\omega$$

$$\tau = v't$$

Perturb equation 2.3.1 by:

$$\bar{p}\bar{h} = \bar{P}_o + \epsilon\bar{P}_1 \qquad 2.3.3$$

neglecting higher orders of ϵ other than the first to get:

$$\frac{\partial^2\bar{P}_o^2}{\partial\xi^2} = 0, \text{ implying a line feed source if } \bar{P}_o \text{ is independant of } \theta. \qquad 2.3.4$$

$$\frac{\partial^2(\epsilon\bar{P}_o\bar{P}_1)}{\partial\theta^2} + \frac{\partial^2(\epsilon\bar{P}_o\bar{P}_1)}{\partial\xi^2} - \frac{\Lambda}{\bar{P}_o}\left(1-2\nu'\frac{\partial\phi}{\partial z}\right)\frac{\partial(\epsilon\bar{P}_o\bar{P}_1)}{\partial\theta} - \frac{2\nu'\Lambda}{\bar{P}_o}\frac{\partial(\epsilon\bar{P}_o\bar{P}_1)}{\partial\tau} = -\epsilon\cos\theta\,\bar{P}_o^2 \qquad 2.3.5$$

Assume a harmonic journal centre motion relative to the bearing centre such that:

$$\epsilon = \epsilon_o + \epsilon_1 e^{v't} \qquad 2.3.6$$

$$\phi = \phi_o + \phi_1 e^{v't} \qquad 2.3.7$$

$$\epsilon\bar{P}_o\bar{P}_1 = \epsilon_o g_o + \epsilon_1 e^{v't} g_1 + \epsilon_o\phi_1 e^{v't} g_2 \qquad 2.3.8$$

Restrict the motion to the condition of neutral stability i.e. v' purely imaginary. Set:

$$v' = jv \;;\; \nu' = j\nu. \qquad 2.3.9$$

Assume the steady state and dynamic pressure profiles to be harmonic with respect to θ and rewrite equation 2.3.8:

$$\epsilon \bar{P}_o \bar{P}_1 = \epsilon_o g_o + \epsilon_1 g_1 + \epsilon_o \phi_1 g_2 \qquad 2.3.10$$

where
$$g_o = Re_i [G_o(\xi) e^{i\theta}]$$
$$g_1 = Re_{ij} [G_1(\xi) e^{i\theta} e^{j\nu t}] \qquad 2.3.11$$
$$g_2 = Re_{ij} [G_2(\xi) e^{i\theta} e^{j\nu t}]$$

Substituting equations 2.3.9 to 2.3.11, and collecting terms according to ϵ_o, ϵ_1 and $\epsilon_o \phi_1$, equation 2.3.5 reduces to:

$$\frac{d^2 G_o}{d\xi^2} - \left(1 + i\frac{\Lambda}{\bar{P}_o}\right) G_o = -\bar{P}_o^2 \qquad 2.3.12$$

$$\frac{d^2 G_1}{d\xi^2} - \left(1 + i\frac{\Lambda}{\bar{P}_o} + j\frac{2\nu\Lambda}{\bar{P}_o}\right) G_1 = \bar{P}_o^2 \qquad 2.3.13$$

$$\frac{d^2 G_2}{d\xi^2} - \left(1 + i\frac{\Lambda}{\bar{P}_o} + j\frac{2\nu\Lambda}{\bar{P}_o}\right) G_2 = -ij\frac{2\nu}{\bar{P}_o} G_o \qquad 2.3.14$$

2.3.2 Boundary Conditions

The geometry of the bearing is indicated in Fig. 2.3.1.

At $\xi = L/D = \bar{\xi}$, the pressure is ambient i.e. $\bar{p} = 1$ such that $\bar{p}\bar{h} = 1 + \epsilon\cos\theta$. Hence from equations 2.3.3, 2.3.10 and 2.3.11

$$\bar{P}_o(\xi) = G_o(\xi) = G_1(\xi) = 1 \qquad 2.3.15$$
$$G_2(\xi) = 0$$

At $\xi = 0$, for continuity of flow, equate the mass flow rates of the bearing and the orifices, assuming the discrete feeding holes to be replaced by a line source, to give:

$$-\bar{h}\frac{\partial(\bar{p}\bar{h})}{\partial\xi} = \Lambda_t \bar{P}_s m \qquad 2.3.16$$

where $\Lambda_t = \dfrac{6\mu N a^2 \sqrt{RT}}{p_a C^3}$ (orifice compensated)

$$m = \frac{M_T \sqrt{RT}}{\pi N a^2 \bar{p}_s}$$

Expand the dimensionless orifice flow $m(p_c/p_s)$ in a Taylor series:

$$m = m_o + \frac{1}{\bar{p}_s} \frac{\partial m}{\partial(\bar{p}_c/\bar{p}_s)}\bigg|_o (\bar{p} - \bar{p}_o)_c \qquad 2.3.17$$

where the subscript "c" refers to downstream of the orifice.

Perturbing the pressure $\bar{p}_c$ according to equation 2.3.3, with the aid of equation 2.3.10 yields:

$$(\bar{p} - \bar{p}_o)_c = \frac{1}{\bar{p}_{oc}} \left[\epsilon_o (g_o - \bar{p}_o^2 \cos\theta) + \epsilon_1 (g_1 - e^{j\nu t} \bar{p}_o^2 \cos\theta) + \epsilon_o \phi_1 g_2\right]_c \qquad 2.3.18$$

For convenience write:

$$\psi' = -\frac{\Lambda_t}{2\bar{p}_{oc}} \frac{\partial m}{\partial(\bar{p}_c/\bar{p}_s)}$$

$$q = \Lambda_t \bar{p}_s m_o$$

Introduce equations 2.3.2, 2.3.3, 2.3.17 and 2.3.18 into equation 2.3.16. Collecting the constant, ϵ_o, ϵ_1 and $\epsilon_o\phi_1$ terms gives the boundary conditions at $\xi = 0$. Note, for example, that $e^{j\nu t} q \cos\theta$ can be written as $Re_{ij}(q e^{i\theta} e^{j\nu t})$ when equating real quantities, since q is real

$$\frac{d\bar{p}_o^2}{d\xi} = -q \qquad 2.3.19$$

$$\frac{dG_o}{d\xi} = \frac{1}{2} q - \psi' \bar{p}_{oc}^2 + \psi' G_{oc} \qquad 2.3.20$$

$$\frac{dG_1}{d\xi} = \frac{1}{2} q - \psi' \bar{p}_{oc}^2 + \psi' G_{1c} \qquad 2.3.21$$

$$\frac{dG_2}{d\xi} = \psi' G_{2c} \qquad 2.3.22$$

From equations 2.3.4, 2.3.15 and 2.3.19

$$\bar{P}_o^2 = 1 + q(\xi - S) \qquad 2.3.23$$

$$\therefore \bar{P}_{oc}^2 = 1 + q\xi \qquad 2.3.24$$

Equation 2.3.24 can be solved by trial and error and hence q determined. The three remaining unknowns G_o, G_1 and G_2 are solved by numerical integration as discussed later in section 2.3.5.

2.3.3 Line Feed Correction

The replacement of the discrete feeding holes by a continuous line feed has the effect of smoothing out the pressure p_{oc}. By the method of sources and sinks, Lund obtains a correction factor which should be applied to equation 2.3.24 such that:

$$\bar{P}_{oc}^2 = 1 + q\xi\lambda \qquad 2.3.25$$

where $$\lambda = \frac{1}{N\xi} \ln\left[\frac{\cosh N\xi - 1}{1 - \cos(Nd/D)}\right]$$

In the same connection ψ' should be replaced by ψ in equations 2.3.20 to 2.3.22 where:

$$\psi = \frac{\lambda + \psi'\xi\lambda}{1 + \psi'\xi\lambda}$$

2.3.4 Evaluation of Gas Film Dynamic Coefficients

The dimensionless radial and tangential force components due to the gas film pressure, shown in Fig. 2.3.2 are given by:

$$f_r = -\frac{1}{2\xi}\int_0^{\xi}\int_0^{2\pi} \bar{p}\cos\theta \; d\theta \, d\xi \qquad 2.3.25$$

$$f_t = \frac{1}{2\xi}\int_0^{\xi}\int_0^{2\pi} \bar{p}\sin\theta \; d\theta \, d\xi \qquad 2.3.26$$

where $f_r = \dfrac{F_r}{p_a L D}$; $f_t = \dfrac{F_t}{p_a L D}$

The forces may be separated into steady state and time dependant parts:

$$f_r = f_{ro} + f_{rt}$$

$$f_t = f_{to} + f_{tt}$$

Resolving f_r and f_t along the fixed axes x and y, assuming ϕ_1 to be small, gives for steady state:

$$f_{ro}\cos\phi_o + f_{to}\sin\phi_o = \bar{W} \qquad 2.3.27$$

$$f_{ro}\sin\phi_o - f_{to}\cos\phi_o = 0 \qquad 2.3.28$$

where $\bar{W} = \dfrac{W}{p_a L D}$.

From which the attitude angle $\phi_o = \tan^{-1} f_{to}/f_{ro}$.

The remaining time dependant parts can be written in terms of the dimensionless dynamic coefficients and displacements by:

$$\begin{cases} (\bar{K}_{xx} + j\gamma\omega\bar{C}_{xx})\epsilon_1 e^{j\omega t} + (\bar{K}_{yx} + j\gamma\omega\bar{C}_{yx})\epsilon_o\phi_1 e^{j\omega t} = f_{rt} + f_{to}\phi_1 e^{j\omega t} & 2.3.29 \\ (\bar{K}_{xy} + j\gamma\omega\bar{C}_{xy})\epsilon_1 e^{j\omega t} + (\bar{K}_{yy} + j\gamma\omega\bar{C}_{yy})\epsilon_o\phi_1 e^{j\omega t} = -f_{tt} + f_{ro}\phi_1 e^{j\omega t} & 2.3.30 \end{cases}$$

where $\bar{K}_{xx} = \dfrac{CK_{xx}}{p_a L D}$ etc ; $\omega\bar{C}_{xx} = \dfrac{C\omega C_{xx}}{p_a L D}$ etc.

The integration of equations 2.3.25 and 2.3.26 with respect to θ are carried out in Appendix I. The coefficients become:

$$f_{ro} = \frac{\pi}{\xi}\left[\frac{\epsilon_o}{\eta(1+\eta)}\left(\int_o^\xi \bar{P}_o\, d\xi - \int_o^\xi \frac{G_{or}}{\bar{P}_o}\, d\xi\right)\right] \qquad 2.3.31$$

$$f_{to} = \frac{\pi}{\xi}\left[\frac{\epsilon_o}{1+\eta}\int_o^\xi \frac{G_{oi}}{\bar{P}_o}\, d\xi\right] \qquad 2.3.32$$

$$\bar{K}_{xx} + j\nu\omega\bar{C}_{xx} = \frac{\pi}{\xi}\left[\frac{(1+\eta-\eta^2)}{\eta^3(1+\eta)}\int_o^\xi \bar{P}_o\, d\xi - \frac{(1-\eta)(1+2\eta)}{\eta^3(1+\eta)}\int_o^\xi \frac{G_{or}}{\bar{P}_o}\, d\xi - \frac{1}{\eta(1+\eta)}\int_o^\xi \frac{G_{1r}}{\bar{P}_o}\, d\xi\right] \qquad 2.3.33$$

$$\bar{K}_{xy} + j\nu\omega\bar{C}_{xy} = -\frac{\pi}{\xi}\left[\frac{1}{1+\eta}\int_o^\xi \frac{G_{oi}}{\bar{P}_o}\, d\xi + \frac{1}{\eta(1+\eta)}\int_o^\xi \frac{G_{2r}}{\bar{P}_o}\, d\xi\right] \qquad 2.3.34$$

$$\bar{K}_{yx} + j\nu\omega\bar{C}_{yx} = -\frac{\pi}{\xi}\left[\frac{(1-\eta)}{\eta(1+\eta)}\int_o^\xi \frac{G_{oi}}{\bar{P}_o} + \frac{1}{1+\eta}\int_o^\xi \frac{G_{1i}}{\bar{P}_o}\, d\xi\right] \qquad 2.3.35$$

$$\bar{K}_{yy} + j\nu\omega\bar{C}_{yy} = \frac{\pi}{\xi}\left[\frac{1}{\eta(1+\eta)}\left(\int_o^\xi \bar{P}_o\, d\xi - \int_o^\xi \frac{G_{or}}{\bar{P}_o}\, d\xi\right) - \frac{1}{1+\eta}\int_o^\xi \frac{G_{2i}}{\bar{P}_o}\, d\xi\right] \qquad 2.3.36$$

where $\eta = \sqrt{(1-\epsilon_o^2)}$

$G_o = G_{or} + iG_{oi}$ and similarly for G_1 and G_2

2.3.5 Numerical Integration of G Functions

Equations 2.3.12 to 2.3.14 are of the form:

$$\frac{d^2G}{d\xi^2} - EG = F \qquad 2.3.37$$

where: $E = \begin{cases} 1 + i\Lambda/\bar{P}_o & \text{for } G_o \\ 1 + i\dfrac{\Lambda}{\bar{P}_o} + j\dfrac{2\nu\Lambda}{\bar{P}_o} & \text{for } G_1 \text{ and } G_2 \end{cases}$

$F = \begin{cases} -\bar{P}_o^2 & \text{for } G_o \text{ and } G_1 \\ -ij\dfrac{2\nu}{\bar{P}_o}G_o & \text{for } G_2 \end{cases}$

From the boundary conditions given by equations 2.3.15 and 2.3.20 to 2.3.22:

$$G(\xi) = \begin{cases} 1 & \text{for } G_0 \text{ and } G_1 \\ 0 & \text{for } G_2 \end{cases} \qquad 2.3.38$$

$$G'(0) = a + a_1 G_c \qquad 2.3.39$$

where $G_c = G(0)$

$$a = \begin{cases} \frac{1}{2} q - \psi \bar{P}_{oc}^2 & \text{for } G_0 \text{ and } G_1 \\ 0 & \text{for } G_2 \end{cases}$$

$$a' = \psi \qquad \text{for } G_0, G_1 \text{ and } G_2$$

Integrating Equation 2.3.37 gives:

$$\frac{dG}{d\xi} = \int (EG + F)\, d\xi + \text{const} \qquad 2.3.40$$

From the boundary condition of equation 2.3.39

$$\text{const} = a + a_1 G_c$$

Set $H = EG + F$ and subdivide the bearing length ξ into m increments of length $\Delta\xi = \xi/m$. Equation 2.3.40 can be given a finite difference form and using the trapezoidal rule for numerical integration becomes:

$$G_{n+1} = G_n + (\Delta\xi)^2 \left[\tfrac{1}{2} H_0 + H_1 + \ldots H_n\right] + \Delta\xi (a + a_1 G_c) \qquad 2.3.41$$

$$0 \leq n \leq m-1$$

Since G_c is initially unknown it is necessary to express the G function in the general form:

$$G = t_r + i t_i + j(u_r + i u_i) + [v_r + i v_i + j(w_r + i w_i)] G_c$$

Equation 2.3.41 may be evaluated step by step keeping G_c as unknown. At n=m-1 the boundary condition given by equation 2.3.38 can be used to determine G_c. G_n may then be evaluated by the back-substitution of G_c.

A computer programme has been written for the evaluation of the G functions and their integrals in equations 2.3.31 to 2.3.36 This is discussed later in section 3.3.

CHAPTER 3

3.0 THEORETICAL INVESTIGATION OF PARAMETERS AFFECTING BEARING STABILITY

3.1 The Rotor-Bearing System

The rotor-bearing system to be analysed is shown diagrammatically in Fig. 3.1.1(a). It comprises a rigid, perfectly symmetrical rotor, of mass m_r per bearing, supported horizontally in two bearings each of mass m_b. The bearing film is represented by the coefficients K_{xx}, C_{xx} etc., while the bearings themselves are mounted on isoelastic springs K_p whose damping C_p is assumed to be viscous.

3.2 Equations of Motion for Translatory Whirl

For the system described, two modes of whirl can occur if the bearings are rigidly supported. The rotor axis can translate uniformly along its length with all points in-phase. For a circular motion of the journal centre the rotor axis will then generate a cylinder about its steady state operating position. Alternatively, if the opposite ends of the rotor move in anti-phase with circular motions, the rotor axis will generate two cones having a common apex at the middle of the rotor. With flexible bearing supports the whirl modes are more complex, but the system will possess two translatory modes, analogous to the in-phase and anti-phase motions of the masses m_r and m_b.

It is convenient to adopt a fixed set of axes which pass through the equilibrium position of the bearing centre O_b and are rotated through the attitude angle ϕ_o, as indicated in Fig. 3.1.1(b). Let the displacement vectors of the instantaneous bearing centre O_b' and journal centre O_j' have components x_1 y_1 and x_2 y_2 respectively along the X and Y axes where, neglecting any phase difference:

$$x_1 = Re\,(X_1 e^{j\omega t}) \quad ; \quad y_1 = Im\,(Y_1 e^{j\omega t}).$$
$$x_2 = Re\,(X_2 e^{j\omega t}) \quad ; \quad y_2 = Im\,(Y_2 e^{j\omega t}). \qquad 3.2.1$$

The equations of motion for translatory whirl are:

$$m_r \ddot{x}_2 + C_{xx}(\dot{x}_2 - \dot{x}_1) + K_{xx}(x_2 - x_1) + C_{xy}(\dot{y}_2 - \dot{y}_1) + K_{xy}(y_2 - y_1) = 0$$
$$m_r \ddot{y}_2 + C_{yx}(\dot{x}_2 - \dot{x}_1) + K_{yx}(x_2 - x_1) + C_{yy}(\dot{y}_2 - \dot{y}_1) + K_{yy}(y_2 - y_1) = 0$$
$$m_b \ddot{x}_1 + C_p \dot{x}_1 + K_p x_1 - C_{xx}(\dot{x}_2 - \dot{x}_1) - K_{xx}(x_2 - x_1) - C_{xy}(\dot{y}_2 - \dot{y}_1) - K_{xy}(y_2 - y_1) = 0$$
$$m_b \ddot{y}_1 + C_p \dot{y}_1 + K_p y_1 - C_{yx}(\dot{x}_2 - \dot{x}_1) - K_{yx}(x_2 - x_1) - C_{yy}(\dot{y}_2 - \dot{y}_1) - K_{yy}(y_2 - y_1) = 0 \qquad 3.2.2$$

To make equations 3.2.2 dimensionless set:

$$\Omega = \frac{m_r P_a}{\mu^2 L \left(\frac{R}{C}\right)^5}$$

$$\bar{m} = \frac{m_b}{m_r}$$

$$\bar{C}_p = \frac{C_p}{\mu L \left(\frac{R}{C}\right)^3}$$

$$\bar{K}_p = \frac{K_p C}{P_a L D}$$

$\bar{X}_1 = X_1/C$ and similarly for, Y_1, X_2 and Y_2.

Then introducing equations 3.2.1 and dividing through by $e^{j\omega t}$ gives:

$$-\Omega \frac{\gamma^2 \Lambda^2}{72} \bar{X}_2 + (\bar{K}_{xx} + j\gamma\omega\bar{C}_{xx})(\bar{X}_2 - \bar{X}_1) + (\bar{K}_{xy} + j\gamma\omega\bar{C}_{xy})(\bar{Y}_2 - \bar{Y}_1) = 0$$
$$-\Omega \frac{\gamma^2 \Lambda^2}{72} \bar{Y}_2 + (\bar{K}_{yx} + j\gamma\omega\bar{C}_{yx})(\bar{X}_2 - \bar{X}_1) + (\bar{K}_{yy} + j\gamma\omega\bar{C}_{yy})(\bar{Y}_2 - \bar{Y}_1) = 0$$
$$\left(-\Omega \frac{\bar{m}\gamma^2\Lambda^2}{72} + j\frac{\gamma\Lambda}{12}\bar{C}_p + \bar{K}_p\right)\bar{X}_1 - (\bar{K}_{xx} + j\gamma\omega\bar{C}_{xx})(\bar{X}_2 - \bar{X}_1) - (\bar{K}_{xy} + j\gamma\omega\bar{C}_{xy})(\bar{Y}_2 - \bar{Y}_1) = 0$$
$$\left(-\Omega \frac{\bar{m}\gamma^2\Lambda^2}{72} + j\frac{\gamma\Lambda}{12}\bar{C}_p + \bar{K}_p\right)\bar{Y}_1 - (\bar{K}_{yx} + j\gamma\omega\bar{C}_{yx})(\bar{X}_2 - \bar{X}_1) - (\bar{K}_{yy} + j\gamma\omega\bar{C}_{yy})(\bar{Y}_2 - \bar{Y}_1) = 0. \qquad 3.2.3$$

where $(\bar{K}_{xx} + j\gamma\omega\,\bar{C}_{xx})$ etc., are given by equations 2.3.33 to 2.3.36.

Equations 3.2.3 can be arranged in matrix form as follows:

$$\begin{bmatrix} -\frac{\Omega\gamma^2\Lambda^2}{72}, & 0, & \bar{K}_{xx}+j\gamma\omega\bar{C}_{xx}-\frac{\Omega\gamma^2\Lambda^2}{72}, & \bar{K}_{xy}+j\gamma\omega\bar{C}_{xy}, \\ 0, & -\frac{\Omega\gamma^2\Lambda^2}{72}, & \bar{K}_{yx}+j\gamma\omega\bar{C}_{yx}, & \bar{K}_{yy}+j\gamma\omega\bar{C}_{yy}-\frac{\Omega\gamma^2\Lambda^2}{72}, \\ -\frac{\Omega\bar{m}\gamma^2\Lambda^2}{72}+j\frac{\gamma\Lambda}{12}\bar{C}_p+\bar{K}_p, & 0, & -\bar{K}_{xx}-j\gamma\omega\bar{C}_{xx}, & -\bar{K}_{xy}-j\gamma\omega\bar{C}_{xy} \\ 0, & -\frac{\Omega\bar{m}\gamma^2\Lambda^2}{72}+j\frac{\gamma\Lambda}{12}\bar{C}_p+\bar{K}_p, & -\bar{K}_{yx}-j\gamma\omega\bar{C}_{yx}, & -\bar{K}_{yy}-j\gamma\omega\bar{C}_{yy} \end{bmatrix} \times \begin{bmatrix} \bar{X}_1 \\ \bar{Y}_1 \\ \bar{X}_2-\bar{X}_1 \\ \bar{Y}_2-\bar{Y}_1 \end{bmatrix} = 0 \qquad 3.2.4$$

To test the stability of the prescribed motion set the determinant of the coefficients of equations 3.2.4 to zero. This results in a determinantal equation containing both real and imaginary (j) terms. The frequency (γ) solution is first obtained numerically from the imaginary terms, since the coefficients $\bar{K}_{xx}, \gamma\omega - \bar{C}_{xx}$ etc., are frequency dependent. For a threshold condition the real part of the determinantal equation must be simultaneously zero.

3.3 Computer Programmes

The programmes have been written so as to investigate the stability of the system with ϵ_o and Λ as input variables. Values of ϵ_o and Λ corresponding to a fixed rotor mass (Load) and set of bearing conditions are first obtained by solving equations 2.3.27 and 2.3.28. This involves setting a range of ϵ_o and Λ values to obtain values of dimensionless load, which can be plotted to obtain the desired relationships between ϵ_o and Λ.

Initially the parameters $p_s, \xi, \Lambda_t, \Omega$, m, $\bar{6}_p$ and $\bar{K}_p$ are set. The frequency ratio γ is then set to some value below the expected solution, say 0.4.

For a given point on the journal centre locus (ϵ_o, Λ) the G functions are evaluated numerically, as outlined in section 2.3.5, and the dynamic coefficients determined from equations 2.3.33 to 2.3.36. The imaginary part of the determinantal equation is evaluated and for a non-zero value γ is increased by a small increment. The process is repeated until the value of the determinant just changes sign, indicating a solution for γ. At this stage the real part of the determinant is evaluated. For a small increase in Λ new values of ϵ_o and Λ are fed in and the procedure is repeated until the real part of the determinant simultaneously changes sign, indicating a threshold condition. A change in one of the parameters, typically $\bar{K}_p$, is then made. A sample print out of the results run on the IBM 360/50 computer is shown in Fig. 3.3.1.

From the results of many experiments it is known that if the journal speed (Λ in this case) is sufficiently low, then the system will always be stable, so that a stable or unstable region can be identified.

In order to economize on computer time, the programme has been designed to "Lock-on" to a stability boundary, rather than perform a series of sweeps.

Some runs were made with the programmes to check a sample of results directly against those given by Lund in reference [17]. Fig. 3.3.2 compares the dimensionless load versus compressability number for the case L/D = 1 and $\Lambda_t = 1.0$, with $\bar{p}_s = 2$ at $\epsilon = 0.1$, $\bar{p}_s = 2$ at $\epsilon = 0.5$ and $\bar{p}_s = 5$ at $\epsilon = 0.1$. The load is seen to be consistently about 10 per cent below Lund's values. A careful scrutiny of the analysis and programme was made, but the discrepancy could not be accounted for. The division of bearing length in the numerical computation was increased from 10 to 100 with no significant effect.

Stability checks were made for the same conditions and Fig. 3.3.3 compares the instability threshold parameters $\frac{MC\omega^2}{(p_s - p_a)LD}$ against compressability number. The curves for $\bar{p}_s = 2$ and 5 at $\epsilon = 0.1$ are generally in satisfactory agreement, whereas the curves for $\bar{p}_s = 2$ at $\epsilon = 0.5$ differ considerably at lower compressability numbers.

3.4 Results of the Analysis

In view of the large number of variables involved in the problem, it was decided to fix the bearing dimensions, feeding geometry and load and examine the effects of support stiffness and damping on the threshold speeds for various supply pressures. Sample results have been obtained for a bearing having the following details:-

Length	1.0 in
Diameter	1.0 in
Radial clearance	0.001 in
Rotor weight per bearing	2.96 lbf
Bearing weight	0.296 lbf
Feeding parameter (Λ_f)	1.0

Calculated from the above

Load parameter $(\bar{W}) = 0.2$

Dimensionless rotor mass $(\Omega) = 524$

Mass ratio $(\bar{m}) = 0.1$

In all the numerical results a line feed correction factor $\lambda = 1.5$ and an orifice discharge coefficient $C_D = 1.0$ have been used. The bearing axial length was divided into 10 increments.

3.4.1 Steady State Locus of Journal Centre

In Fig. 3.4.1 the steady state eccentricity ratio ϵ_o and attitude angle ϕ_o are shown plotted against compressability number Λ for various supply pressure ratios $\bar{p}_s$ up to 10 and the hydrodynamic case ($\Lambda_t = 0$). At $\Lambda = 0$, the hydrostatic stiffness is found to be fairly linear with $\bar{p}_s$ above a value of about 5, but below this the stiffness falls progressively faster as $\bar{p}_s$ is reduced. As $\Lambda \rightarrow 10$ the hydrodynamic effects begin to assert themselves, which is apparent from the closing together of the ϵ_o curves.

3.4.2 Gas Film Dynamic Coefficients

Before attempting a general theoretical survey a further check was made to see if the computer programme would correctly generate the gas film dynamic coefficients. Comparisons were made against some curves in the 1969 MTI Gas Bearing Design Manual, which were for the synchronous whirl case ($\gamma = 1.0$) of a plain cylindrical hydrodynamic journal bearing. It is believed that these curves are also based on a linearized ph analysis and that the coefficients are referred to axes along and perpendicular to the load line. For values of $\epsilon_o = 0.1$ and L/D = 1.0, agreement between the direct stiffness and damping coefficients was generally to within 10 percent over the range of Λ from 0 to 5. However, major discrepancies were found to exist between the cross stiffness and damping coefficients, which could not be accounted for, even when allowing for a transformation through the angle ϕ_o between the two pairs of axes. An exhaustive series of checks were then made on the present computer programme without revealing the source of the discrepancy. As the result of a private communication with Drs. Pan and Lund, who kindly made some spot checks using reference [30], the validity of the present results was confirmed.

Curves of these coefficients are shown in Fig. 3.4.2 and in Figs. 3.4.3 and 3.4.4. Similar curves are given for pressure ratios of 2 and 5, which may provide useful checks in the future.

The frequency dependence of the dynamic coefficients is demonstrated in Fig. 3.4.5 for the case $\bar{p}_s = 2$ and $\epsilon_o = 0.2$ at $\Lambda = 1$, 5 and 10.

3.4.3 Stability Maps

Figs. 3.4.6 to 3.4.9 show the effects of support stiffness $\bar{K}_p$ and damping $\bar{C}_p$ on the threshold speeds for the hydrodynamic case and for supply pressure ratios of 2, 5 and 10. The overall effect of a flexible support is seen to introduce a lower and upper threshold boundary for a given value of $\bar{C}_p$. In Fig. 3.4.8 for example, taking $\bar{C}_p = 1.0$, for values of $\bar{K}_p$ below about 0.35 the speed of the rotor is limited by the upper threshold boundary i.e. $\Lambda \simeq 4$. Above $\bar{K}_p = 0.35$ the speed is limited by the lower threshold boundary and as $\bar{K}_p \to \infty$ (fixed bearing) the value becomes asymptotic at about $\Lambda = 1.0$. The threshold is thus increased by a factor of about 4. However, to achieve this order of improvement the bearing support must be sufficiently "forgiving" and it may be unacceptable to have a value which is below the hydrostatic film stiffness. In the example cited this corresponds to $\bar{K}_p = 1.43$. This can be overcome by increasing $\bar{C}_p$ to 10 say, which has the effect of folding back the threshold boundaries to give a stable system at all speeds below $\bar{K}_p = 1.4$. There are however practical limitations on the amount of damping that can be readily incorporated in the support and this is discussed later in chapter 4.

Plots of threshold frequency ratio corresponding to the curves of Figs. 3.4.6 to 3.4.9 are shown in Figs. 3.4.11 to 3.4.14.

It is well known that for an ordinary hybrid journal bearing the threshold speed for a rigid rotor occurs at about twice the synchronous whirl speed based upon the hydrostatic film stiffness. A comparison of the stability maps in Figs. 3.4.7 to 3.4.9 with the rigid body synchronous whirl speeds in Fig. 3.4.15 for the same system, shows a similar correlation. Generally the lower and upper stability boundaries all branch out from, and lie above, the respective synchronous whirls scaled up by a factor of two. The correlation is further emphasised by a comparison of the stability map of Fig. 3.4.10, which shows the effect of bearing mass, and the synchronous whirl curves in Fig. 3.4.16.

CHAPTER 4

4.0 EXPERIMENTAL BEARING TEST RIG

4.1 The Design of the Experiment

The large number of design variables associated with the stability problem has been previously referred to in the theoretical discussion. It was considered to be impracticable to attempt an experimental investigation of the effects of all of these on a single test rig. Accordingly, it was decided to restrict the parametric investigation by fixing the bearing and feeder hole geometries to fairly typical values and to arrange for variations in support stiffness and damping, supply pressure and rotational speed over as wide a range as possible.

A number of alternative design schemes were considered for the rotor/bearing system. Emphasis has already been laid on the need for accurate alignment in a two bearing machine. Marsh [7] advocated the use of a single, long bearing, free from external loading devices, as the ideal laboratory arrangement for testing bearing stability theory. An early test rig was also built along these lines by the present author, in connection with the theoretical investigation reported in Appendix II. Some difficulty was experienced in grinding the internal bearing diameter (2 in) to the required accuracy over the bearing length (6 in). In order to vary the support stiffness the bearing was held isoelastically at each end, firstly, by sets of tension springs and later by taut piano wires. It was, however, difficult to achieve a satisfactory range of stiffness as the springs tended to be very flexible and the wires, for adequate strength, very stiff compared to the film stiffness.

An attempt was also made to introduce external damping to the bearing using miniature "Kinetrol" torsional dampers, but as the motion of the bearing itself was of the order of 0.001 in, the linkage was required to have virtually no backlash or deflection in order to be effective. However, for the usual hybrid bearing length/diameter ratios, it was not thought to be feasible to support a shaft of sufficient length to incorporate a drive turbine and the necessary instrumentation in a single bearing.

Another proposal was to have a single test bearing supported on a shaft rotating in two slave bearings, on the general lines of the stability test rig used by Whitley and Betts [31]. While such a scheme appears to be suitable for steady state performance measurements, it was felt that, because of the interaction of the rotor with the slave bearings, it would be unsuitable for dynamic tests. In any case the restraint of the shaft by the slave bearings would limit the results to threshold of bearing whirl.

A symmetrical two bearing arrangement, with a central air turbine to drive the rotor, was used by Larson and Richardson [14], Gross [15] and Taniguchi et al [16]. Larson and Richardson employed rubber O-rings for self alignment of the bearings, whereas Gross fitted the bearing sleeves into an outer casing, with slight interference, prior to the final grinding of the bores.

It was finally decided to design the test rig along the conventional lines just described, taking great care during the course of manufacture to ensure accurate alignment of the bearing centres.

Ideally it was required to vary support stiffness and damping independently which, in practice, implied having a separate variable damping device.

This tended to conflict with previously unsuccessful attempts with the springs, wires and dampers, from which it seemed imperative to incorporate both variables within the same element. In their experiments into flexibly supported bearings, Kerr [22] used rubber O-rings of various hardness and Mori [25] employed externally pressurized air lubricated sub-bearings.

From a mechanical design point of view rubber O-rings have the advantages of simplicity and of acting as seals in the pressurization of the bearings. Rubbers of various compositions also offer a fairly wide range of stiffness and damping ratios. For laboratory use they have the disadvantage of frequency dependant, and to a lesser extent, amplitude dependent properties [32]. The results of the stability survey contained in Figs. 3.4.6 to 3.4.9 showed that substantial increases in threshold speed could be obtained with sufficiently high ratios of $\overline{C}_p/\overline{K}_p$. For example, taking $\overline{C}_p = 10$, $\overline{C}_p/\overline{K}_p = 25$, 7 and 4 at $\overline{p}_s = 2$, 5 and 10 respectively. Translated into actual coefficients these represent ratios of 5.6, 1.6 and 0.9 x 10^{-4} sec respectively. Based on the rotor mass and $\overline{K}_p = 1.0$, $\overline{C}_p = 10$ corresponds to a damping rate of about 15 per cent of the critical rate. Kerr measured the "equivalent" viscous damping rates of some rubber O-rings by the decay method. The results indicated rates between 3.6 per cent (30° shore hardness) and 12.8 per cent (70°) of critical. The actual damping/stiffness ratios varied between 1.07 - 1.7 x 10^{-4} sec, which were within the range required.

Pressurized sub-bearings require additional accuracy in manufacture and there is no independent control over stiffness and damping.

Increasing supply pressure increases stiffness and reduces damping. Provided the dimensionless squeeze number $\frac{12\mu\omega}{p_a}\left(\frac{R}{C}\right)^2$ is made sufficiently low, say < 1.0, the dynamic radial coefficients are independant of frequency (ω), see Figs. 5.8.1 and 5.8.5 of reference [33]. Estimates of dimensionless damping/stiffness from these curves gave values of approximately 10 and 4 for supply pressure $\bar{p}_s$ of 2 and 3 respectively, which were comparable with the values for the rubber O-rings.

It was decided to adopt the O-rings for the support system, primarily on the grounds of simplicity.

4.2 Mechanical Details

4.2.1 The Rotor and Bearings

A photograph of the test rig and air supply system is shown in Fig. 4.2.1. A drawing of the test rig, showing a section through one of the two identical bearing supports, is given in Fig. 4.2.2. The two steel pedestal blocks are bolted to a 1 in thick steel base plate and the rotor is located axially by a small carbon brush in the centre drilled in the end of the rotor. The base plate is slightly tilted so that the brush exerts a light pressure against the ground face of an adjustable bolt located in a fixed bracket. The carbon brush also acts as an earthing device when observing the displacements of the rotor by means of capacitance probes. This system is preferable to one employing air jets which can give poor axial stability.

The nominal bearing length and diameter is 1 in. Pressurized air is supplied to the side of each pedestal block and into the annular chamber between the two O-rings.

The restrictors comprise 8 equi-spaced holes of 0.0135 in dia. in the central plane of the bearing. The rotor and bush assembly is inserted axially into the pedestals which do not therefore have to be disturbed when once aligned. To allow the O-rings to be compressed without damage, the entrances to the pedestal bores are flared on one side.

To avoid possible seizure due to the fillets at the steps in the rotor running into the bearings, the shaft is slightly undercut at these sections. Also, the corners of the ends of the rotor and bushes are chamfered to avoid damaging the bearing surfaces during assembly.

Full details of the rotor and bearings are given in Table I.

4.2.2 Drive Turbine

The rotor is driven by means of an impulsive type air turbine located at its centre. Three nozzles, mutually inclined at 120 degrees, direct jets of air tangentially into the twelve pairs of buckets of the turbine, which are milled in the surface of the rotor. The convergent-divergent nozzles, from the earlier test rig, had been designed for the maximum airflow from a portable compressor of 6.8 cu ft of free air per minute and a pressure ratio of 6.1. The nozzles were made of brass in two halves which were hard soldered together.

An estimate of the maximum speed of the rotor can be made by equating the power loss in the bearings and the power developed by the drive turbine. Assuming Petroffs formula for concentric cylinders i.e. a lightly loaded bearing, the power dissipation in a bearing due to friction is given by:

$$E = \frac{\mu \pi^3 D^3 L N^2}{C}$$

The power developed by an impulse turbine having 180 deg buckets is given by:

$$P = 2m u (v_j - u) \eta_T$$

where m = mass flow rate through nozzle

u = peripheral speed of turbine buckets

v_j = jet velocity

η_t = turbine efficiency

Estimates for the test rig showed that the bearing power loss was very small and that the turbine speed was close to the "runaway" speed i.e. $u \rightarrow v_j$, indicating a probable maximum speed in excess of 100,000 r.p.m.

4.2.3 Rubber O-rings

The following standard rubber type materials were obtained in BS size No. 225

Material	Shore Hardness
Nitrile	60° 75° 90°
Viton	60° 75°
Silicon	75°

The groove and pedestal bore dimensions were made in accordance with the manufacturers instructions to give a minimum cross-section squeeze of 0.01 in.

4.2.4 Manufacturing and Inspection Procedures

The rotor and bearing sleeves were machined from free-cutting stainless steel, which was selected for its good machining and non-corrosive properties.

The anti-galling properties of stainless steel/stainless steel were not regarded as so important as it was intended to stop and start the test rig with adequate air always supplied to the bearings.

The rotor and internal bearing surfaces were precision ground and finished to the required accuracy using lead laps impregnated with oil and carborundum paste. Between the grinding and various lapping operations the rotor and bush dimensions were measured on a Society Genevoise Universal Measuring Apparatus, Type MU 214B, in a temperature controlled room at 70°F. With a little experience it is possible to measure to within ± 0.00002 in. The rotor was held horizontally between centre supports at each end. A feeler microscope was used which could be traversed in three directions relative to the workpiece. It was first necessary to traverse the feeler vertically against the side of the rotor in order to determine the diametral plane in the horizontal direction. At the correct height the diameter was then measured by taking the difference between the reading on each side of the rotor, less the calibrated width of the feeler. The ovality of the rotor, as indicated by the difference in two diameters perpendicular to one another, was found to average about 0.0001 in. As a check on the straightness of the rotor the ordinate of the centre was estimated at each axial location, for both angular positions, by adding half the local diameter to the corresponding reading on the side of the rotor. The maximum deviation from the average ordinate or "true" geometrical centre was found to be 0.0001 in and in general was less than half this value. These results were considered to be reasonably good having regard to the facilities of the Departmental Workshop and the infrequent demand for such precision.

The bearing bushes were clamped flat on the instrument table and the internal diameter was measured with the feeler microscope in two perpendicular directions at three different heights. The mean radial clearance of each bearing, given by half the difference between the rotor and bush sizes, was found to be 0.00056 in[2], which was close to the nominal design value of 0.0006 in.

For the machining of the pedestals the procedure was as follows. A cylindrical plug to fit the box size was first made. One of the pedestal faces to contain the bore was machined flat and then clamped to the magnetic chuck of the lathe for boring out, thus ensuring the bore axis to be perpendicular to the pedestal face. The bore was machined until the special plug could be fitted with slight interference. The same procedure was carried out for the other pedestal and the grinding of their bases was performed in a single operation with both pedestals fitted to the plug. The top surface of the main base plate was also finished on the surface grinding machine.

4.3 AIR SUPPLIES

For pressurized air bearings it is necessary to have a supply of clean and reasonably dry compressed air. The quality of air supplied by the usual type of small industrial compressor is not sufficiently good for direct use in air bearings and requires to be carefully filtered.

The compressed air supply is obtained from a Broomwade compressor with a maximum delivery pressure of 150 psig and maximum flow rate of about 26.0 cu ft of free air per minute.

(2) Later increased, see Chapter 5.

As the air has to pass along about 50 feet of pipe to reach the test rig, no special cooling arrangements are provided.

From the common delivery pipe the filtering and control of the bearing and turbine air supplies is separate. On the bearing supply line the air first enters a Norgren 25 micron filter which removes any water droplets and larger contaminants. It then passes through a pressure regulating valve which can maintain a steady downstream pressure when there are pressure fluctuations upstream. A pressure gauge is incorporated with the valve so that the desired bearing supply pressure can be set. After the valve the air is passed through a fine filter to remove any further moisture and sub-micron particles and then to a block with multiple tappings. The connections to the pedestals are made with flexible plastic tubing. The air to the drive turbine passes through a single filter and is then regulated by a precision controller, to enable the turbine speed to be set as accurately as possible. The three nozzles are fed independently through plastic tubing from a common block.

4.4 INSTRUMENTATION

4.4.1 Vibration and Displacement Measurements

For a complete study of the whirl behaviour of the system it is necessary to monitor continuously the motions of the journal and bearing relative to a fixed point in space. This is experimentally more convenient than attempting to measure the motion of the journal relative to the bearing, which involves mounting probes and leads (with damping) on the small bushes.

The motions at the threshold of a whirl are necessarily very small and require extremely sensitive measuring instruments to detect them. The position of the rotor or bearing is measured by capacitance probes which are mounted, with a small air gap, close to the smooth surface of the metallic object. In the single channel Wayne-Kerr System used, the standard probes give direct readings of the distance and peak to peak vibration amplitude across the gap, which are indicated on separate meters. The two readings are not interdependant i.e. the accuracy of the measurement of distance is unaffected by variations in vibration amplitude, and vice-versa. Although the instrument is designed for use with flat surfaces, the makers supply correction curves for cylindrical surfaces.

The probes which were used have a peak to peak amplitude range of 0.005 in and a stated accuracy of 100μ in (about 8 per cent of the bearing radial clearance). They are clamped in brackets attached to each pedestal block in the vertical and horizontal directions. By this means it is possible to discriminate between cylindrical and conical whirl, by comparing the phase of the signals at each end of the rotor, and study the orbital motion in a given plane on an oscilloscope, using a second instrument in parallel. A junction box is also used which enables any one of up to six probes to be switched into the measuring circuit.

4.4.2 Rotor Speed

The speed of the rotor is measured by using the buckets of the turbine to produce a change in the capacitance between the probe of a fixed transducer and the shaft.

The frequency of the signal generated is thus proportional to the speed of the rotor. The probe, comprising a short length of brass strip of rectangular section and clamped to the transducer, is mounted with a gap between 0.01 and 0.02in. The transducer is supplied by Racal Instruments and is encapsulated in a block about 1 in cube which is bolted to the nozzle support bracket. Batteries are used to provide the necessary 12 volts d.c. power supply. With the help of Mr. C.H.C. Mathews, of Electrical Engineering Department, a transistorized electrical circuit was built in order to improve the size and shape of the output pulse and remove the carrier frequency of 1.6 Mc/s. The output leads are also screened. These precautions were found to be necessary to ensure reliable triggering of the counter/timer used for accurate frequency measurement.

5.0 EXPERIMENTAL PROCEDURE AND RESULTS

5.1 Dynamic Test on O-rings.

5.1.1 Method of Analysis

The stiffness and damping of a single degree of freedom mass/spring system with viscous damping can be conveniently obtained by subjecting the system to a forced resonance test. Provided the magnitude of the applied force (P_o) is kept constant, it can be shown [34] that the damping rate (c) is given by:

$$c \simeq M \Delta\omega \qquad 5.1.1$$

where M = mass

$\Delta\omega$ = circular frequency bandwidth between the amplitudes of the response which have a value of $1/\sqrt{2}$ of their peak.

The damping rate may also be estimated by considering the energy of the system. At the resonant frequency (ω_n), the work done by the applied force is wholly dissipated by the damper. Equating energies gives:

$$c = \frac{P_o}{x_o\ \omega_n} \qquad 5.1.2$$

where x_o = amplitude of response at ω_n.

For practical purpose x_o may be taken as the peak amplitude, since the natural frequency and frequency of maximum amplitude are very close for damping rates up to 0.2 of critical.

The stiffness (k) can be calculated from the equation

$$\omega_n = \sqrt{\frac{k}{M}} \qquad 5.1.3$$

Rubber-like materials are not perfectly elastic - they exhibit hysteresis damping and their stiffness tends to increase as the frequency of loading is increased.

However, as an approximation, the O-rings are regarded as being perfectly elastic and the damping as having an "equivalent" viscous value. This can be justified on the grounds of the assumptions made in the analysis with respect to the support conditions. The frequency dependence of the material properties are taken into account by performing a series of resonance tests at different natural frequencies.

5.1.2 Apparatus for Measurement of O-ring Properties

The apparatus used for the dynamic tests on the various O-ring materials is shown in Fig. 5.1.1. Basically this consists of a rigid beam, hinged at one end with a mass M at the other end, as shown below. At distance a from the hinge the O-ring is represented by a spring of stiffness k and a viscous damper of rate c.

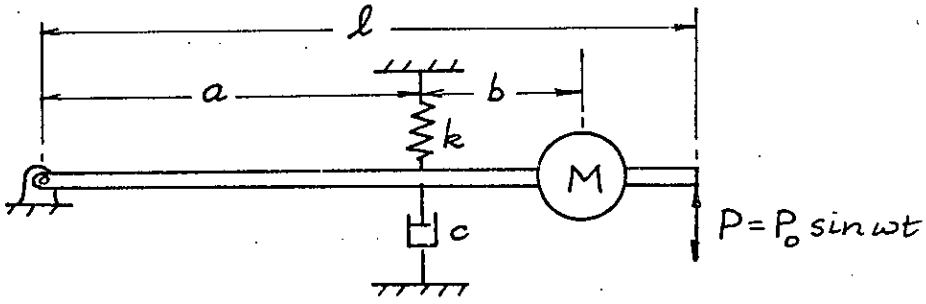

This system is equivalent to:

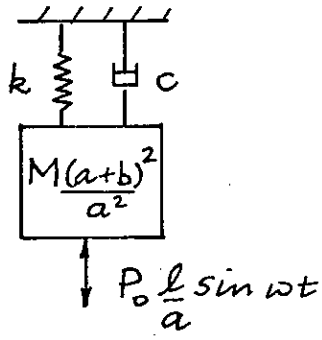

The moment of inertia of the beam and the drive system is allowed for by adding an appropriate mass to M.

The apparatus is designed so that the bending stiffness of the beam is relatively high compared with the maximum radial stiffness of the O-rings, thus avoiding any undesirable resonances over the test frequency range. In order to keep the external damping as low as possible the beam pivots on ball bearings. For a given O-ring the resonant test frequency can be altered by varying the loading weights and also by moving the pedestal nearer to the pivot, giving a resonant frequency range capability of more than 10:1.

The applied force is obtained from a moving coil vibration generator, fed from a variable frequency oscillator through a power amplifier. The output from the oscillator is also fed into a digital counter for accurate frequency measurement. A Brüel and Kjaer Type 8001 Impedance Head is incorporated in the drive from the vibration generator, so that a known force can be maintained constant by feeding the output signal into a calibrated oscilloscope. The makers supply a force gauge sensitivity for the impedance head.

5.1.3 Dynamic Properties

Resonance tests on the 60°, 75° and 90° Nitrite rubber O-rings were carried out with weights of 10, 4 and 2 lbf with the pedestal positioned as in Fig. 5.1.1. The amplitude of the applied force in the drive rod was maintained constant at 0.915 lbf. For the 75° Silicon rubber O-rings weights of 3, 2 and 1 lbf were attached with a constant force of 0.152 lbf. Only one test was performed on each of the 60° and 75° Viton O-rings, with a weight of 10 lbf and a constant force of 0.457 lbf.

Samples of the resonance curves for each type of material are shown in Fig. 5.1.2. For example, taking the curve for the 60^{o} Nitrile rubber and using the notation of the previous sections:

$$P_o = 0.915 \text{ lbf}$$

$$M = 10 + 1.55 = 11.55 \text{ lb}$$

$$a = 6.0 \text{ in}$$

$$b = 1.8 \text{ in}$$

$$\ell = 10.6 \text{ in}$$

$$\Delta f = 21.5 \text{ c/s}$$

$$x_o = 8.1 \times 10^{-4} \text{ in p-p}$$

$$f_n = \omega_n/2\pi = 80 \text{ c/s}$$

From equation 5.1.1

$$c = 11.55 \times (\frac{7.8}{6.0})^2 \times 2\pi \times 21.5/386 = 6.8 \text{ lbfs/in.}$$

From equation 5.1.2

$$c = \frac{2 \times 0.915 \times 10^4}{8.1 \times 2\pi \times 80} = 4.25 \text{ lbfs/in}$$

From equation 5.1.3

$$k = (2\pi \times 80)^2 \times 11.55 \times (\frac{7.8}{6.0})^2/386 = 12{,}800 \text{ lbf/in}$$

The estimate of the damping rate by the latter method is found to give results which are less consistent and always below those of the former. Since the bandwidth method is an averaging process and does not rely upon the absolute accuracy of the force and displacement measurements, it is regarded as the more reliable.

The response of the Viton rings do not conform to the behaviour of the other materials.

The response continues to increase down to 15 c/s, with no peak, and the force and displacement are found to have a phase difference of 90° at 250 c/s for the 60° shore. A static stiffness test was also carried out and the material was found to be quite anelastic. Between each loading the material was allowed to "recover" and the displacement reading was taken as soon as each load was applied. The stiffness of the 60° and 75° O-rings on this basis are estimated to be about 3 and 6 x 10^{3} lbf/in respectively. Using equation 5.1.2 the damping rate works out at about 11.5 lbfs/in for the 60° shore.

Fig. 5.1.3 shows the estimated stiffness and damping rates (from equation 5.1.1) plotted against frequency for the Nitrile and Silicon O-rings. These results show the characteristic increase in stiffness and decrease in damping as the frequency of loading is increased.

5.2 Balance of Rotor

During a preliminary run on the test rig a bearing seizure was experienced when attempting to run through the lowest synchronous whirl speed. This was at first attributed to excessive dynamic unbalance in the turbine buckets milled into the surface of the rotor. The rotor and bearing surfaces had to be re-ground and lapped, and measured as previously described in Section 4.2.1. The final mean radial clearances for the two bearings are estimated to be 0.00128(1) and 0.00132(0) in.

The rotor was then sent to an industrial firm for balancing. On a trial run in the rig afterwards the amplitude of vibration on approaching the synchronous whirl speed was found to be much larger than it had previously been .

The writer attributes this fault to a coupler which had to be locked onto the rotor to drive it during the balancing operation. Both shoulders of the rotor had to be machined back by $\frac{1}{4}$ in to remove the offending balance holes. A check was made on the rotor in the Genevoise Measuring Instrument and by rotating it slowly between centres against the feeler microscope, it was discovered that the axis of the main body of the rotor was 0.0006 in eccentric relative to the axis through the centre of the journals. This was rectified by re-grinding the surface of the main body.

A small E.M.I. balancing machine in the laboratory was then used to further improve the balance of the rotor. With this machine the rotor under test is cradled in floating ball bearings and driven at about 2500 r.p.m. by a light belt from an electric motor. Bearing movement is detected by transducers which produce an oscillating signal, the phase and amplitude of which are measures of angular position and amount of unbalance. The oscillations produced by the lateral bearing movements are amplified and used to flash a strobe lamp which "freezes" the rotor at the angular position of the unbalance. For this purpose a band of numbered sellotape is fixed circumferentially round the work piece. One of the cradles is locked and small pieces of plasticine are placed at the opposite end of the work piece, in the angular position indicated, until the meter reading is a minimum. The other cradle is then locked instead and the same procedure followed. By alternating between the two bearings the meter reading can be made substantially zero, indicating the optimum balance obtainable with the machine. The pieces of plasticine are carefully weighed and located and the appropriate balance holes drilled diametrically opposite. This procedure was followed and it was then found to be possible to run the rotor safely through the translational and conical synchronous whirls, with amplitudes of less than half the radial clearance.

5.3 Steady State Performance of Bearings

Tests were conducted in order to determine the hydrostatic stiffness of the gas film without rotation. A loading beam, with a central pivot, was supported horizontally with one end underneath the centre of the rotor. Weights could be suspended from the other end of the beam thus giving an upward thrust to the rotor. Initially, sufficient weight was added just to counter balance the weight of the rotor, so that with pressurized air supplied to the bearings the journals were assumed to be concentric with the bearings i.e. $\epsilon = 0$. The meter readings indicated by the two vertical displacement probes, one at each end of the rotor, were recorded. For a given supply pressure the upward thrust on the rotor was increased by steps of 2 lbf up to 10 lbf and the meter readings noted. The tests were carried out for various supply pressures over the range 30 to 80 psig.

The above displacement readings include the small deflections of the O-rings (90^{o} Nitrile), and hence indicates the in-series stiffness of the gas film and O-rings from the slopes of the load versus displacement plots.

With the air supply to the bearings cut off the stiffness of the O-rings was obtained separately, as previously described, thus enabling the film stiffness to be estimated from two sets of results.

The load versus displacement plots for the gas film at the various values of supply pressure are quite linear up to $\epsilon = 0.5$. Fig. 5.3.1 shows the variation of hydrostatic film stiffness with supply pressure for each bearing obtained from these plots.

5.4 Dynamic Performance of Bearings

A preliminary test was conducted to determine how constant the rotor speed could be maintained for a given setting of the precision pressure regulator on the air line to the turbine. The regulator was set and the rig allowed to run for several minutes to stabilize and the digital speed counter was then recorded over a period of 20 minutes. It was found that the speed "hunted" cyclically over periods of roughly 6 minutes, the range of speed variation being 46 r.p.m. at the nominal speed of 8350 r.p.m. Over the three cycles observed there was also a slight increase in the mean speed by 32 r.p.m.

With a given type of O-ring fitted the bearing supply pressure was turned on and off a number of times and the change in the vertical displacement of the rotor observed to ensure that the alignment of the two bushes was satisfactory. At various values of bearing supply pressure the rotor was run up through the first synchronous whirl speed (translational mode) and then allowed to run back freely through resonance and the speed of maximum amplitude determined. The same procedure was carried out for the second synchronous whirl speed (conical mode). The speeds of the latter are always found to be in the range 1.75 - 1.80 times the former, for a given pressure.

At the same values of supply pressure the rotor speed was increased very slowly above the conical whirl speed until a threshold of instability was encountered. A synchronous whirl component of amplitude $\epsilon = 0.15$ existed over this part of the speed range, tending to mask the lower frequency signal of the instability on the oscilloscope, which was intermittent at a very low level, sometimes over a range of several thousand r.p.m. before showing a positive growth.

On other tests, notably at the lower supply pressures and with those O-ring materials which gave least improvement in threshold speed, the growth of the instability was quite explosive in character and caused metal/metal contact, fortunately with only local damage to the bearing surfaces. The bearing surfaces had been rubbed with Molybdenum Disulphide powder to reduce friction. It is suggested that the variation in the growth rate of the instability is related to the direction in which the boundary is traversed i.e. an oblique approach is characterised by a slower rate of increase of amplitude. This makes an experimental definition of threshold speed somewhat difficult. It was decided, where possible, to adopt the speed at which the amplitude of the instability was half that of the synchronous component.

In a final series of tests both bushes were "fixed" to the pedestals with Araldite to enable a direct comparison of the effectiveness of the various O-ring materials to be made.

Fig. 5.4.1 shows the synchronous whirl and threshold speeds, in the translational mode, plotted against bearing supply pressure. The figures adjacent to each point denote the ratio of the threshold speed/synchronous speed, or whirl ratio, as used by Larson and Richardson(14). Those points marked with small vertical arrows indicate the bearing to be stable at the maximum speed of the test run and the corresponding figure denotes the maximum speed/ synchronous speed. Larson and Richardson performed a number of tests with various radial clearances and comparing their curve for C = 0.0014 in with the "fixed" whirl ratio values in Fig. 5.4.1 the present results generally agree well. The effect of the O-rings is clearly seen to bring about some substantial increases in threshold speed.

The effect of increasing supply pressure is to increase the whirl ratio, which is compatible with the theoretical predictions of Figs. 3.4.7 to 3.4.9. For the 60° Viton material in particular the bearing is stable over the entire speed range of the test rig, up to a whirl ratio of 5.2.

In general no attempt was made to measure the frequency of the instability on the oscilloscope, due to the risk of a rub. The frequency was well below half-speed and at the lower point on the 75° Silicon curve the frequency ratio was observed to be close to 0.25.

The maximum speed obtained on the test rig was 42,500 r.p.m., which was well below the estimated design speed of 100,000 r.p.m. The Petroff Equation has previously been found to give reliable estimates of bearing power loss, which implies a much lower turbine efficiency than that assumed in the design. The maximum speeds obtained also varied, due to either excessive water in the rig supply line or fluctuations in the compressor output pressure, as indicated by pressure variations on the gauge downstream of the pressure regulator.

CHAPTER 6

6.0 COMPARISON OF THEORY AND EXPERIMENT

6.1 Test Rig Parameters

In order to compute the steady state performance of the test bearings it is required to estimate the feeding parameter (Λ_t), dimensionless load ($\overline{W}$) and line feed correction factor (λ). From the data of Table I, the "curtain area" $\pi.2a.h \ll \pi a^2$, the orifice area, so that the flow to the bearing film is controlled by the former area and the restrictor is of the inherently compensated type. The feeding parameter becomes:

$$\Lambda_t = 6\mu \frac{Nd\sqrt{GRT}}{p_a C^2} = 0.82$$

based on the average radial clearance of 0.0013 in.

$$\overline{W} = \frac{W}{p_a LD} = 0.195$$

$$\lambda = 1.46$$

The additional dimensionless parameters of rotor mass (Ω) and bearing /rotor mass ($\overline{m}$) are required in the stability analysis. Estimated from the data in Table I these are:

$$\Omega = \frac{m_r p_a}{\mu^2 L(\frac{R}{C})^5} = 1920$$

$$\overline{m} = \frac{m_b}{m_r} = 0.385$$

It has been established in the results of the analytical section, and generally supported by experimental observation, that the effect of increasing support damping is to increase threshold speed and at the same time reduce the frequency ratio (γ) at threshold, for example see Figs. 3.4.8 and 3.4.13.

For low damping the threshold frequency ratio is usually in the range 0.45 - 0.50, and the whirl ratio in the range 2.0 - 2.5. As an approximation therefore the frequency of the unstable motions of the system near threshold can be taken as similar to the synchronous whirl speed and to be independant of the actual threshold speed. This enables the support paramters $\overline{K}_p$ and $\overline{C}_p$ to be estimated relatively easily from the frequency dependant properties of the O-rings.

From the experimental results of Fig. 5.4.1, the synchronous whirl speeds were estimated for each O-ring material at a representative bearing supply pressure of 65 lbf/in^2. The frequencies obtained were then used to read off the dynamic stiffness and damping rates of the different O-rings from the curves in Fig. 5.1.3, as tabulated below.

O-ring Material	Synchronous Frequency $c/_s$	Stiffness lbf/in	Damping lbfs/in	$\overline{K}_p$	$\overline{C}_p$
75° Silicon	128	5,400	0.83	0.95	11.1
60° Nitrile	158	17,300	5.40	3.06	72.4
75° "	155	15,800	6.20	2.80	83.3
90° "	167	29,000	6.40	5.13	86.0

6.2 Gas Film Stiffness

The hydrostatic stiffness was obtained theoretically for various values of supply pressure, with discharge coefficients (C_D) of 1.0 , 0.8 and 0.6, and the results for $\epsilon \rightarrow 0$ are compared with the experimental values in Fig. 6.2.1. The theoretical curve for C_D = 0.6 agrees sufficiently well with the experimental curves to justify the use of this value of discharge coefficient in the subsequent estimates of threshold speed.

6.3 Threshold Speeds

The procedure for determining the theoretical values of threshold speed was similar to that outlined in section 3.3.

A comparison of the theoretical and experimental curves of threshold speed against bearing supply pressure is made in Fig. 6.3.1. The experimental results are seen to confirm the theoretical predictions of threshold speed, generally to within 10 percent which is regarded as satisfactory for design purposes. With the exception of the curves for the "rigid" bearing, the theory tends to overestimate the threshold speed. For the "rigid" bearing the two experimental points at $p_s = 30$ and 45 lbf/in^2 in Fig. 5.4.1 probably indicate some erratic behaviour in the Araldite "fixing", since the theoretical results do not show a corresponding trend. It is possible that the Araldite could possess sufficient damping/stiffness to account for the relative increase in the experimental threshold speeds in this case.

The theoretical curves for the 75° Silicon and 75° Nitrile rubbers are less steep than their experimental counterparts, which may be due to the use of fixed "mean" values for $\overline{K}_p$ and $\overline{C}_p$ in the computed results. Allowance for the variations in the values of $\overline{K}_p$ and $\overline{C}_p$, on the basis of the earlier discussion, would tend to increase the slope of the theoretical curves, particularly over a part of the stability boundary such as this, which is relatively sensitive to changes in damping/stiffness.

At $p_s = 45$ lbf/in^2 the predicted threshold frequency ratio of 0.21 for the 75° Silicon O-rings compares with the observed value of 0.25.

The dynamic stiffness of the 60° Viton O-rings at frequencies in the range 150 - 200 C/S is clearly comparable with that of the 75° Nitrile O-rings, as can be seen from the experimental plots of the synchronous whirl speeds in Fig. 5.4.1. From the O-ring tests the damping rate was estimated to be 11.6 lbfs/in at 250 C/S . With these support conditions ($\bar{K}_p$ = 2.80 and $\bar{C}_p$ = 156) the computed threshold speeds at p_s = 45 and 55 lbf/in^2, are 40,000 and 50,000 r.p.m. respectively, which are in reasonable agreement with the experimental evidence.

6.4 The Possible Extension of Flexibly Mounted Systems

The success of using a flexible damped bearing support to postpone, or inhibit, the onset of self-excited whirl has been demonstrated theoretically and confirmed experimentally. This can be achieved with values of support stiffness which are substantially higher than the gas film stiffness, thus overcoming a possible design objection to ~~their use~~ flexibly mounted systems.

Gas bearings are also prone to another form of instability known as pneumatic hammer. The instability usually occurs in both hydrostatic journal and thrust bearings which have a pocket after the orifice restrictor. It is suggested that an investigation could be undertaken to study the behaviour of such a system with external damping and stiffness.

CHAPTER 7

7.0 CONCLUSIONS

Employing Lund's "linearised ph" solution to the time dependant Reynolds Equation, in order to evaluate the gas film dynamic coefficients, an analysis has been developed which can predict the threshold speed of self-excited whirl of a rigid rotor in an externally pressurised journal bearing having a flexible damped support. The principal results of the analysis show that:

(1) There are two threshold speeds in translational whirl, which are related to the corresponding rigid body synchronous whirl speeds of the system.

(2) On a plot of threshold speed against support stiffness, with zero support damping, the threshold speeds occur at approximately twice the synchronous whirl speeds. Both threshold speeds then increase with increase in support damping.

(3) If the support contains sufficient damping/stiffness then the stability boundaries can be folded back in such a way as to achieve a system which is stable at all speeds.

(4) The effect of an increase in bearing supply pressure is to increase both threshold speeds. The threshold speed associated with bearing whirl (in this case the upper one)is increased if the mass of the bearing is reduced.

An experimental gas journal bearing test rig has been designed and operated in which a flexible support is provided by rubber O-rings. Variations in support damping/stiffness are obtained by using different O-ring materials. Separate tests were conducted on the O-rings to determine their dynamic properties.

Owing to the large number of design variables the experimental programme was restricted to the study of threshold speed at values of bearing supply pressure for the different O-rings. The results of the experiments show that substantial increases in threshold speed can be achieved with certain O-ring materials. For one material in particular, called Viton, the bearing is stable up to the maximum speed of the test rig (42,500 r.p.m.) at the lowest supply pressure (45 lbf/in^2), which is 5.2 times the corresponding synchronous whirl speed.

A comparison of the theoretical and experimental results shows that the threshold speed is predicted to within 10 percent, which is considered to be satisfactory for design purposes.

NOMENCLATURE

a = orifice radius

C = radial clearance

C_D = restrictor discharge coefficient

C_p = support damping coefficient

$\bar{C}_p$ = $\dfrac{C_p}{\mu L(\frac{R}{C})^3}$, dimensionless support damping coefficient

C_{xx}, C_{xy}, C_{yx}, C_{yy} = damping coefficients of the gas film (1st index force direction; 2nd index displacement direction)

$\omega\bar{C}_{xx}$, etc. = $\dfrac{C\omega C_{xx}}{p_a LD}$ dimensionless damping coefficients of gas film

D = bearing diameter

d = feed hole diameter

F_r, F_t = radial and tangential bearing force components

f_r, f_t = $\dfrac{F}{p_a LD}$, dimensionless bearing force components

f_{ro}, f_{to} = steady state components of f_r and f_t

f_{rt}, f_{tt} = time dependant components of f_r and f_t

h = $C(1+\epsilon\cos\theta)$, film thickness

$\bar{h}$ = $\dfrac{h}{C}$, dimensionless film thickness

i = $\sqrt{-1}$, denotes a spatial rotation through 90°

j = $\sqrt{-1}$, denotes a phase change through 90°

k = adiabatic gas exponent

K_p = support stiffness coefficient

$\bar{K}_p$ = $\dfrac{CK_p}{p_a LD}$ dimensionless support stiffness

K_{xx}, K_{xy}, K_{yx}, K_{yy} = stiffness coefficients of gas film (1st index force direction, 2nd index displacement direction)

K_{xx}, etc. = $\dfrac{CK_{xx}}{p_a LD}$, dimensionless stiffness coefficients of gas film

X $\bar{K}_{xx}$?

L = bearing length

M_T = total steady state mass flow

m = dimensionless orifice flow

$= C_D\sqrt{\frac{2k}{k+1}} \cdot \left(\frac{2}{k+1}\right)^{\frac{1}{k-1}}$ for super-critical flow

$= C_D\sqrt{\frac{2k}{k-1}} \cdot \left(\frac{p_c}{p_s}\right)^{\frac{1}{k}} \cdot \sqrt{1 - \left(\frac{p_c}{p_s}\right)^{\frac{k-1}{k}}}$ for sub-critical flow

m_o = dimensionless orifice flow, concentric journal

m_b = bearing mass

m_r = rotor mass

$\bar{m}$ = $\frac{m_b}{m_r}$

N = number of feed holes

P = gas film pressure

$\bar{p}$ = $\frac{p}{p_a}$, dimensionless gas film pressure

p_a = ambient pressure

$\bar{p}_c$ = dimensionless film pressure downstream of orifice

$\bar{p}_o$ = dimensionless film pressure for concentric journal

p_s = bearing supply pressure

$\bar{p}_s$ = $\frac{p_s}{p_a}$, dimensionless bearing supply pressure

q = $\Lambda_t p_s m_o$

R = bearing radius

$\mathcal{R}.T$ = gas constant x absolute temperature

t = time

W = bearing load

$\bar{W}$ = $\frac{W}{p_a LD}$, dimensionless bearing load

X, Y = co-ordinate system parallel and perpendicular to steady state line of centres

X_1, Y_1 = bearing centre amplitudes

X_2, Y_2 = journal centre of amplitudes

$\overline{X}_1$, etc = $\frac{X_1}{C}$ dimensionless amplitude

x_1, y_1 = bearing displacements

x_2, y_2 = journal displacements

γ = ν/ω, frequency ratio

ϵ = eccentricity ratio

ϵ_o = steady state eccentricity ratio

$\epsilon_1, \epsilon_o\phi_1$ = dynamic journal centre amplitudes

ξ = axial distance divided by bearing radius

η = $\sqrt{1-\epsilon_o^2}$

θ = angular co-ordinate relative to instantaneous line of centres

Λ = $\frac{6\mu\omega}{p_a}(\frac{R}{C})^2$, compressability number, dimensionless

Λ_t = $\frac{6\mu N a^2\sqrt{RT}}{p_a C^3}$, feeding parameter, dimensionless

λ = line feed correction factor

μ = gas viscosity

ν = frequency

ξ = L/D

ρ = density of gas

τ = jvt, dimensionless time

ϕ = attitude angle, relative to fixed load line

ϕ_o = steady state attitude angle

ψ' = orifice flow factor

Ω = $\frac{m_r p_a}{\mu^2 L(\frac{R}{C})^5}$, dimensionless rotor mass

ω = angular velocity

BIBLIOGRAPHY

1. AUSMAN, J.S. "An Improved Analytical Solution for Self-Acting, Gas-Lubricated Journal Bearings of Finite Length". Journal of Basic Engineering, Trans ASME, Vol.83, 1961.

2. PAN, C.H.T. and STERNLICHT, B. "On the Translatory Whirl Motion of a Vertical Rotor in Plain Cylindrical Gas-Dynamic Journal Bearings" Journal of Basic Engineering, Trans ASME, Vol.84, 1962.

3. AUSMAN, J.S. "Linearized ph Stability Theory for Translatory Half-Speed Whirl for Long, Self-Acting Gas-Lubricated Journal Bearings". Journal of Basic Engineering, Trans ASME, Vol.85, 1963.

4. NG. C.W. "Linearized ph Stability Theory for Finite Length, Self-Acting, Gas-Lubricated Plain Journal Bearings". Journal of Basic Engineering, Trans ASME, Vol.87, 1965.

5. CHENG, H.S. and PAN, C.H.T. "Stability Analysis of Gas-Lubricated, Self-Acting, Plain, Cylindrical, Journal Bearings of Finite Length, Using Galerkin's Method". Journal of Basic Engineering, Trans ASME, Vol.87, 1965.

6. CASTELLI, V. and ELROD, H.G. "Solution of the Stability Problem for 360° Self-Acting, Gas-Lubricated Bearings". Journal of Basic Engineering, Trans ASME, Vol.87, 1965.

7. MARSH, H. "The Stability of Aerodynamic Gas Bearings". Mechanical Engineering Science Monograph No. 2, Inst. of Mech. Engs., London, 1965.

8. ELROD, H.G., McCABE, J.T. and CHU, T.Y. "Determination of Gas Bearing Stability by Response to Step-Jump". Journal of Lubrication Technology, Trans ASME, Vol.89, 1967.

9. WHITLEY, S., BOWHILL, A.J. and McEWAN, P. "Half-Speed Whirl and Load Capacity of Hydrodynamic Gas Journal Bearings". Proc. Inst. Mech. Engrs., London, Vol.176 1962.

10. REYNOLDS, D.B. and GROSS, W.A. "Experimental Investigation of Whirl in Self-Acting Air-Lubricated Journal Bearings". ASLE Trans, Vol.5, No. 2, 1962.

11. STERNLICHT, B. and WINN, L.W. "On the Load Capacity and Stability of Rotors in Self-Acting Gas Lubricated Plain Cylindrical Journal Bearings". Journal of Basic Engineering, Trans ASME, Vol.85, 1963.

12. STERNLICHT, B. and WINN, L.W. "Geometry Effects on the Threshold of Half-Frequency Whirl in Self-Acting, Gas-Lubricated Journal Bearings". Journal of Basic Engineering, Trans ASME, Vol.86, 1964.

13. PAN, C.H.T. and STERNLICHT, B. "Comparison Between Theories and Experiments for the Threshold of Instability of Rigid Rotor in Self-Acting, Plain-Cylindrical Journal Bearings". Journal of Basic Eng. Trans ASME, Vol.86, 1964.

14. LARSON, R.H. and RICHARDSON, H.H. "A preliminary Study of Whirl Instability for Pressurized Gas Bearings". Journal of Basic Engineering, Trans ASME, Vol.84, 1962.

15. GROSS, W.A. "Investigation of Whirl in Externally Pressurized Air-Lubricated Journal Bearings". Journal of Basic Engineering, Trans ASME, Vol.84, 1962.

16. TANIGUCHI, O. et al "Experimental Study of Whirl Instability for Externally Pressurized Air Journal Bearings". Bulletin of JSME, Vol.11, No. 43, 1968.

17. LUND, J.W. "A Theoretical Analysis of Whirl Instability and Pneumatic Hammer for a Rigid Rotor in Pressurized Gas Journal Bearings". Journal of Lubrication Technology, Trans ASME, Vol.89, 1967.

18. LUND, J.W. "The Stability of an Elastic Rotor in Journal Bearings with Flexible, Damped Supports". Journal of Applied Mechanics, Trans ASME, Vol.87, 1965.

19. MARSH, H. "The Stability of Self-Acting Gas Journal Bearings with Noncircular Members and Additional Elements of Flexibility". ASME PAPER No 68-LUBS-45

20. BOFFEY, D.A. See Appendix II

21. POWELL, J.W. and TEMPEST, M.C. "A Study of High Speed Machines with Rubber-Stabilized Air Bearings". Journal of Lubrication Technology, Trans ASME, Vol.90, 1968.

22. KERR, J. "The Onset and Cessation of Half-Speed Whirl in Air-Lubricated Self-Pressurized Journal Bearings". Proc. Inst. Mech. Engrs., Vol.180, 1966.

23. LUND, J.W. "Rotor Bearing Dynamics Design Technology, Part III The Three Lobe Bearing and Floating Ring Bearing". MTI Report 67 TR 47 (Feb. 1968).

24. TONDL, A. "The Effects of an Elastically-Suspended Foundation Mass and its Damping on the Initiation of Self-Excited Vibrations of a Rotor Mounted in Air Bearings". Proc. of 5th Biennial Gas Bearing Symposium. Univ. of Southampton, 1971, Vol.1 Paper No. 1.

25. MORI, H. "A Stabilizing Method of the Externally Pressurized Gas Journal Bearing". Proc. of 5th Biennial Gas Bearing Symposium. Univ. of Southampton, 1971, Vol.1, paper No. 4.

26. ELROD, H.G. and GLANFIELD "Computer Procedures for the Design of Flexibly Mounted, Externally Pressurized, Gas Lubricated Journal Bearings". Report for Dept. of Mech. Eng., Univ. of Southampton (Sept. 1970).

27. DIPRIMA "Design of Gas Bearings". MTI Manual Vol.1, 1969, Section 3.

28. CASTELLI, V. and PIRVICS, J. "Review of Numerical Methods in gas Bearing Film Analysis". Journal of Lubrication Technology, Trans ASME, Vol.90, 1968.

29. SHAPIRO, W. "Steady State and Dynamic Analyses of Gas Lubricated Hybrid Journal Bearings". Journal of Lubrication Technology, Trans ASME, Vol.91, 1969.

30. "Design of Gas Bearings" MTI Manual Vol. 1., 1969, Section 6.1.

31. WHITLEY, S. and BETTS, C. "Study of Gas lubricated, Hydrodynamic, Full Journal Bearings" Brit.J.Appl.Phys. 10, No. 10 (1959).

32. COOPER, D.H. "Method of Applying the Results of Dynamic Testing to Rubber Anti-Vibration Systems" Trans. Inst. of the Rubber Industry Vol. 35, No. 5.

33. "Design of Gas Bearings" MTI Manual Vol. 1., 1969.

34. BISHOP, R.E.D. and JOHNSON, D.C. "The Mechanics of Vibration" Cambridge University Press, 1960.

TABLE 1

Details of Test Rotor and Bearings

Bearing details:

diameter	1.0 in.
length	1.0 in.
radial clearance - thrust end (1)	0.00128 in.
free end (o)	0.00132 in.
type of feed -	inherent compensation 8 equi-spaced holes in central plane.
feed hole diameter	0.0135 in.
distance between bearing centres	8.0 in.
mass	1.1 lb.
material	free cutting stainless steel

Rotor details:

overall length	10.0 in.
maximum diameter	2.0 in.
mass	5.7 lb
transverse moment of inertia	27.8 lb in^2
drive turbine	2 rows of 12 buckets, cut to a depth of 0.01 in.
material	free cutting stainless steel.

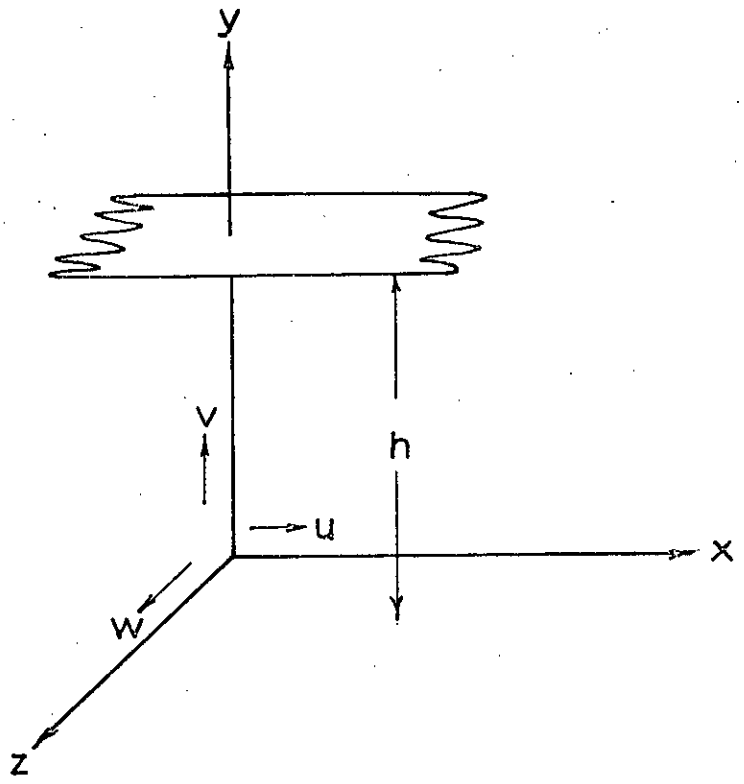

FIG 2.1.1. SYSTEM OF CARTESIAN CO ORDINATES

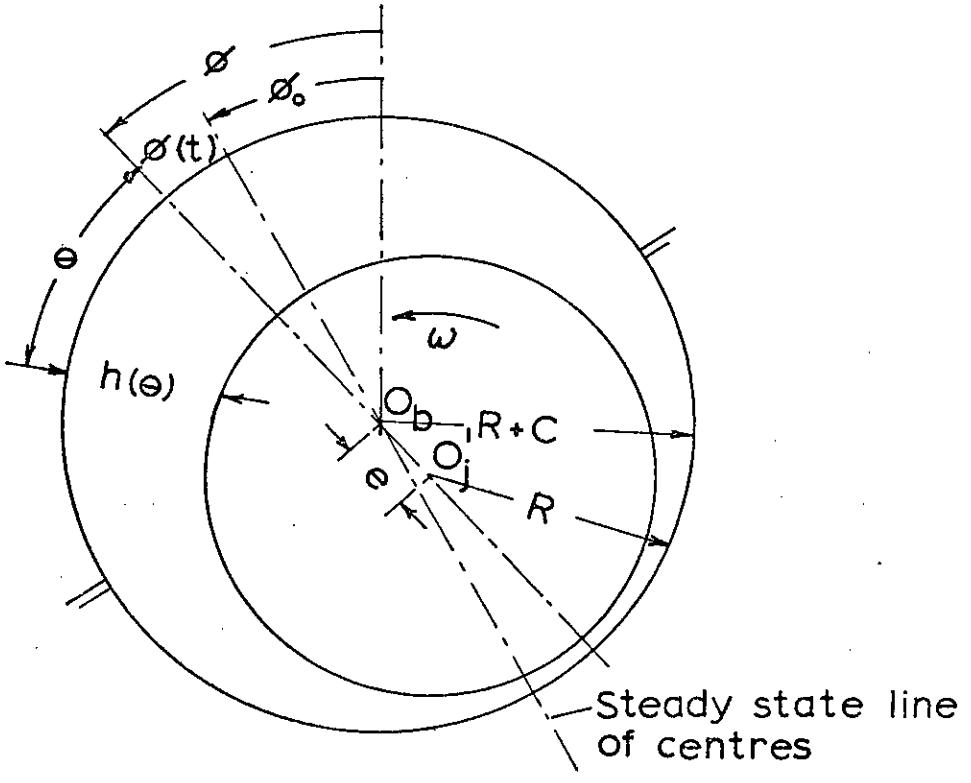

FIG 2.1.2 SYSTEM OF CO ORDINATES FOR A CYLINDRICAL JOURNAL BEARING

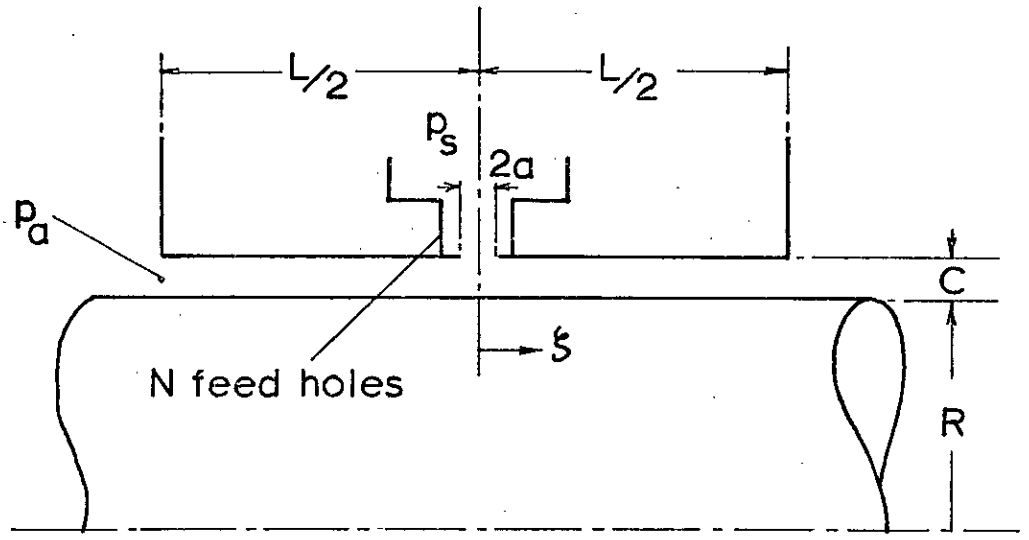

FIG. 2.3.1. BEARING GEOMETRY

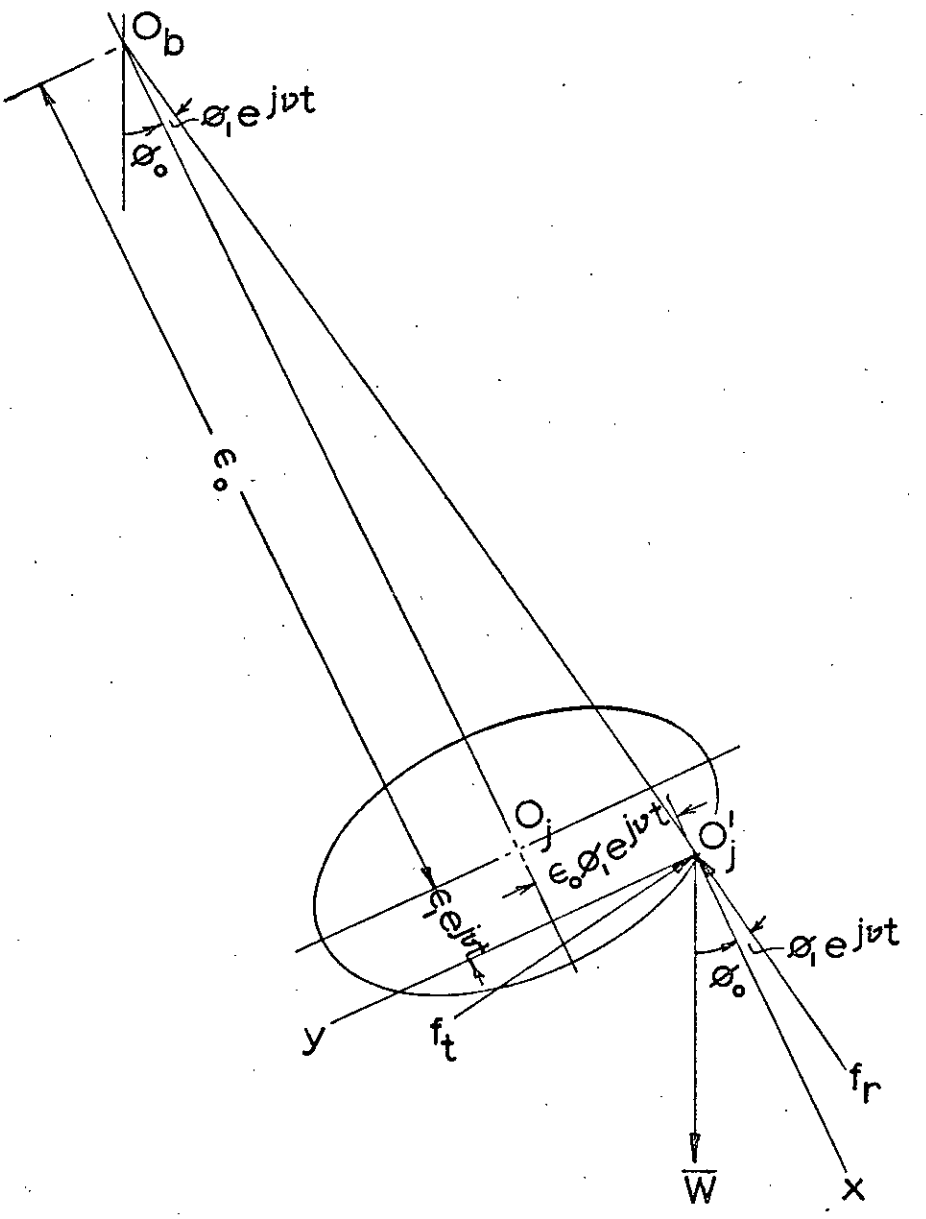

FIG 2.3.2 SYSTEM OF CO ORDINATES FOR PERTURBED JOURNAL CENTRE. FIXED BEARING.

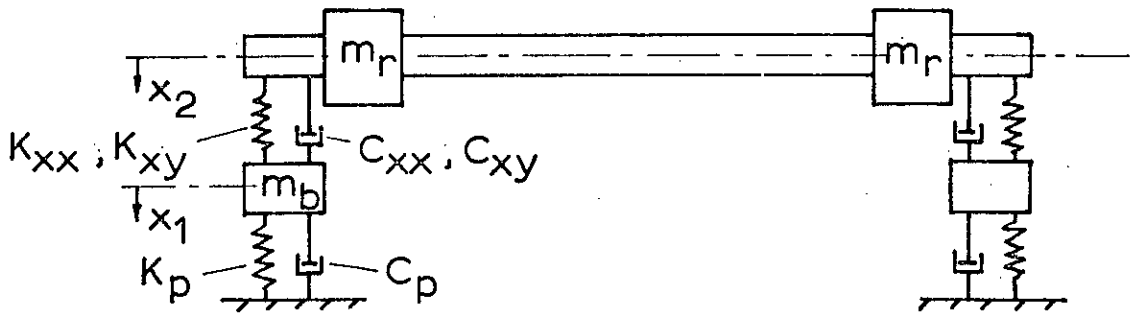

FIG 3.1.1(a) ROTOR-BEARING SYSTEM MODEL

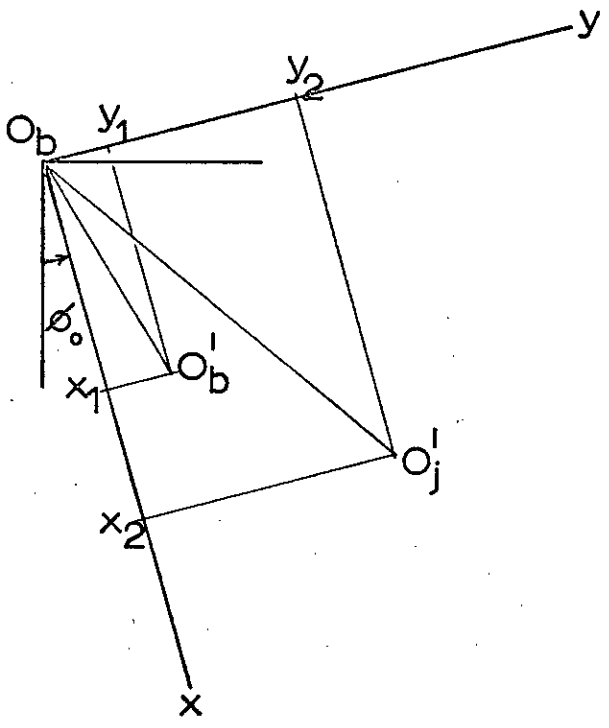

FIG 3.1.1(b) FIXED REFERENCE AXES

```
PRESSURE=   5.0
L/D=   1.0
FEED PARAM=   1.0
LOAD PARAM= 0.20
MASS RATIO= 0.10
MASS PARAM= 524.0000

STIFFNESS    DAMPING
 10.000       10.000
COMP NO   ECC RATIO          GAMMA     ERROR
  0.60       0.136           0.692   -6.5947@ -1

  0.65       0.136           0.638   -5.8463@ -1

  0.70       0.136           0.593   -5.1388@ -1

  0.75       0.136           0.553   -4.2857@ -1

  0.80       0.135           0.518   -3.3576@ -1

  0.85       0.135           0.488   -2.5177@ -1

  0.90       0.135           0.461   -1.5737@ -1

  0.95       0.135           0.436   -3.8804@ -2
                                                  <-- THRESHOLD
  1.00       0.135           0.414    7.5264@ -2

STIFFNESS    DAMPING
  4.000      10.000
COMP NO   ECC RATIO          GAMMA     ERROR
  0.90       0.135           0.422   -6.8901@ -2

  0.95       0.135           0.400   -5.7492@ -2

  1.00       0.135           0.380   -4.5514@ -2

  1.10       0.134           0.345   -1.8937@ -2
                                                  <-- THRESHOLD
  1.20       0.134           0.317    7.1954@ -3
```

FIG.3.3.1. SAMPLE OF COMPUTER PRINTOUT IN STABILITY ANALYSIS.

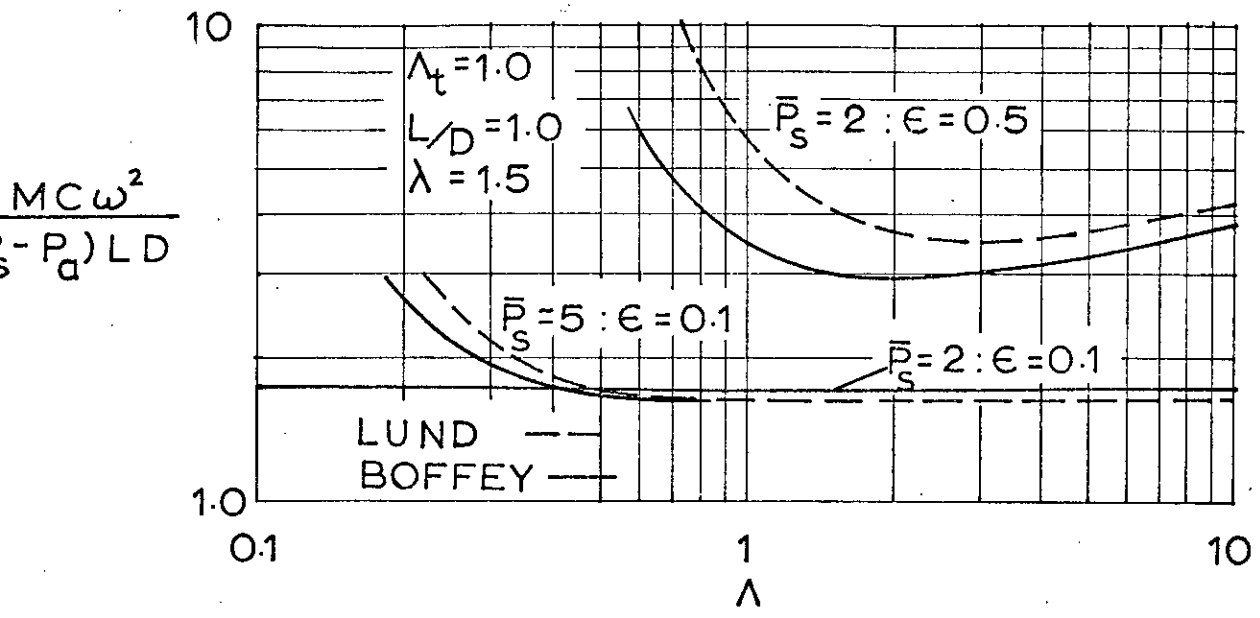

FIG 3.3.3. STABILITY PARAMETER v COMPRESSABILITY NUMBER. COMPARISON WITH LUND(17).

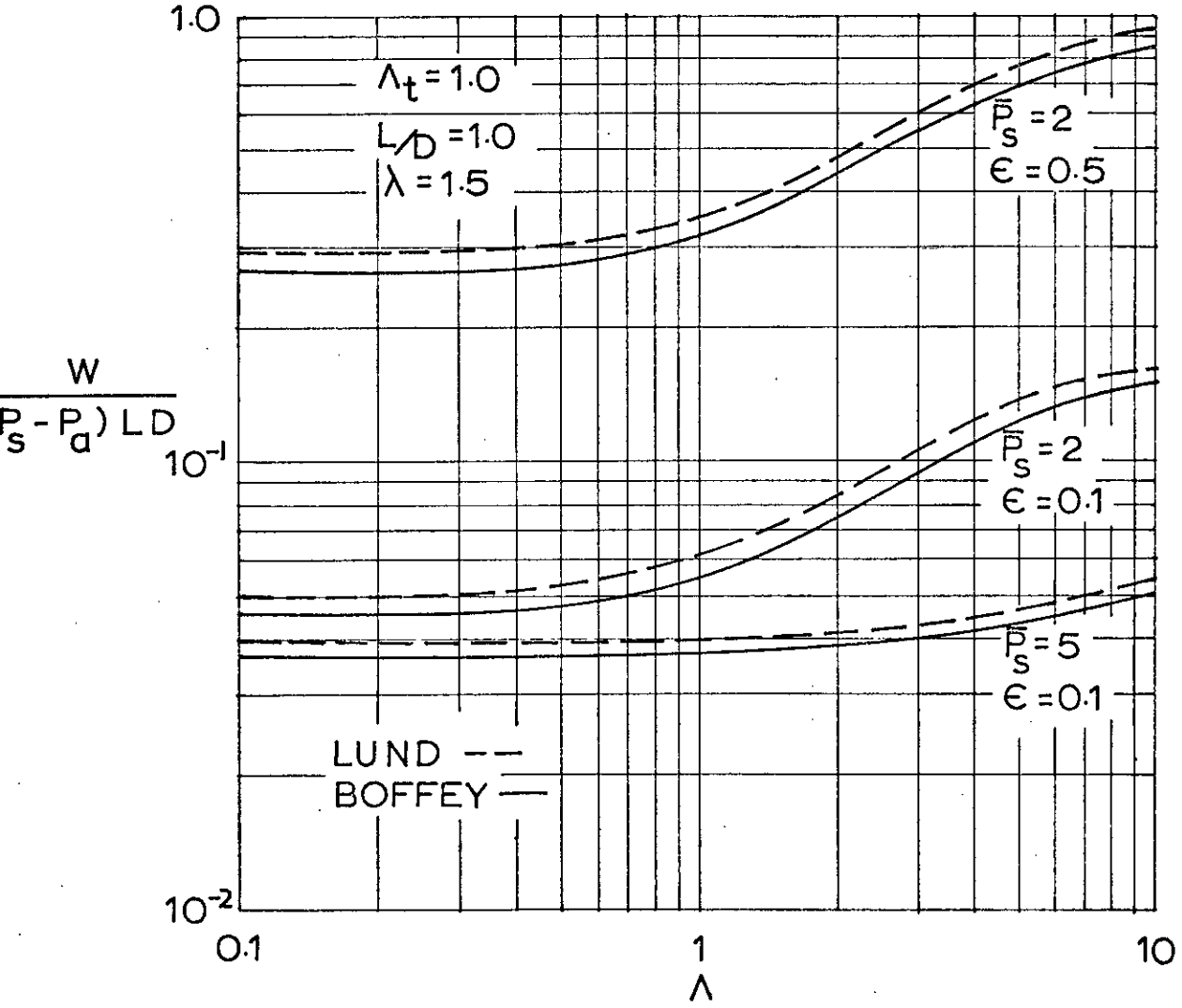

FIG 3.3.2. DIMENSIONLESS LOAD v COMPRESSABILITY NUMBER. COMPARISON WITH LUND(17).

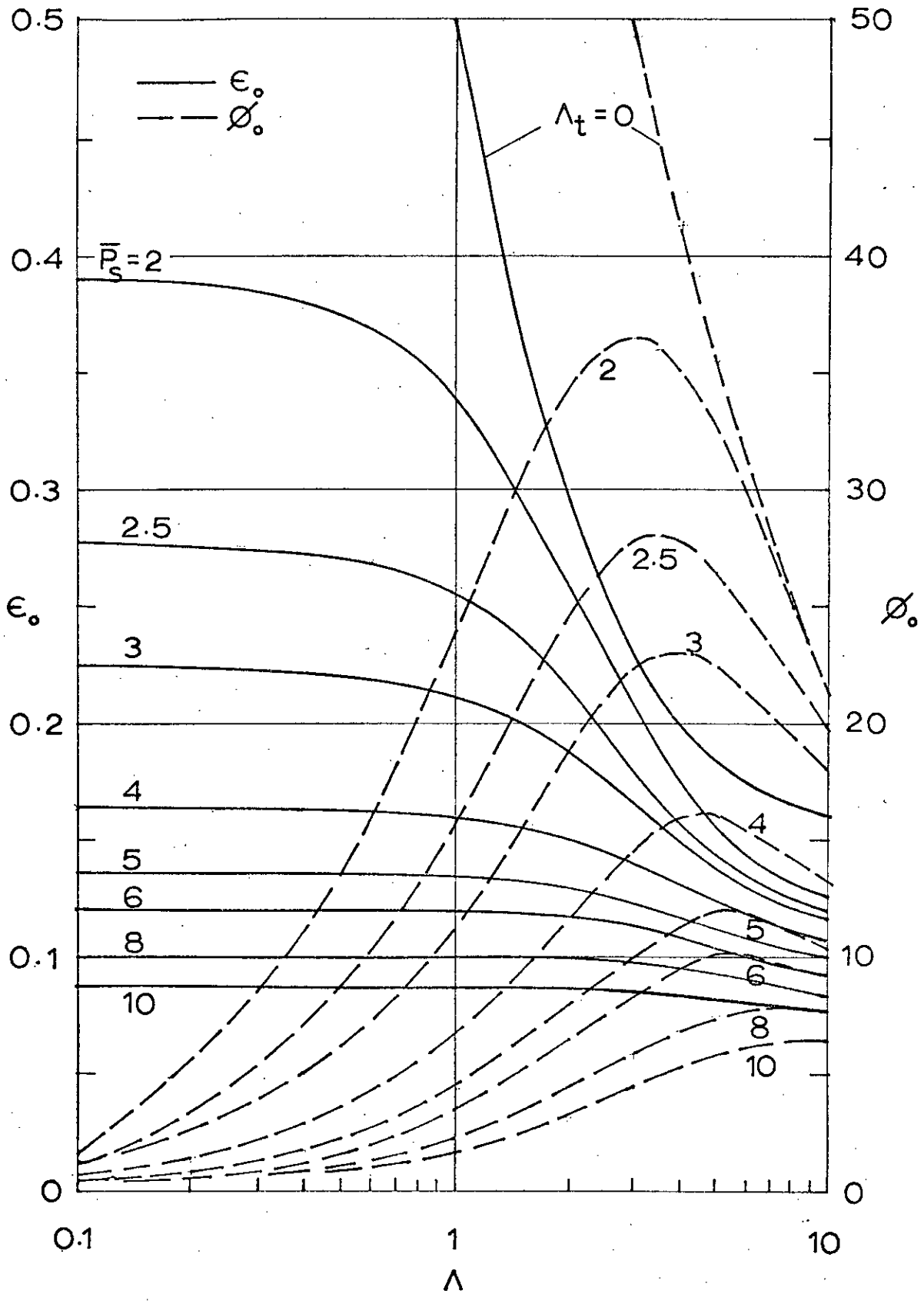

FIG 3.4.1 STEADY STATE ECCENTRICITY RATIO & ATTITUDE ANGLE v COMPRESSIBILITY NUMBER.

$L/D = 1 : \Lambda_t = 1 : \bar{W} = 0.2$.

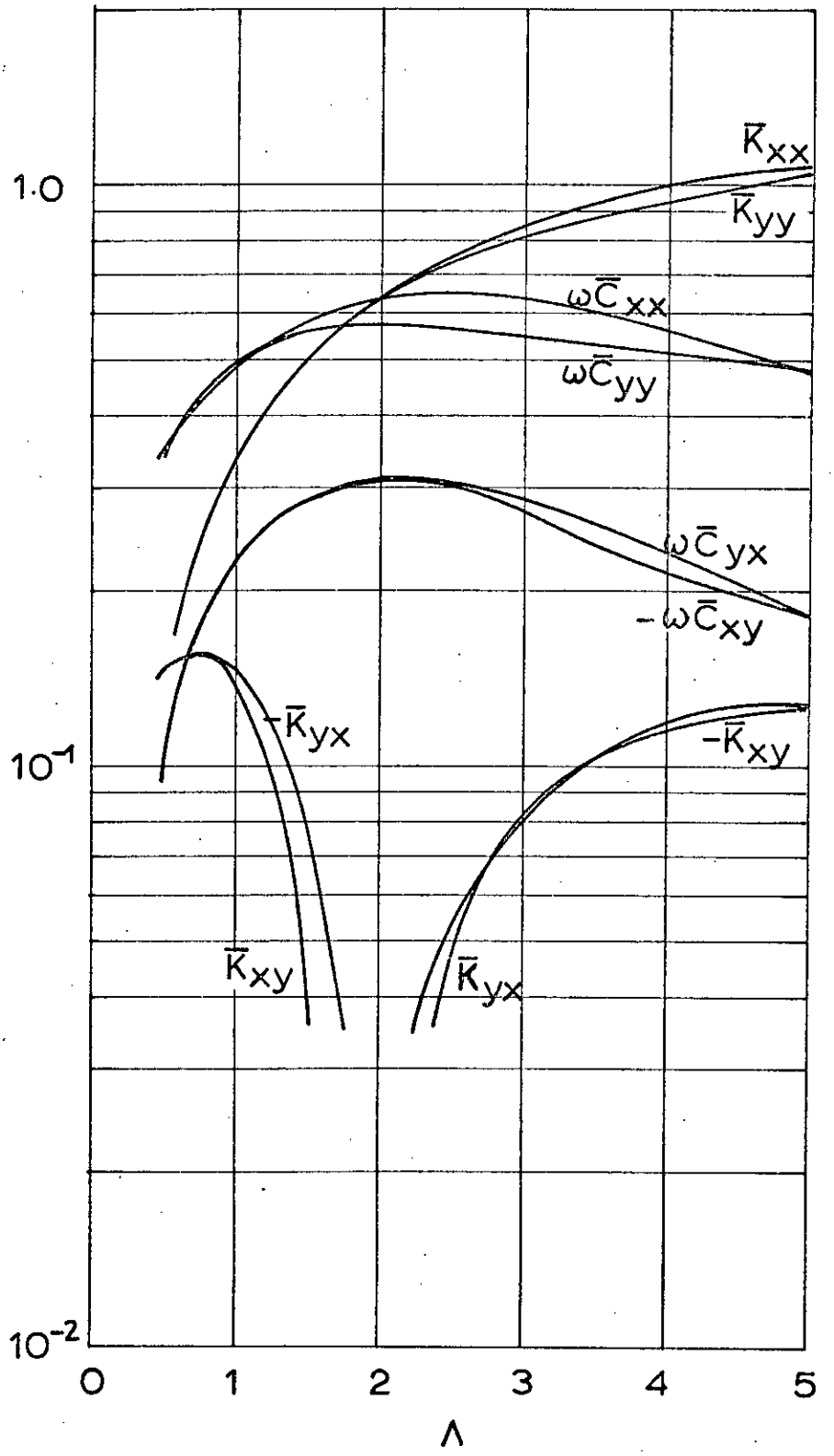

FIG 3.4.2. GAS FILM DYNAMIC COEFFICIENTS

$L/D = 1 : \epsilon = 0.1 : \bar{r} = 1.0.$

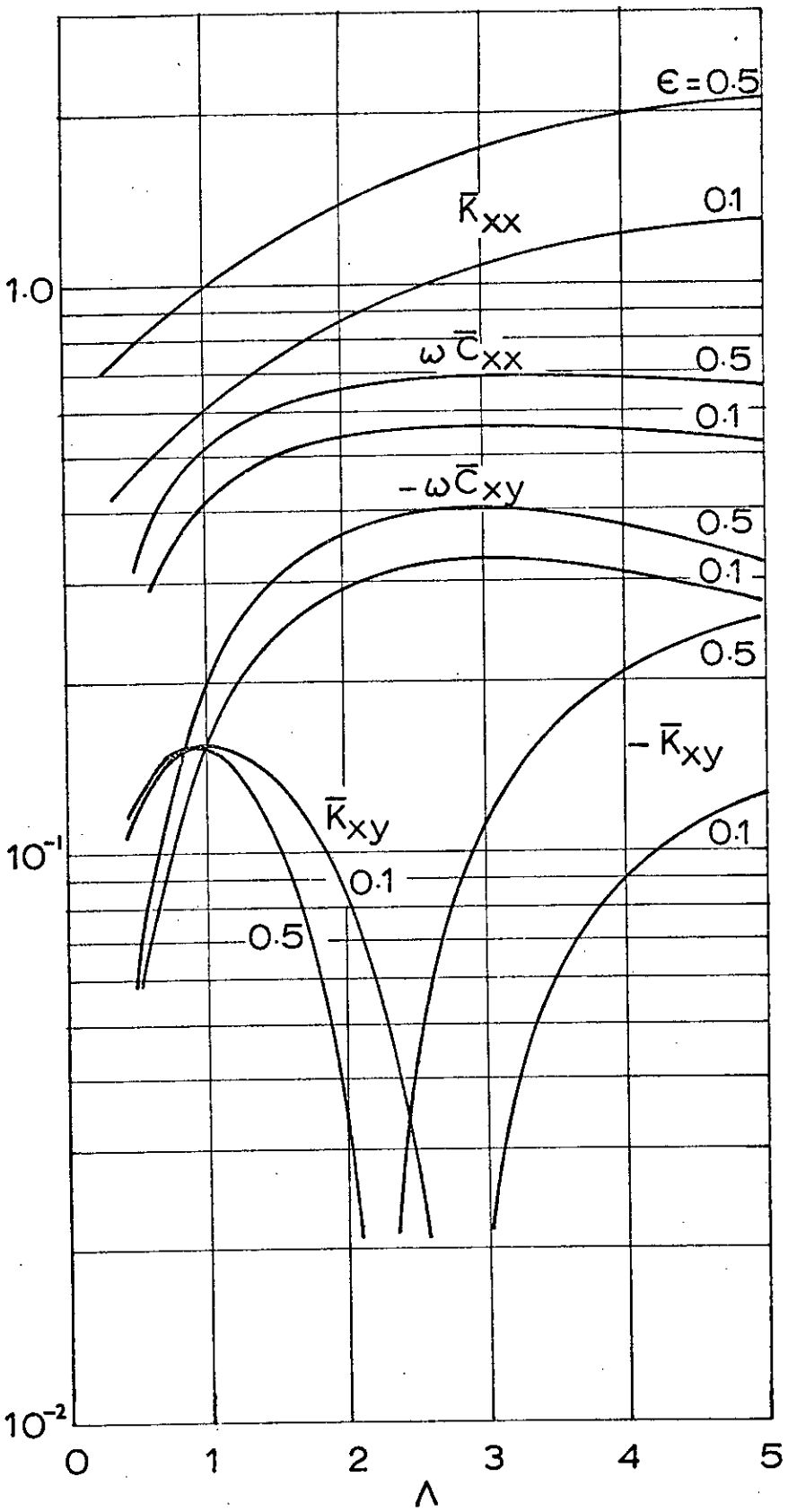

FIG 3.4.3. GAS FILM DYNAMIC COEFFICIENTS

$\bar{P}_s = 2 : L/D = 1 : \Lambda_t = 1 : \gamma = 1.0.$

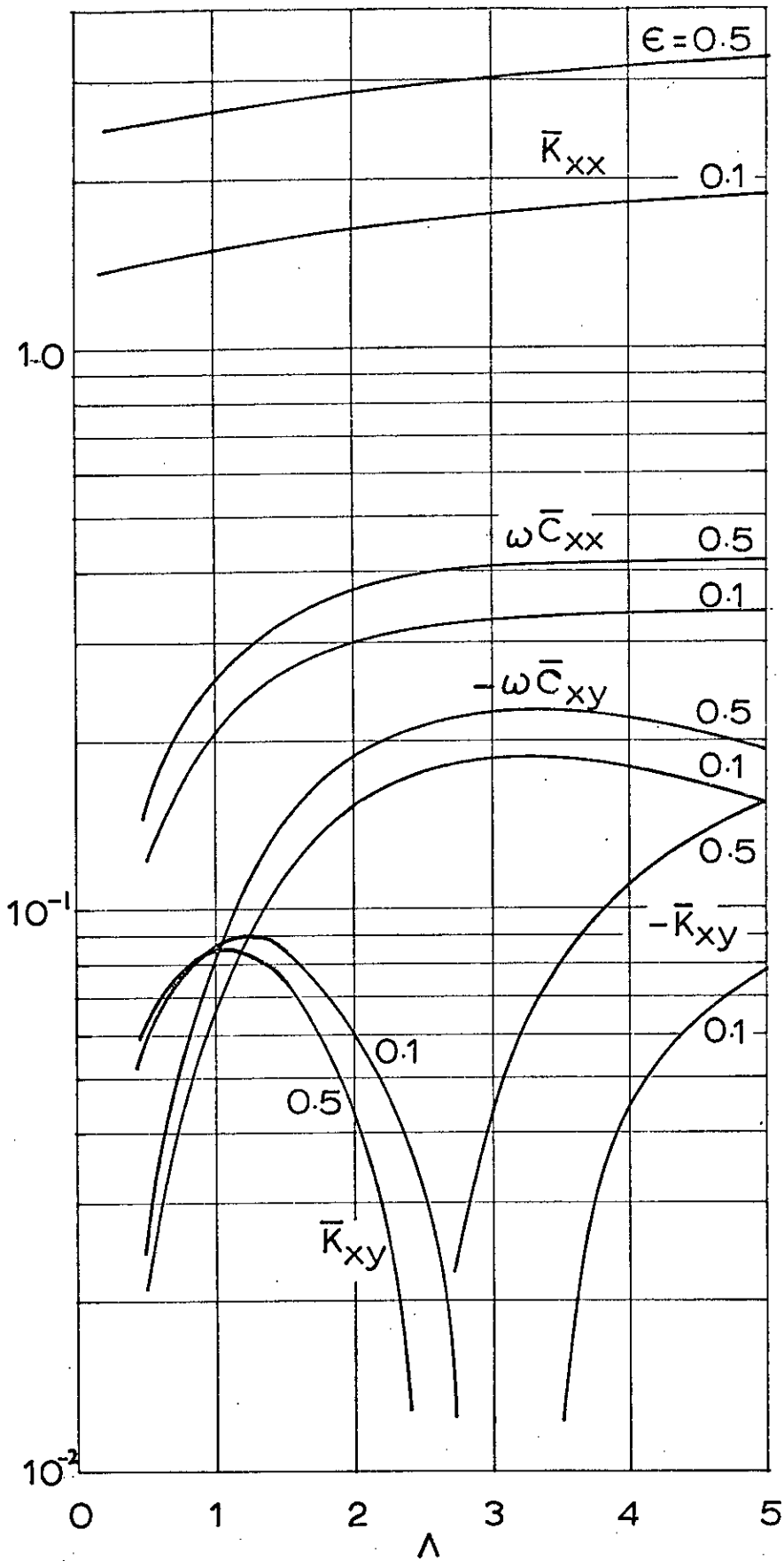

FIG. 3.4.4. GAS FILM DYNAMIC COEFFICIENTS

$\bar{P}_s = 5 : L/D = 1 : \Lambda_t = 1 : \gamma = 1.0$.

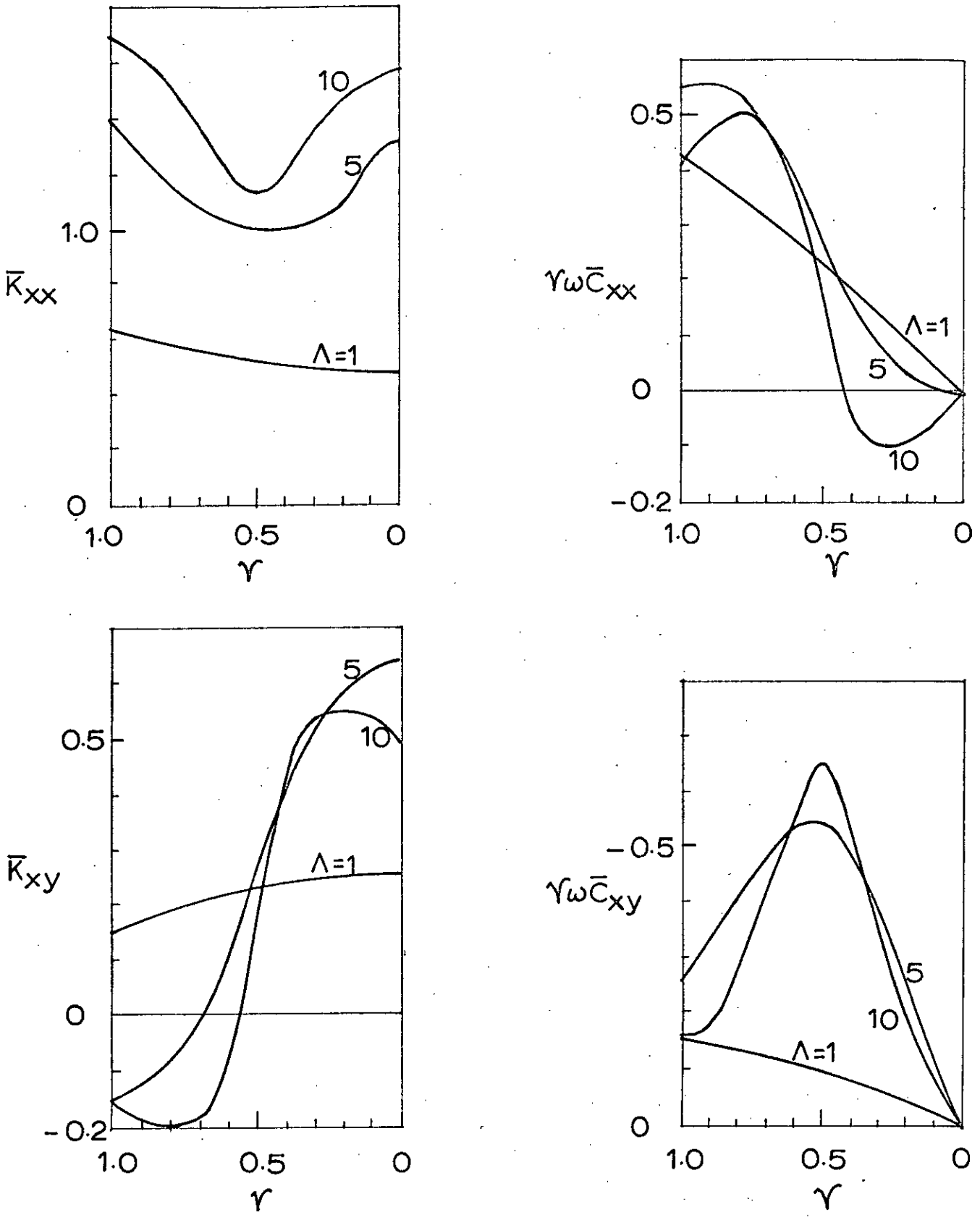

FIG 3.4.5 GAS FILM DYNAMIC COEFFICIENTS

$\bar{P}_s = 2 : L/D = 1 : \Lambda_t = 1 : \epsilon = 0.2$.

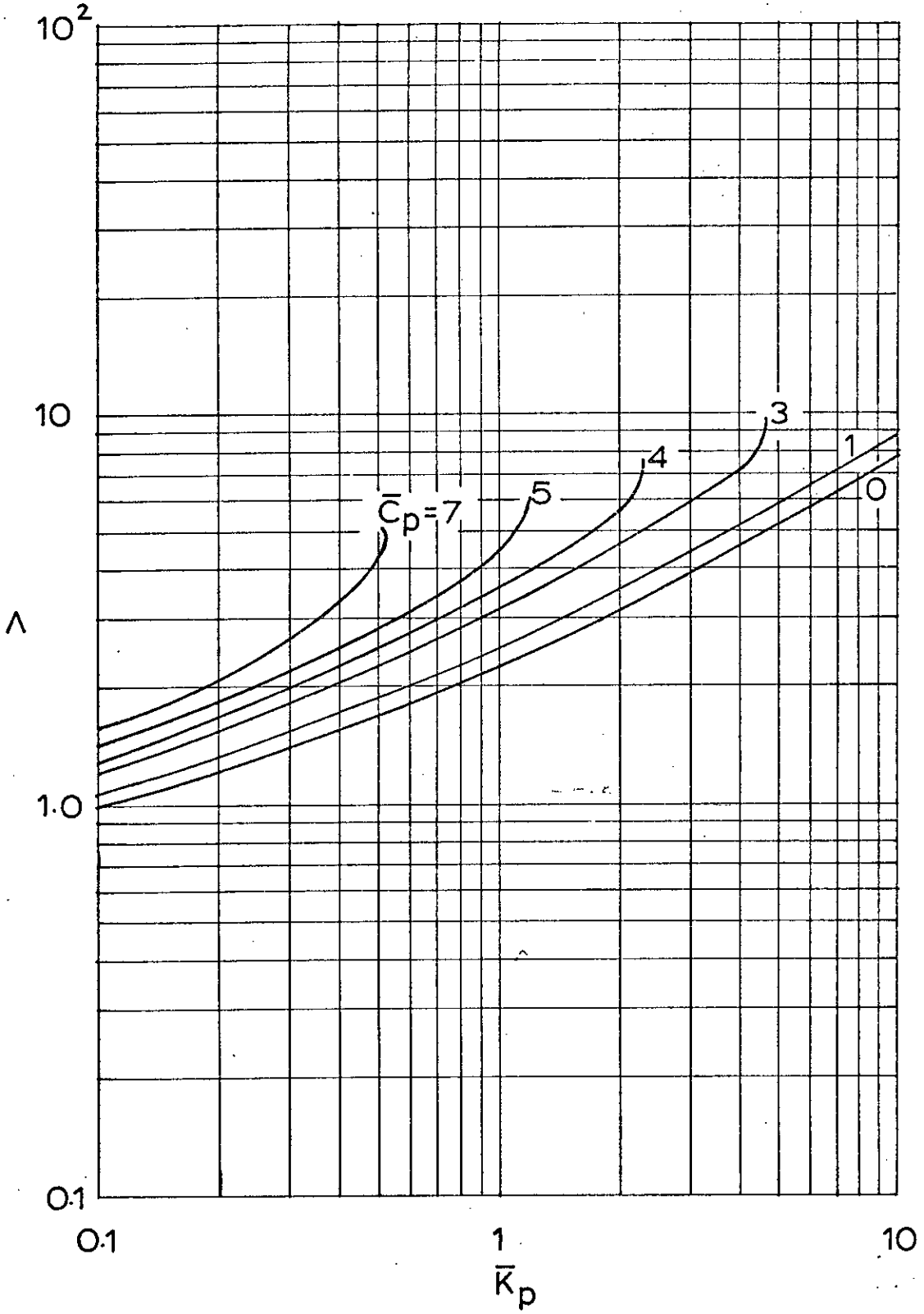

FIG. 3.4.6 THRESHOLD SPEED v SUPPORT STIFFNESS

$L/D = 1 : \Omega = 524 : \bar{W} = 0.2 : \bar{m} = 0.1.$

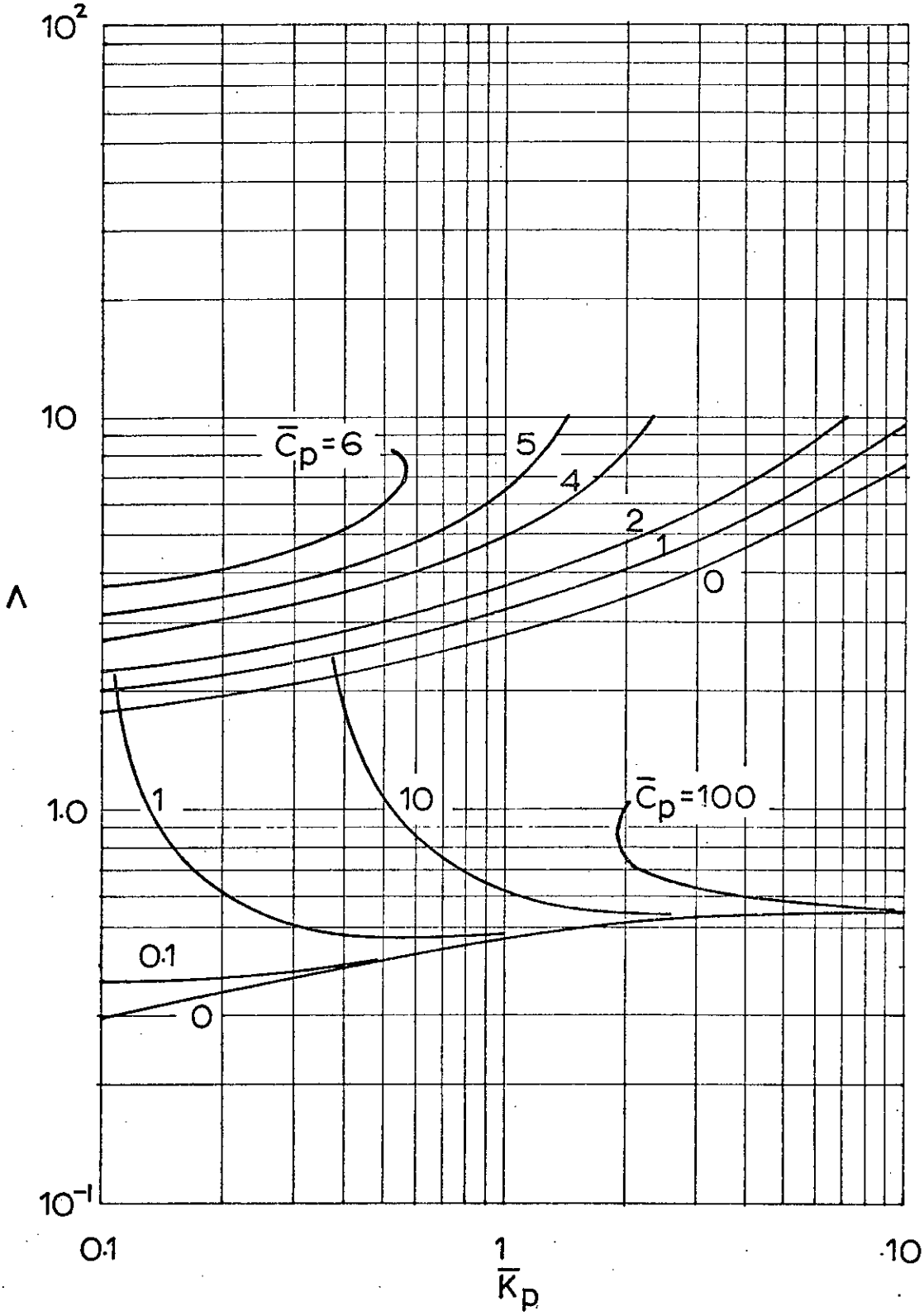

FIG 3.4.7 THRESHOLD SPEED v. SUPPORT STIFFNESS

$\bar{P}_s = 2 : L/D = 1.0 : \Lambda_t = 1.0 : \Omega = 524 : \bar{W} = 0.2 : \bar{m} = 0.1.$

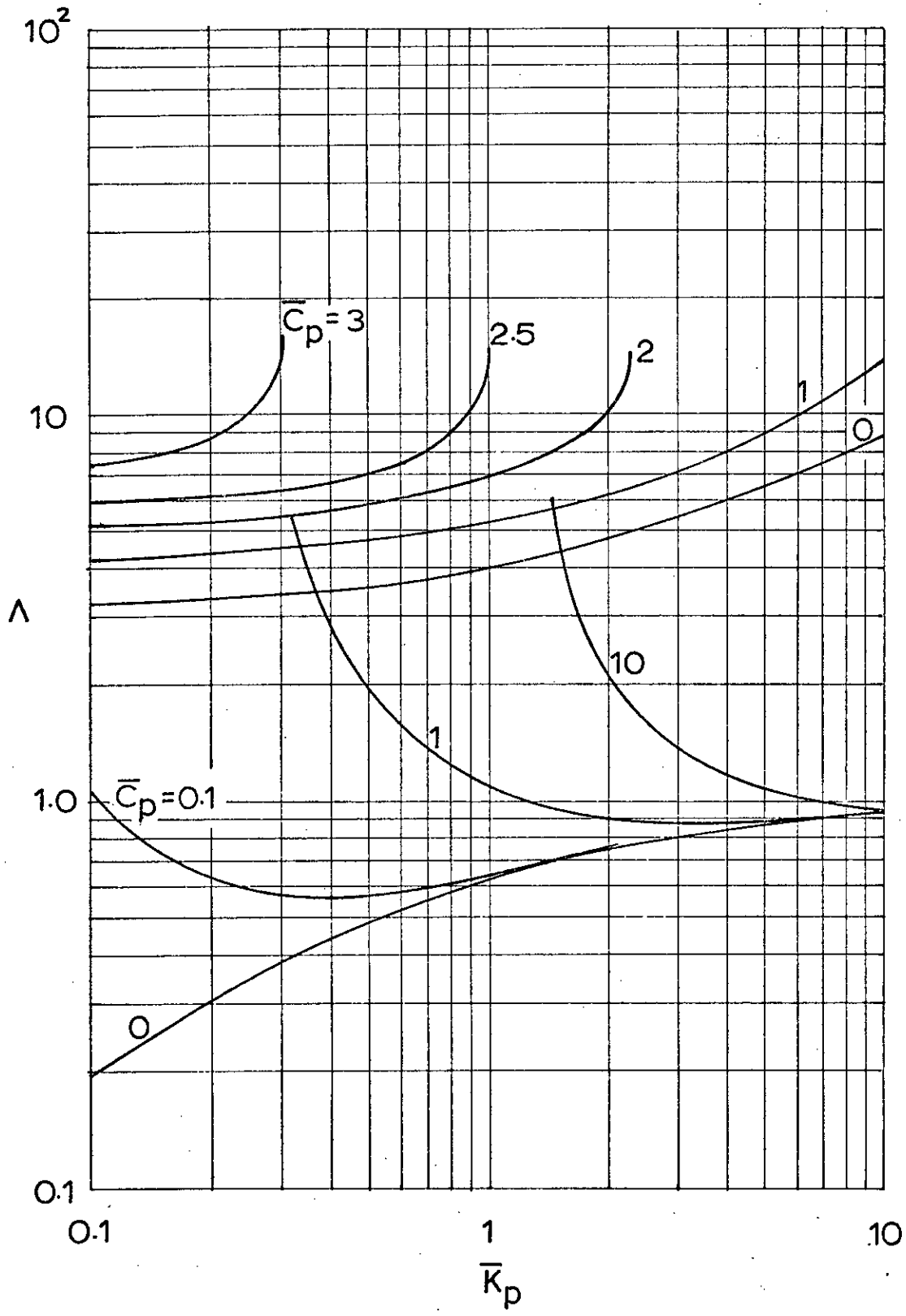

FIG. 3.4.8. THRESHOLD SPEED v SUPPORT STIFFNESS
$\bar{P}_s = 5 : L/D = 1 : \Lambda_t = 1 : \Omega = 524 : \bar{W} = 0.2 : \bar{m} = 0.1$.

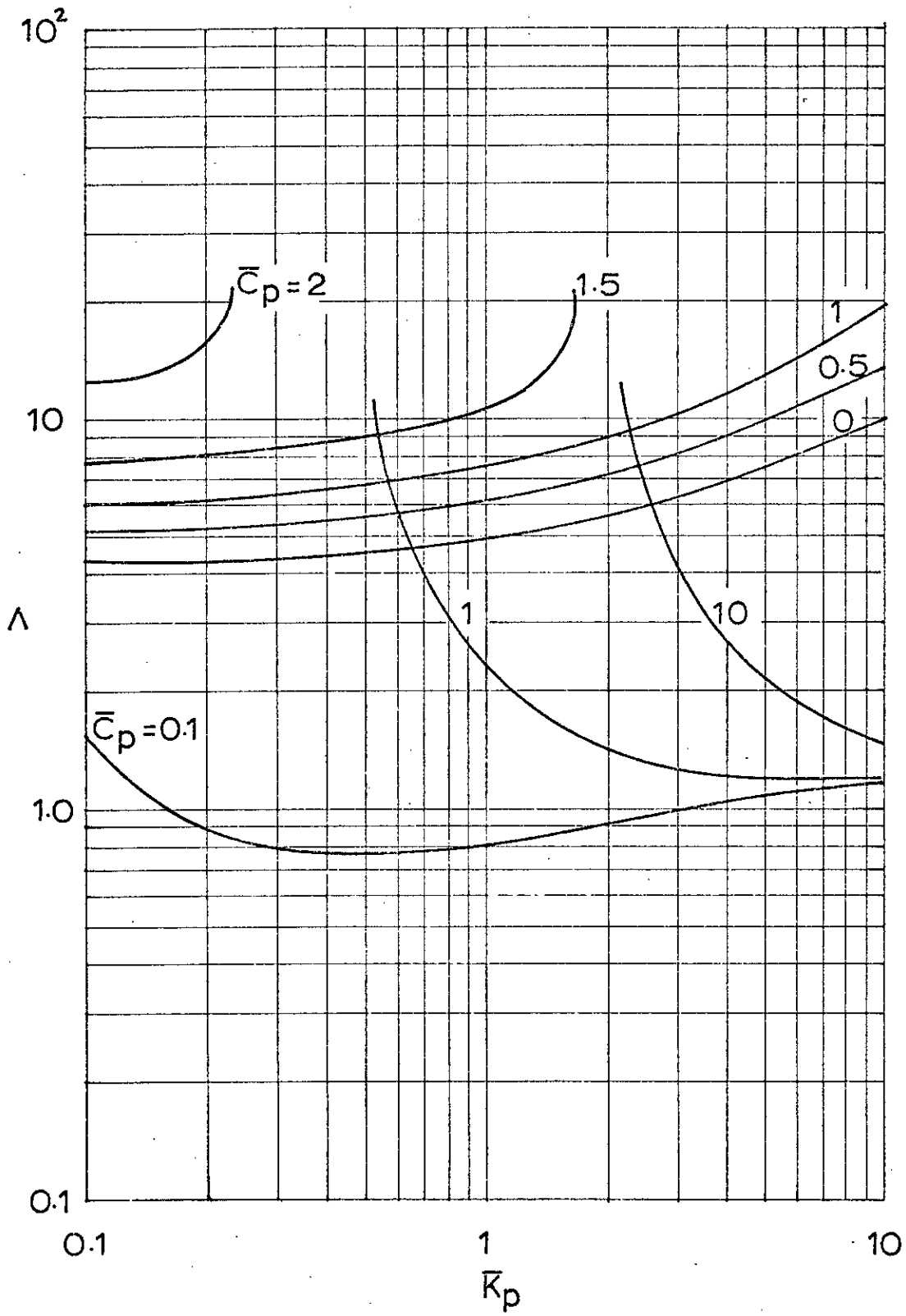

FIG 3.4.9 THRESHOLD SPEED v SUPPORT STIFFNESS.
$\bar{P}_s = 10 : L/D = 1 : \Lambda_t = 1 : \Omega = 524 : \bar{W} = 0.2 : \bar{m} = 0.1.$

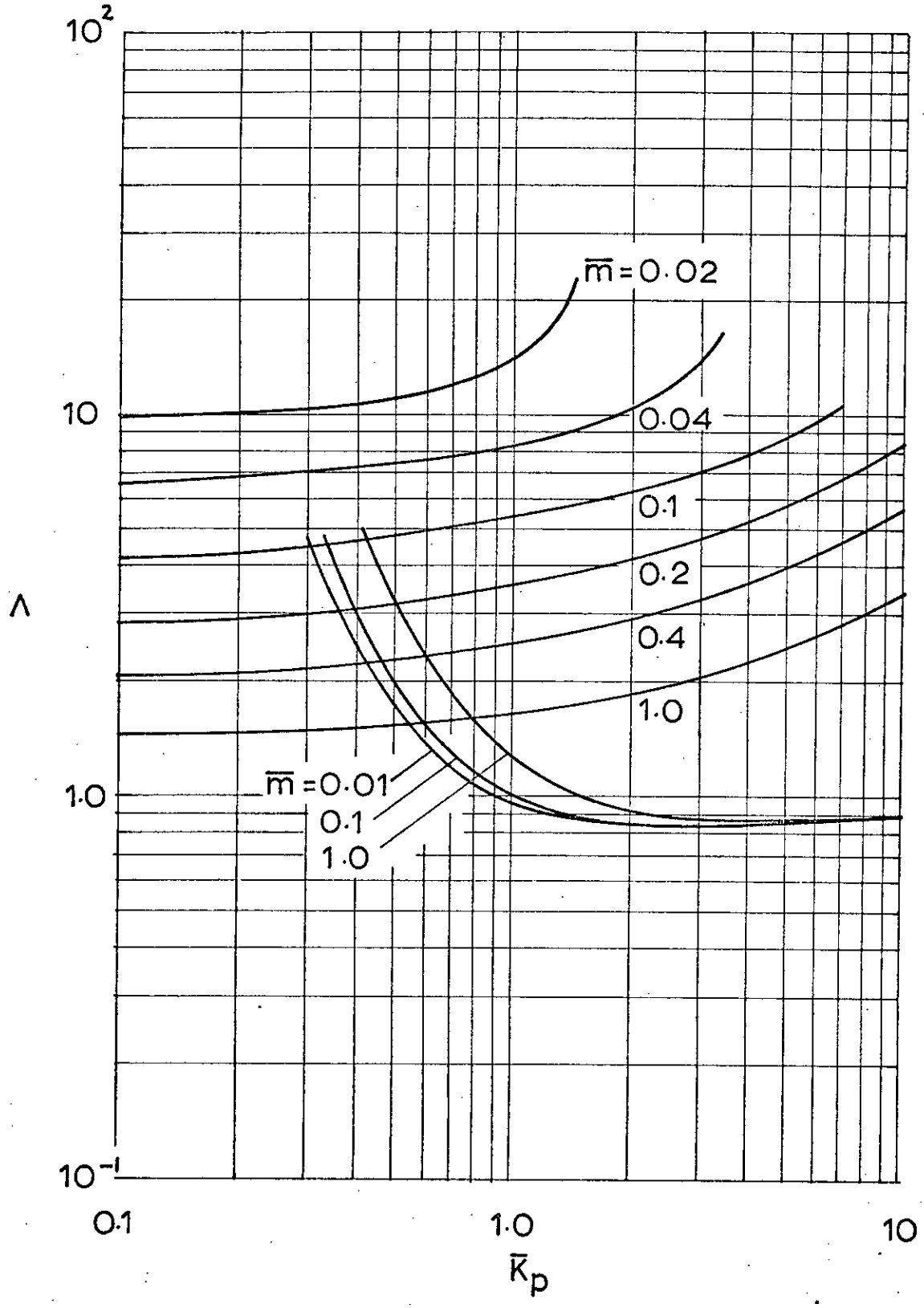

FIG. 3.4.10. THRESHOLD SPEED v SUPPORT STIFFNESS.
$\bar{P}_s = 5$: $L/D = 1{\cdot}0$: $\Lambda_t = 1{\cdot}0$: $\bar{C}_p = 1{\cdot}0$: $\Omega = 524$: $\bar{W} = 0{\cdot}2$.

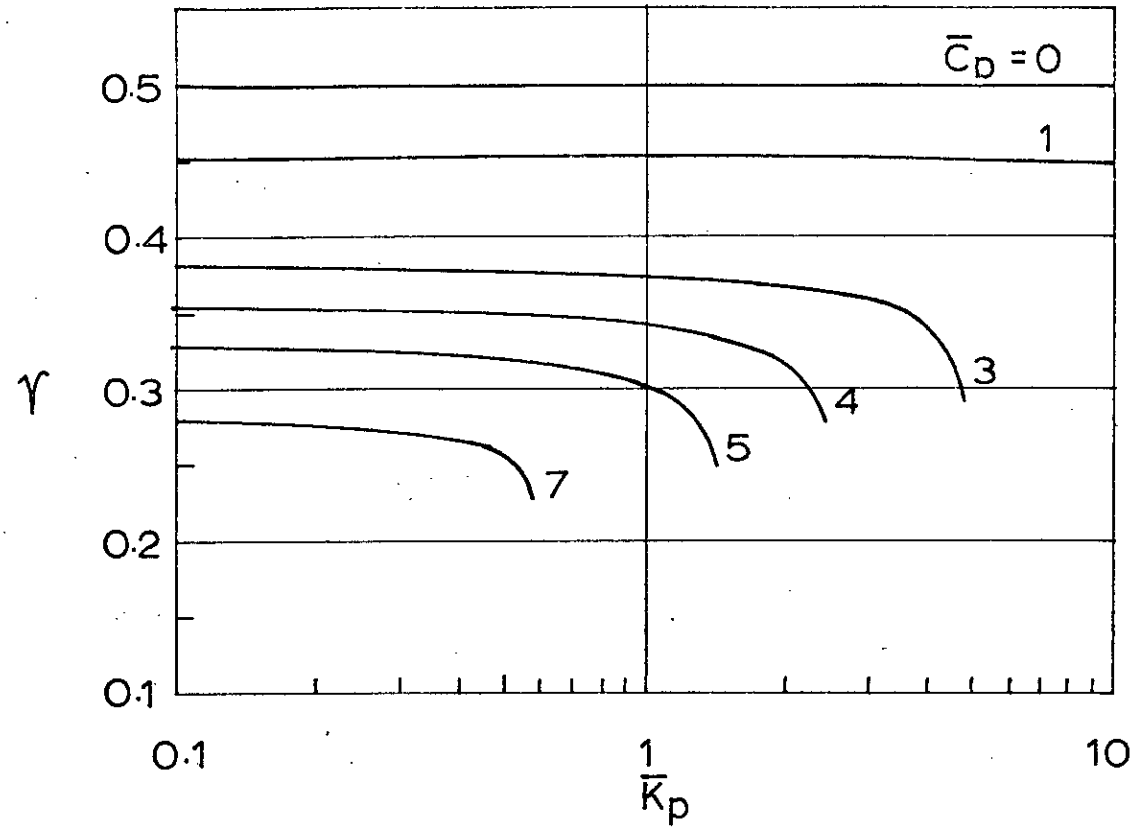

FIG. 3.4.11. THRESHOLD FREQUENCY RATIO v SUPPORT STIFFNESS
$L/D = 1 : \Omega = 524 : \bar{W} = 0.2 : \bar{m} = 0.1.$

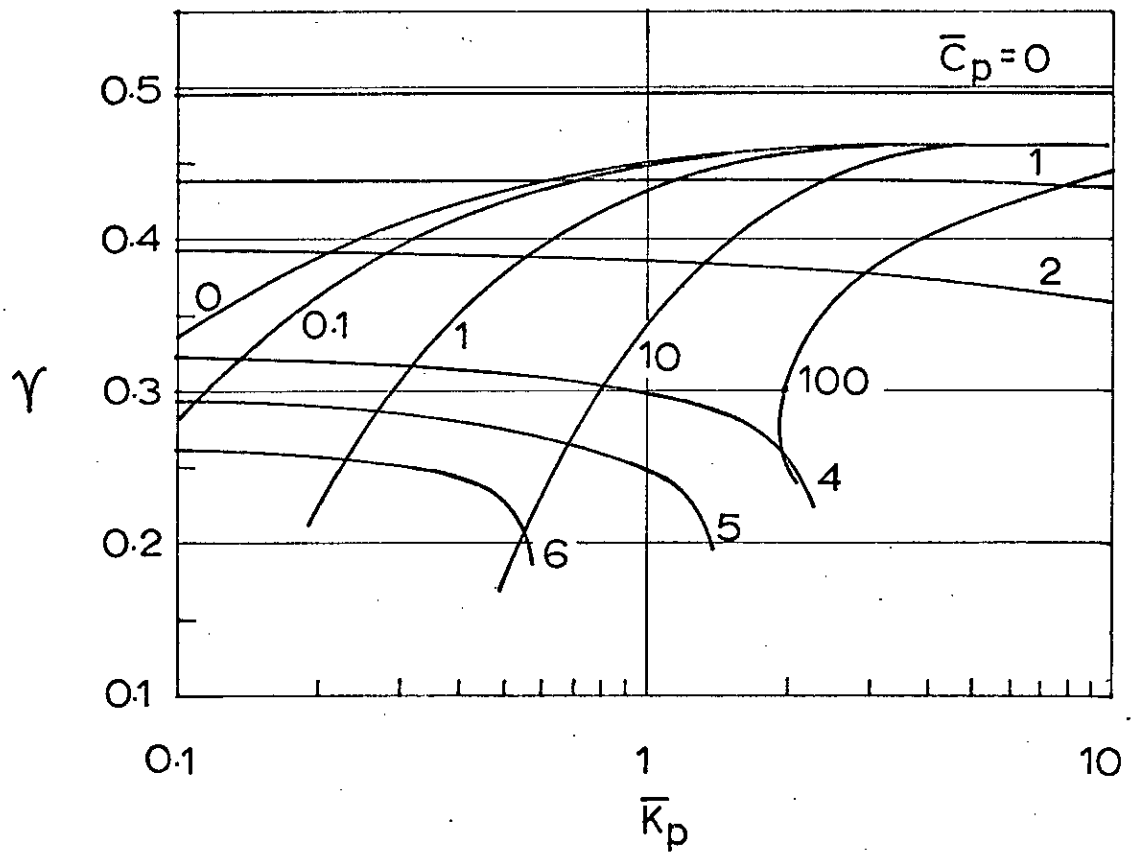

FIG. 3.4.12. THRESHOLD FREQUENCY RATIO v SUPPORT STIFFNESS
$\bar{P}_s = 2 : L/D = 1 : \Lambda_t = 1 : \Omega = 524 : \bar{W} = 0.2 : \bar{m} = 0.1.$

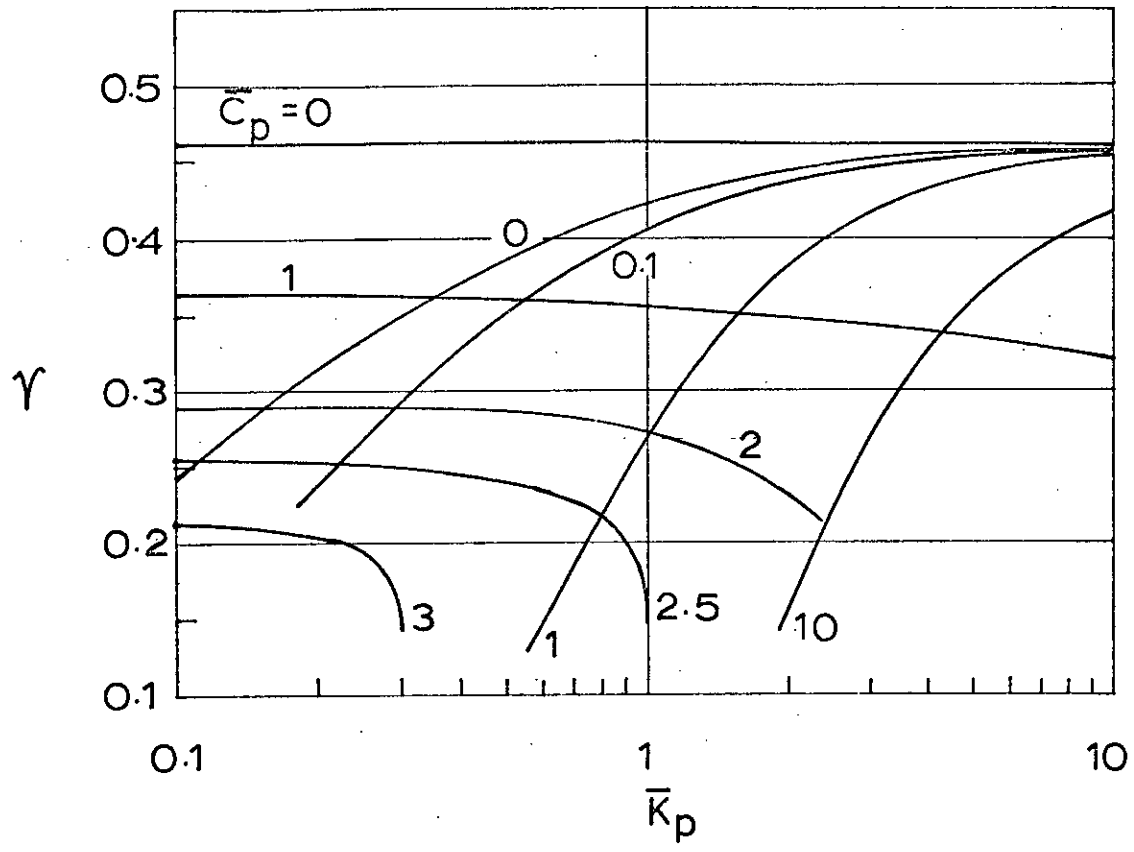

FIG. 3.4.13. THRESHOLD FREQUENCY RATIO v SUPPORT STIFFNESS
$\bar{P}_s = 5 : L/D = 1 : \Lambda_t = 1 : \Omega = 524 : \bar{W} = 0.2 : \bar{m} = 0.1.$

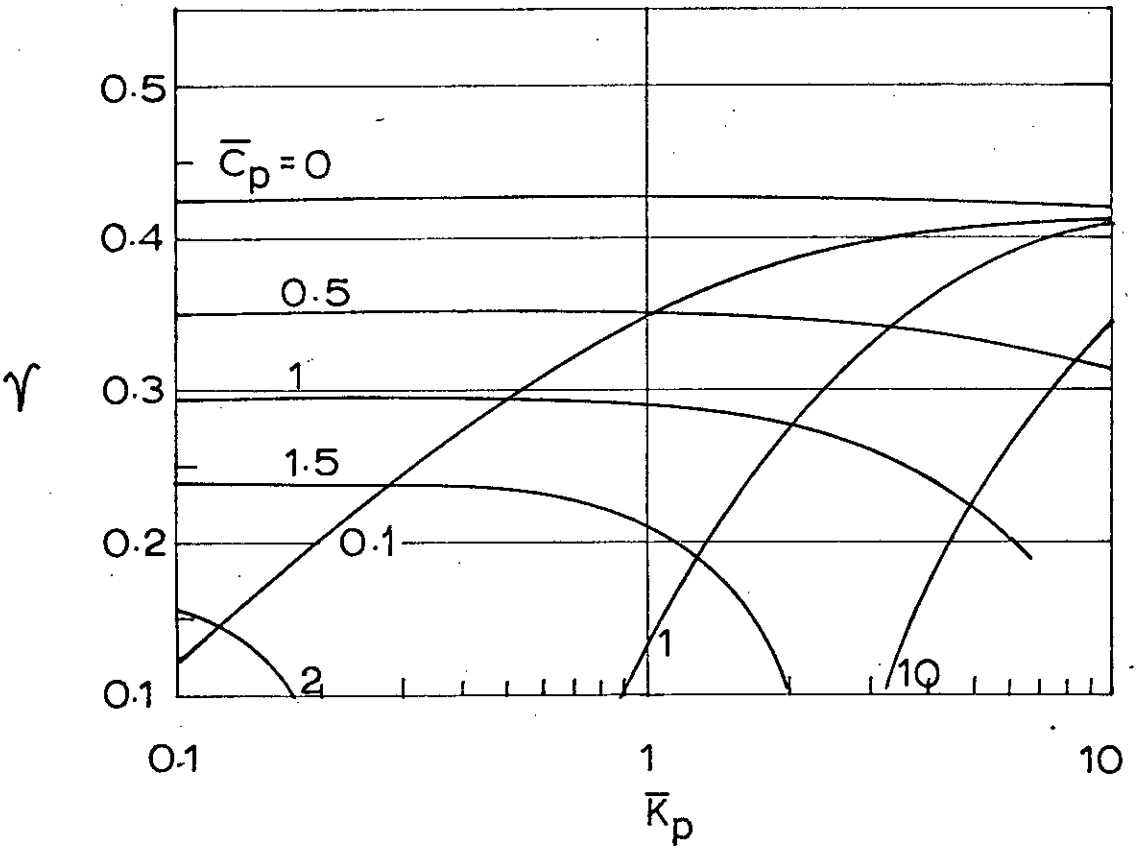

FIG. 3.4.14. THRESHOLD FREQUENCY RATIO v SUPPORT STIFFNESS
$\bar{P}_s = 10 : L/D = 1 : \Lambda_t = 1 : \Omega = 524 : \bar{W} = 0.2 : \bar{m} = 0.1.$

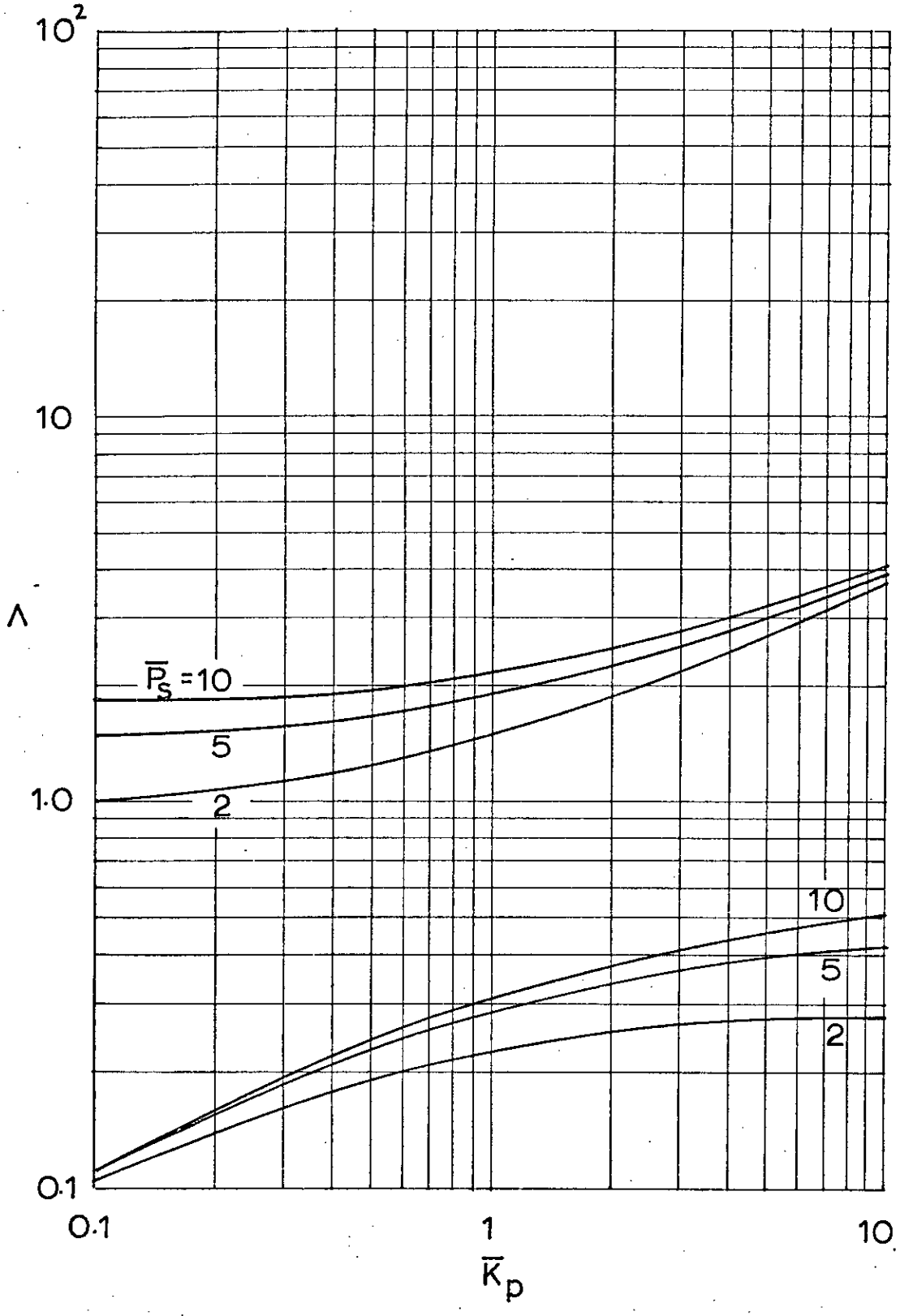

FIG. 3.4.15. SYNCHRONOUS WHIRL SPEED v SUPPORT STIFFNESS

$L/D = 1 : \Lambda_t = 1 : \overline{W} = 0.2 : \overline{m} = 0.1$.

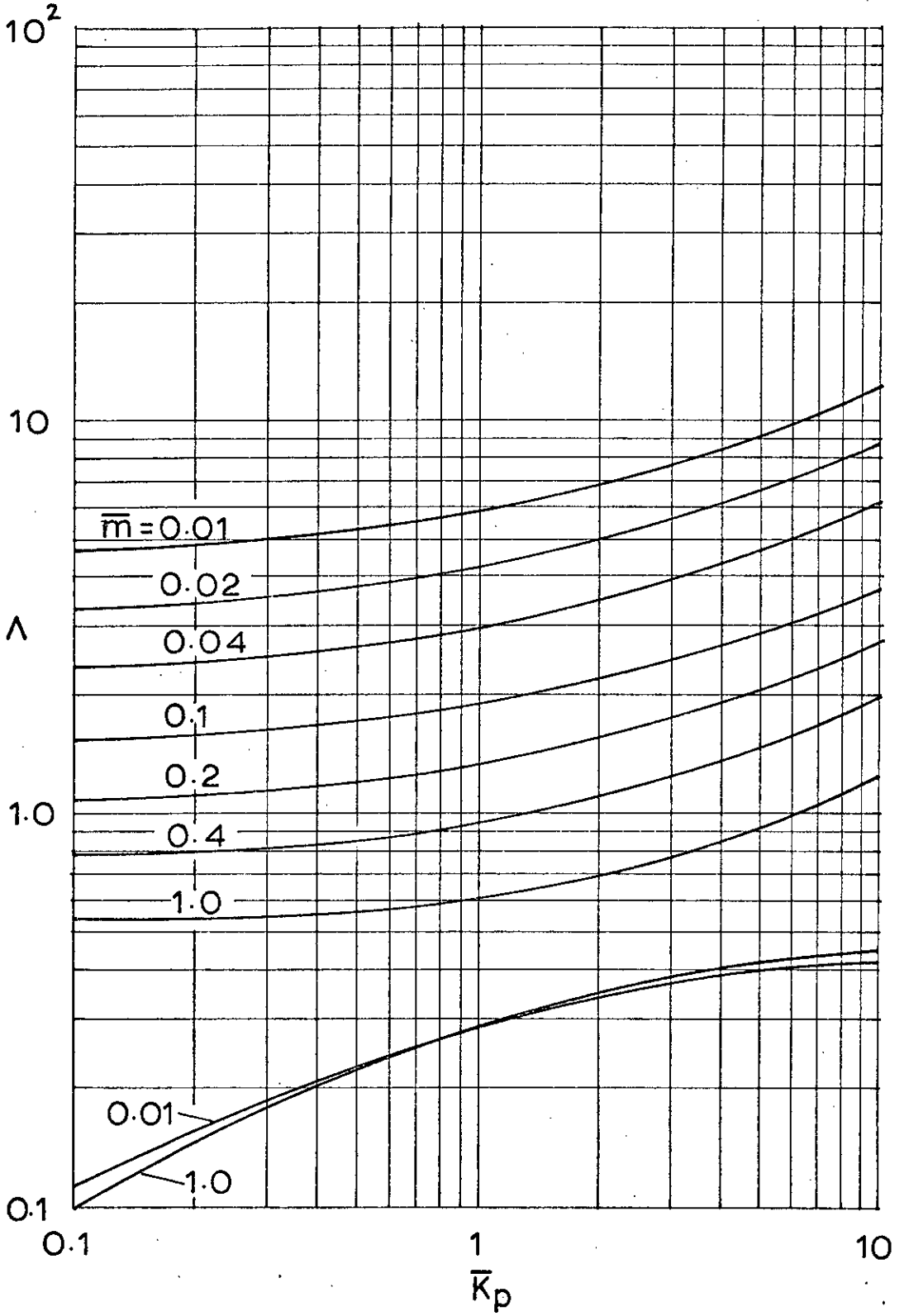

FIG. 3.4.16. SYNCHRONOUS WHIRL SPEED v SUPPORT STIFFNESS

$\bar{P}_s = 5 : L/D = 1 : \Lambda_t = 1 : \bar{W} = 0.2 :$ ~~$\bar{m} = 0.1$~~

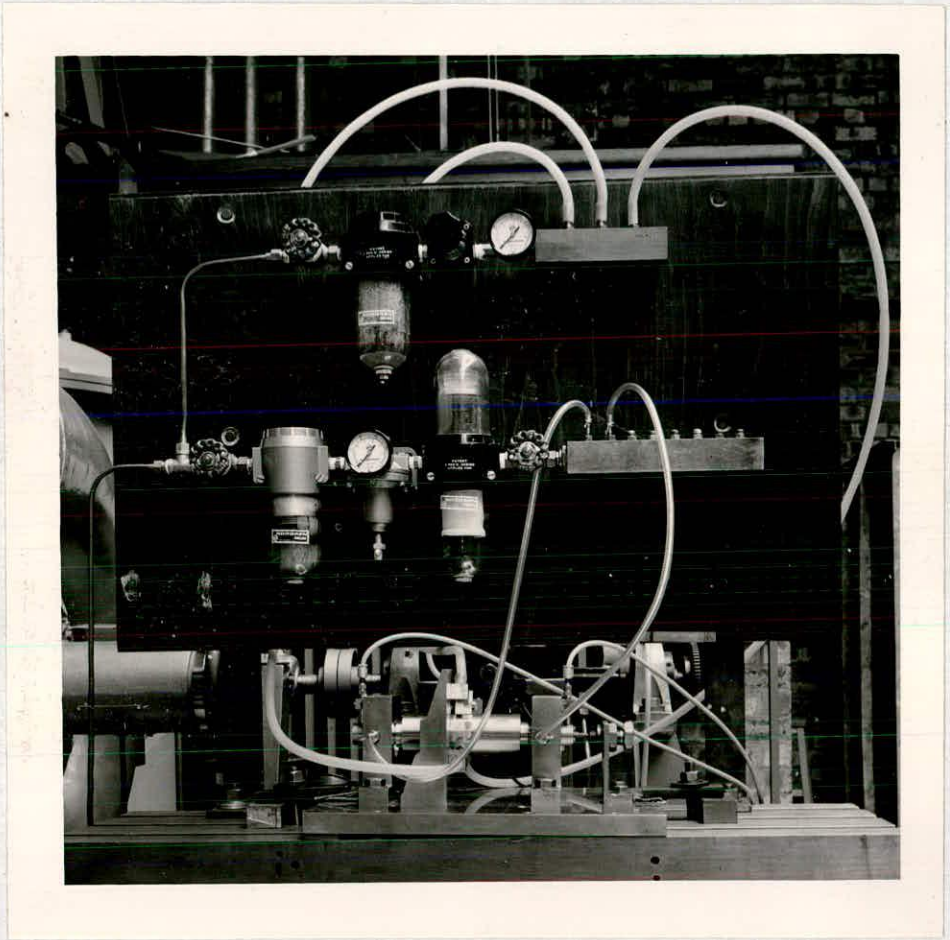

FIG. 4.2.1. VIEW OF GAS BEARING TEST RIG.

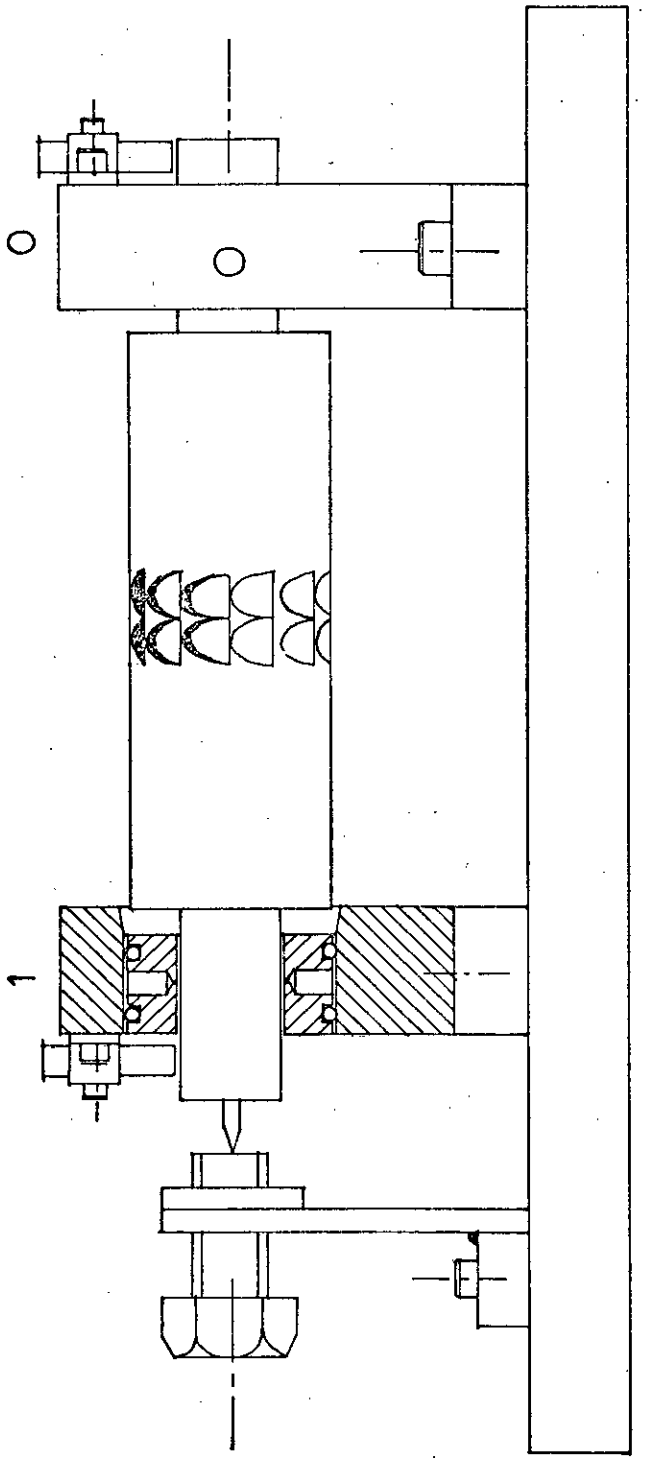

half scale

GAS BEARING TEST RIG

FIG 4.2.2.

FIG. 5.1.1.

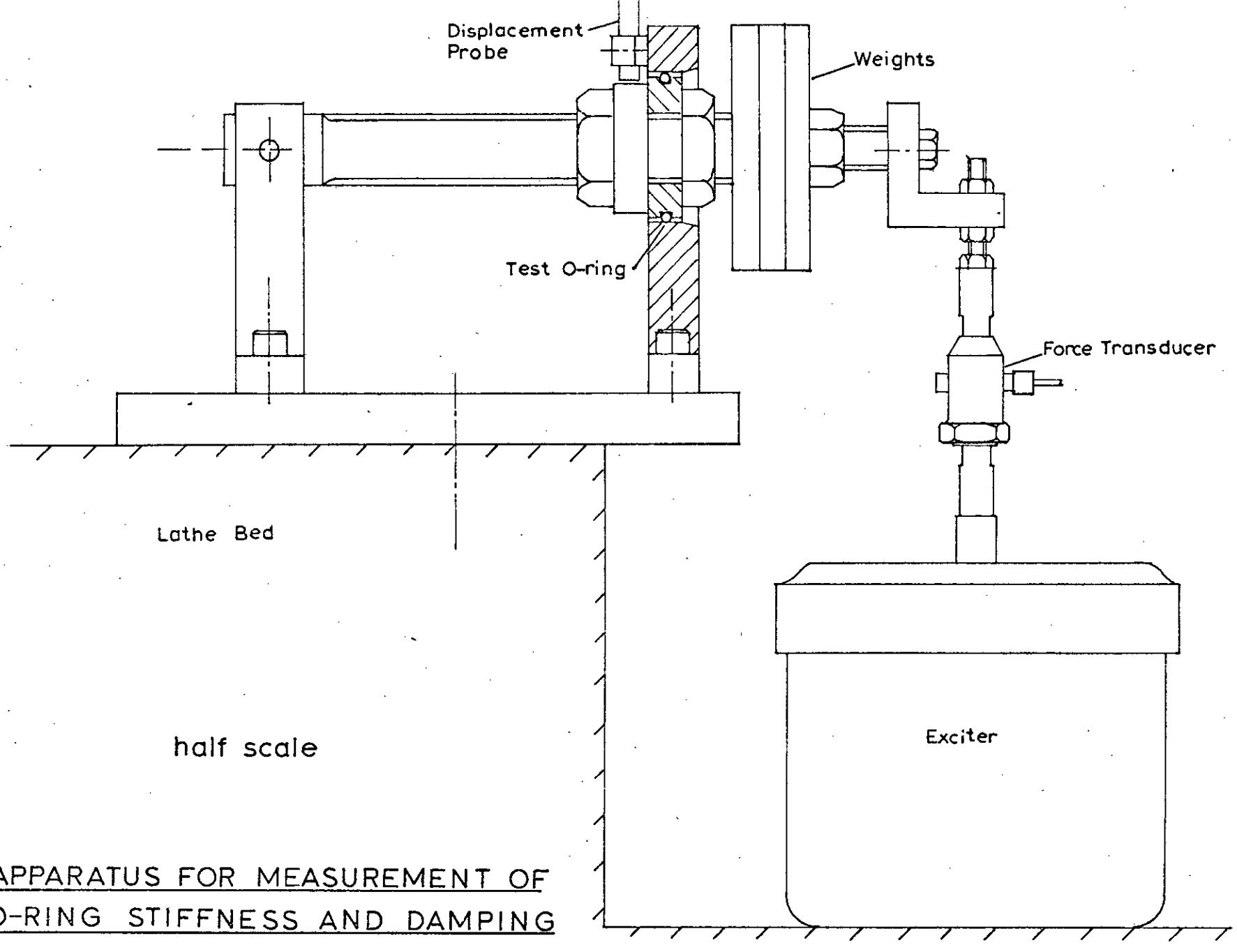

APPARATUS FOR MEASUREMENT OF O-RING STIFFNESS AND DAMPING

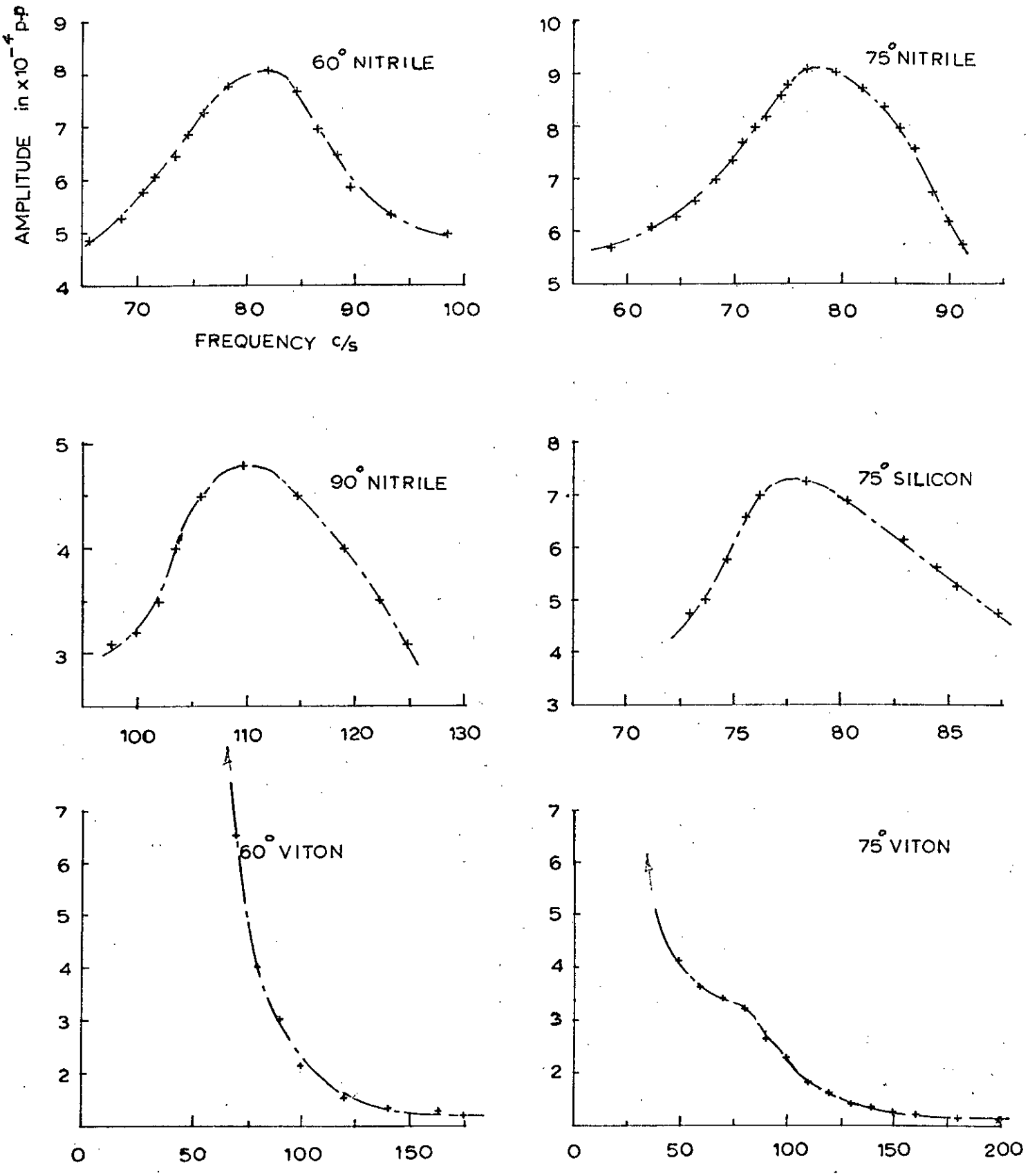

FIG. 5.1.2. TYPICAL RESONANCE CURVES FOR VARIOUS O-RINGS

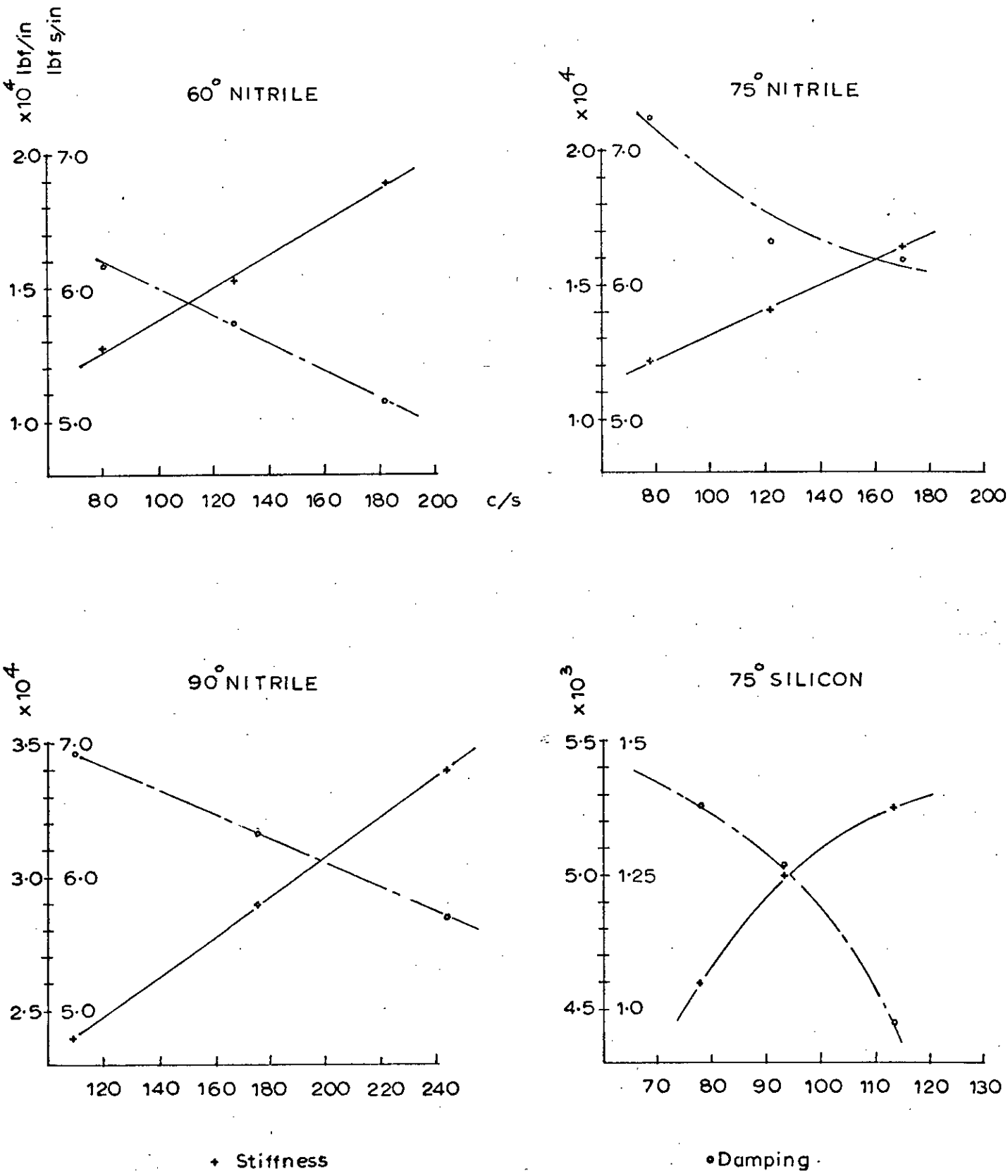

FIG. 5.1.3. O-RING STIFFNESS AND DAMPING v FREQUENCY

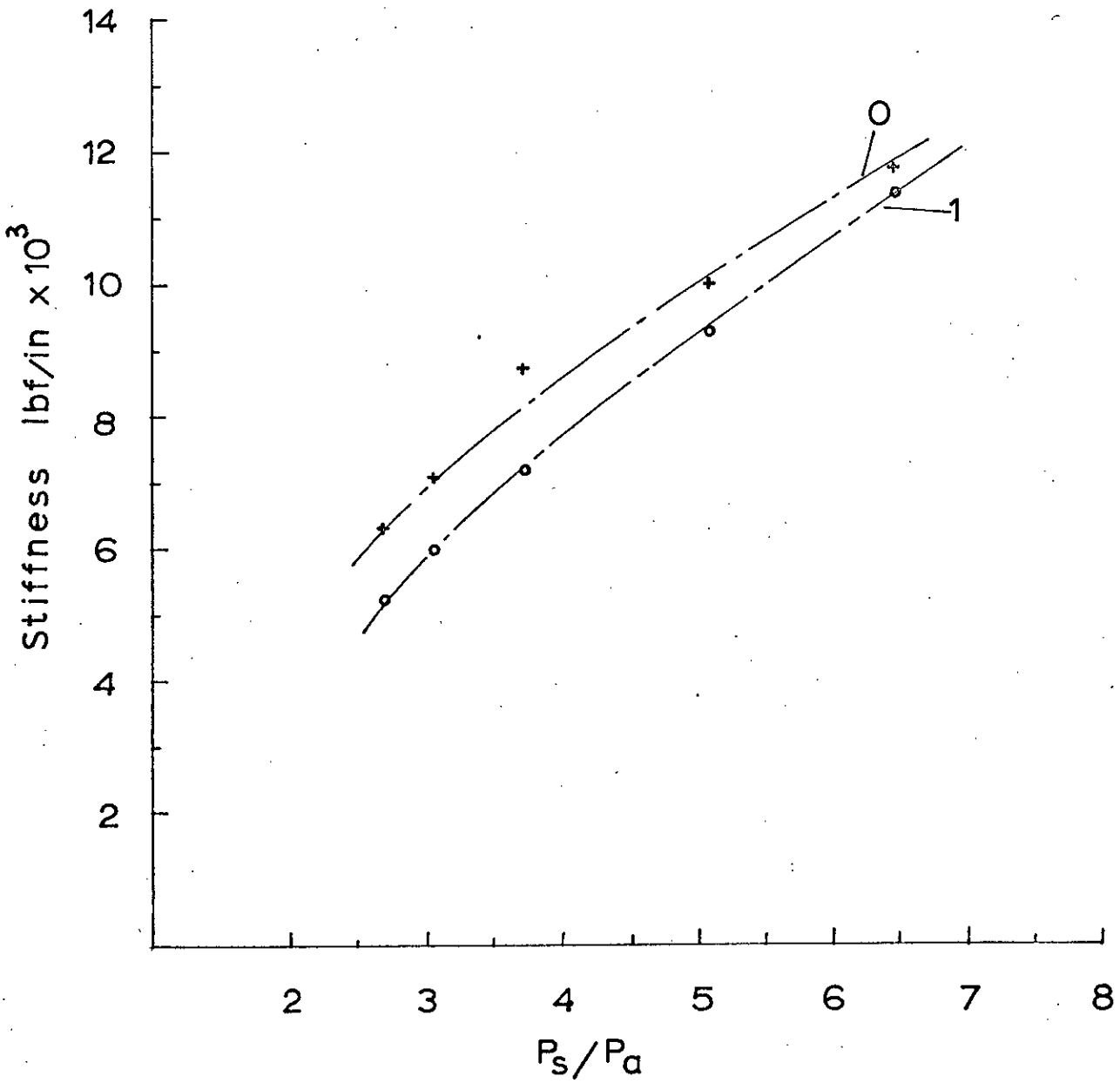

FIG. 5.3.1. BEARING FILM STIFFNESS v SUPPLY PRESSURE RATIO ($\epsilon \to 0$)

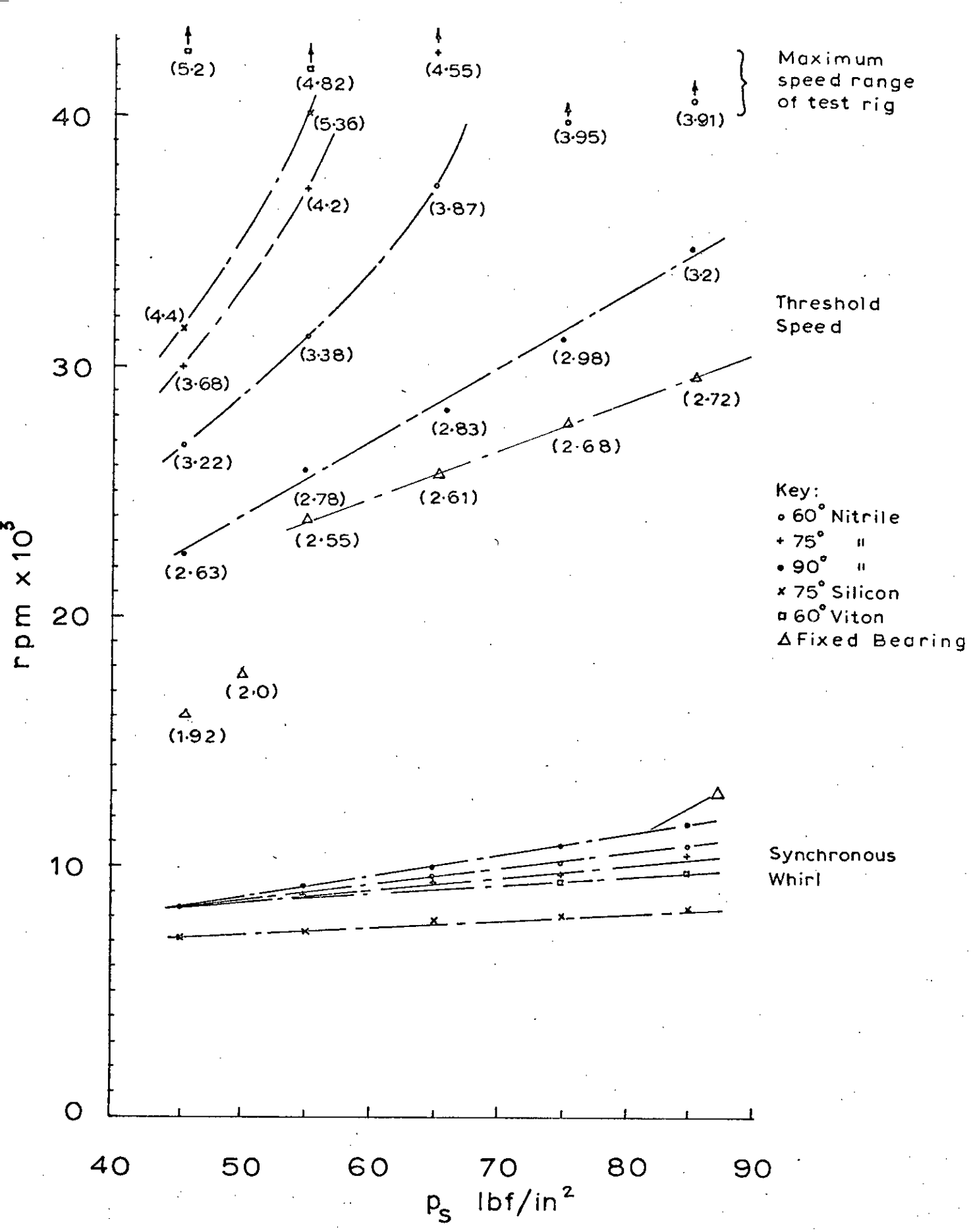

FIG. 5.4.1 THRESHOLD SPEED IN TRANSLATIONAL WHIRL v BEARING SUPPLY PRESSURE

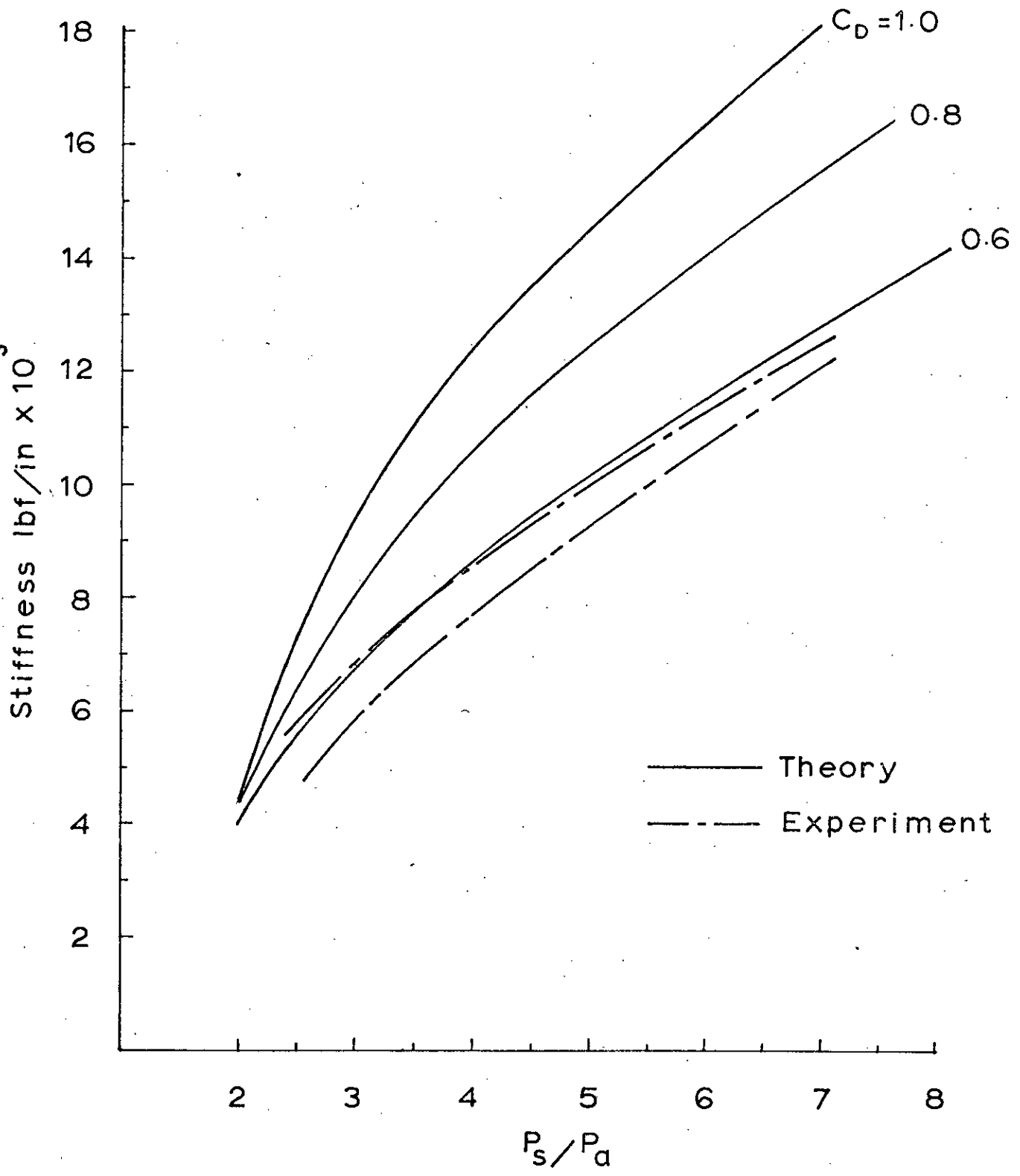

FIG. 6.2.1. BEARING FILM STIFFNESS v SUPPLY PRESSURE RATIO ($\epsilon \to 0$)

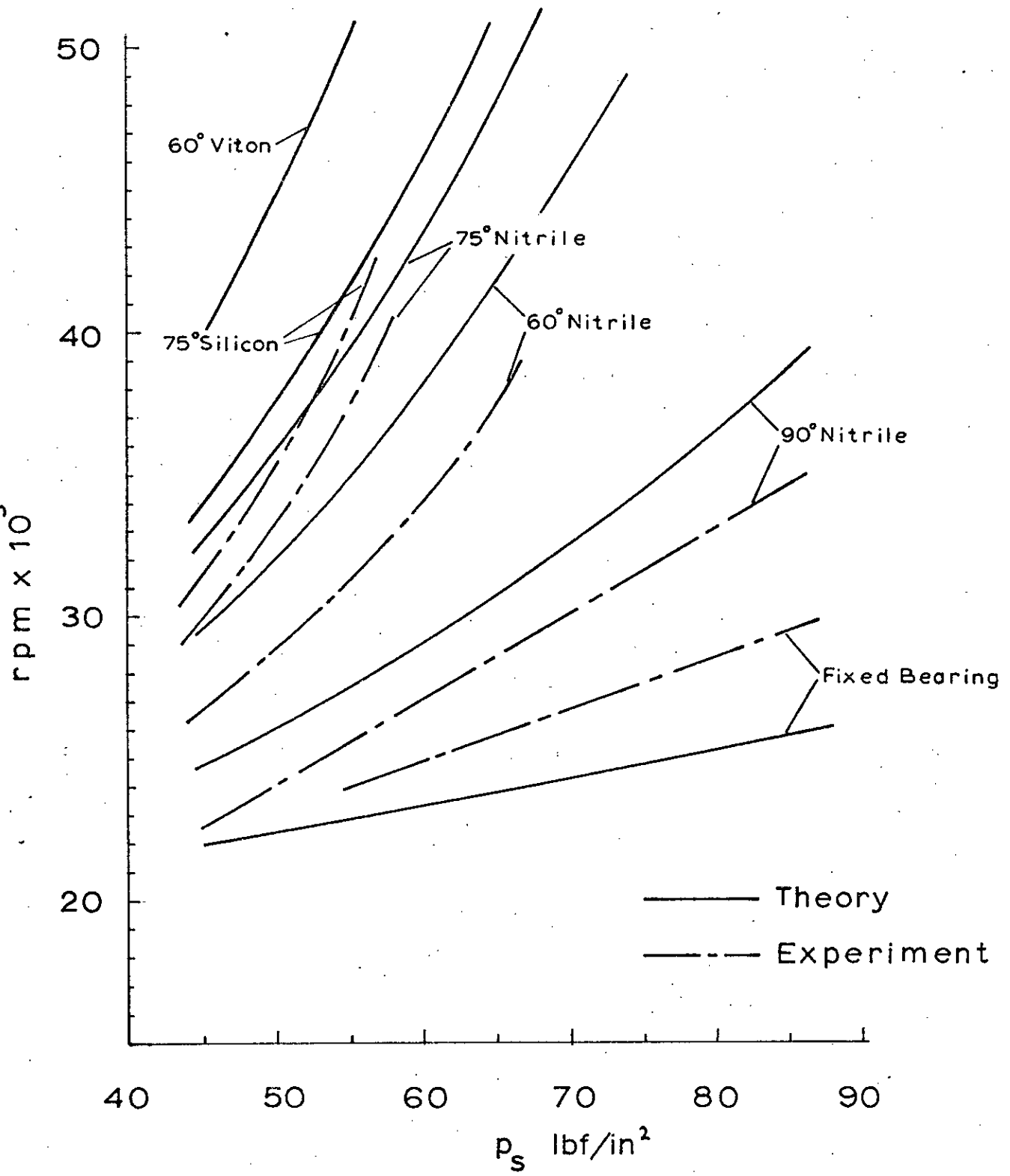

FIG. 6.3.1. THRESHOLD SPEED v BEARING SUPPLY PRESSURE.

APPENDIX I

From equation 2.3.3

$$\bar{P} = \frac{\bar{P}_0 + \epsilon\bar{P}_1}{1+\epsilon\cos\theta}$$

$$\simeq \left[\frac{\bar{P}_0}{1+\epsilon_0\cos\theta} + \frac{\epsilon_0 g_0 + \epsilon_1 g_1 + \epsilon_0\phi_1 g_2}{\bar{P}_0(1+\epsilon_0\cos\theta)}\right]\left[1 - \frac{\epsilon_1 e^{j\omega t}\cos\theta}{1+\epsilon_0\cos\theta}\right]$$

$$= \left[\frac{\bar{P}_0}{1+\epsilon_0\cos\theta} + \frac{\epsilon_0 g_0}{\bar{P}_0(1+\epsilon_0\cos\theta)}\right] + \left[\frac{\epsilon_1 g_1}{\bar{P}_0(1+\epsilon_0\cos\theta)} - \frac{\epsilon_1 e^{j\omega t}\epsilon_0 g_0\cos\theta}{\bar{P}_0(1+\epsilon_0\cos\theta)^2} - \frac{\epsilon_1 e^{j\omega t}\cos\theta\,\bar{P}_0}{(1+\epsilon_0\cos\theta)^2}\right] + \left[\frac{\epsilon_0\phi_1 g_2}{\bar{P}_0(1+\epsilon_0\cos\theta)}\right]$$

Let $G = G_r + iG_i$, where G_r and G_i are, in general, complex in j.

$$f_r = -\frac{1}{2\xi}\int_0^{\xi}\int_0^{2\pi} \bar{P}\cos\theta\, d\theta\, d\xi$$

$$= -\frac{1}{2\xi}\int_0^{2\pi}\left\{\left[\frac{\cos\theta}{1+\epsilon_0\cos\theta}\int_0^{\xi}\bar{P}_0\,d\xi + \frac{\epsilon_0\cos^2\theta}{1+\epsilon_0\cos\theta}\int_0^{\xi}\frac{G_{0r}}{\bar{P}_0}d\xi - \frac{\epsilon_0\cos\theta\sin\theta}{1+\epsilon_0\cos\theta}\int_0^{\xi}\frac{G_{0i}}{\bar{P}_0}d\xi\right]\right.$$

$$+ \epsilon_1 e^{j\omega t}\left[\frac{\cos^2\theta}{(1+\epsilon_0\cos\theta)}\int_0^{\xi}\frac{g_{1r}}{\bar{P}_0}d\xi - \frac{\cos\theta\sin\theta}{(1+\epsilon_0\cos\theta)}\int_0^{\xi}\frac{G_{1i}}{\bar{P}_0}d\xi - \frac{\epsilon_0\cos^3\theta}{(1+\epsilon_0\cos\theta)^2}\int_0^{\xi}\frac{G_{0r}}{\bar{P}_0}\right.$$

$$+ \frac{\epsilon_0\cos^2\theta\sin\theta}{(1+\epsilon\cos\theta)^2}\int_0^{\xi}\frac{G_{0i}}{\bar{P}_0} - \frac{\cos^2\theta}{(1+\epsilon_0\cos\theta)^2}\int\bar{P}_0\,d\xi\Big] + \epsilon_0\phi_1 e^{j\omega t}\left[\frac{\cos^2\theta}{1+\epsilon_0\cos\theta}\int_0^{\xi}\frac{G_{2r}}{\bar{P}_0}d\xi\right.$$

$$\left.\left.\left. - \frac{\cos\theta\sin\theta}{1+\epsilon_0\cos\theta}\int_0^{\xi}\frac{G_{2i}}{\bar{P}_0}d\xi\right]\right\}d\theta$$

$$f_t = \frac{1}{2\xi}\int_0^{\xi}\int_0^{2\pi}\bar{P}\sin\theta\, d\theta\, d\xi$$

$$= \frac{1}{2\xi}\int_0^{2\pi}\left\{\left[\frac{\sin\theta}{1+\epsilon_0\cos\theta}\int_0^{\xi}\bar{P}_0\,d\xi + \frac{\epsilon_0\cos\theta\sin\theta}{1+\epsilon_0\cos\theta}\int_0^{\xi}\frac{G_{0r}}{\bar{P}_0}d\xi - \frac{\epsilon_0\sin^2\theta}{1+\epsilon_0\cos\theta}\int_0^{\xi}\frac{G_{0i}}{\bar{P}_0}d\xi\right]\right.$$

$$+ \epsilon_1 e^{j\omega t}\left[\frac{\cos\theta\sin\theta}{1+\epsilon_0\cos\theta}\int_0^{\xi}\frac{G_{1r}}{\bar{P}_0}d\xi - \frac{\sin^2\theta}{1+\epsilon_0\cos\theta}\int_0^{\xi}\frac{G_{1i}}{\bar{P}_0}d\xi - \frac{\epsilon_0\cos^2\theta\sin\theta}{(1+\epsilon_0\cos\theta)^2}\int_0^{\xi}\frac{G_{0r}}{\bar{P}_0}d\xi\right.$$

$$+ \frac{\epsilon_0\sin^2\theta\cos\theta}{(1+\epsilon_0\cos\theta)^2}\int_0^{\xi}\frac{G_{0i}}{\bar{P}_0}d\xi - \frac{\cos\theta\sin\theta}{(1+\epsilon_0\cos\theta)^2}\int_0^{\xi}\bar{P}_0\,d\xi\Big] + \epsilon_0\phi_1 e^{j\omega t}\left[\frac{\cos\theta\sin\theta}{1+\epsilon_0\cos\theta}\int_0^{\xi}\frac{G_{2r}}{\bar{P}_0}d\xi\right.$$

$$-\frac{\sin^2\theta}{1+e_o\cos\theta}\int_0^{\xi}\frac{q_{2r}}{p_o}\,d\xi\Bigg]\Bigg\}\,d\theta.$$

The various integrals of θ over the range 0 to 2π are given by:

$$\frac{\cos\theta}{1+e_o\cos\theta}\,d\theta = -\frac{2\pi e_o}{\eta(1+\eta)}$$

$$\frac{\cos^2\theta}{1+e_o\cos\theta}\,d\theta = \frac{2\pi}{\eta(1+\eta)}$$

$$\frac{\cos\theta\sin\theta}{1+e_o\cos\theta}\,d\theta = 0$$

$$\frac{\cos^3\theta\,d\theta}{(1+e_o\cos\theta)^2} = -\frac{2\pi(1-\eta)(1+2\eta)}{e_o\eta^3(1+\eta)}$$

$$\frac{\cos^2\theta\sin\theta\,d\theta}{(1+e_o\cos\theta)^2} = 0$$

$$\frac{\cos^2\theta\,d\theta}{(1+e_o\cos\theta)^2} = \frac{2\pi(1+\eta-\eta^2)}{\eta^3(1+\eta)}$$

$$\frac{\sin\theta}{1+e_o\cos\theta}\,d\theta = 0$$

$$\frac{\sin^2\theta}{1+e_o\cos\theta}\,d\theta = \frac{2\pi}{1+\eta}$$

$$\frac{\sin^2\theta\cos\theta}{(1+e_o\cos\theta)^2}\,d\theta = -\frac{2\pi(1-\eta)}{e_o\eta(1+\eta)}$$

where $\eta = \sqrt{(1-e_o^2)}$

From which:

$$f_{ro} = \frac{\pi}{\xi}\left[\frac{e_o}{\eta(1+\eta)}\left(\int_0^{\xi}\bar{p}_o\,d\xi - \int_0^{\xi}\frac{q_{or}}{\bar{p}_o}\,d\xi\right)\right]$$

$$f_{rt} = -\frac{\pi}{\xi}\left\{\left[-\frac{(1+\eta-\eta^2)}{\eta^3(1+\eta)}\int_0^{\xi}\bar{p}_o\,d\xi + \frac{(1-\eta)(1+2\eta)}{\eta^3(1+\eta)}\int_0^{\xi}\frac{q_{or}}{\bar{p}_o}\,d\xi + \frac{1}{\eta(1+\eta)}\int_0^{\xi}\frac{q_{ir}}{\bar{p}_o}\,d\xi\right]e_i e^{\sqrt{}}\right.$$

$$+\left[\frac{1}{\eta(1+\eta)}\int_{0}^{\xi}\frac{q_{2n}}{\bar{p}_0}\,d\xi\right]\epsilon_0\phi_1 e^{j\omega t}\Bigg\}$$

$$f_{t_0} = -\frac{\pi}{\xi}\left[\frac{\epsilon_0}{1+\eta}\int_{0}^{\xi}\frac{q_{0i}}{\bar{p}_0}\,d\xi\right]$$

$$f_{tt} = -\frac{\pi}{\xi}\left\{\left[\frac{1}{1+\eta}\int_{0}^{\xi}\frac{q_{1i}}{\bar{p}_0}\,d\xi + \frac{(1-\eta)}{\eta(1+\eta)}\int_{0}^{\xi}\frac{q_{0i}}{\bar{p}_0}\,d\xi\right]\epsilon_1 e^{j\omega t}\right.$$

$$\left. + \left[\frac{1}{1+\eta}\int_{0}^{\xi}\frac{q_{2i}}{\bar{p}_0}\,d\xi\right]\epsilon_0\phi_1 e^{j\omega t}\right\}$$

APPENDIX II

UNIVERSITY OF SOUTHAMPTON
Department of Mechanical Engineering
GAS BEARING SYMPOSIUM
April 1969 Paper No. 12

"THE STABILITY OF A RIGID ROTOR IN A FLEXIBLY SUPPORTED SELF-ACTING GAS JOURNAL BEARING"

by
D.A. Boffey
University of Edinburgh, U.K.

INTRODUCTION

Extensive theoretical and experimental work has been carried out on the investigation of the stability of self-acting gas lubricated journal bearings in which the bearings are rigidly supported, for example References 1, 2, 3, 4, 5, 6. The onset of the characteristic instability, known as half speed whirl, can now be fairly accurately predicted. As the radial clearances in this type of bearing are extremely small, there is a practical advantage in having the bearings flexibly supported, to facilitate ease of alignment. An application of such a system, in the textile field, was demonstrated recently at the National Engineering Laboratory.

The work of Marsh, Ref. 7, and Kerr, Ref. 8, has shown that the stability characteristics of this system are affected by both the stiffness and damping of the bearing support. Marsh, in his theoretical treatment, finally used a numerical method to obtain the dynamic pressure field of the bearing in solving the equations of motion for the system.

The purpose of the present paper is to examine the stability characteristics of a bearing on a flexible damped support using a purely analytical approach. It is suggested that this may give a further insight into the behaviour of the system. The analysis which is developed is based on the "linearized ph" solution to the time dependent Reynolds Equation, neglecting axial flow, due to Ausman, Ref. 2. The advantage of this solution is that the steady state fluid film forces partially retain the important nonlinear influences of the eccentricity ratio, for the entire range of compressibility numbers, which previous solutions had not achieved.

EQUATIONS OF MOTION

The axially symmetric system to be analysed, shown diagrammatically in Figure 1, comprises a rigid rotor in a non-rotating flexibly supported bearing. To simplify the analysis, the damping in the support is assumed to be viscous, and the stiffness to be isoelastic. Employing the system of co-ordinates given in Figure 2, where O is the static equilibrium position of the bearing centre, the reference lines OZ and O'Z' are parallel while O"Z" is parallel to the bearing axis, for the self-loading condition the equations of motion for translatory whirl are:

$$m_R(\ddot{x}_1 + \ddot{x}_2) - W_x = m_R \cdot g \tag{1}$$

$$m_R(\ddot{y}_1 + \ddot{y}_2) - W_y = 0 \tag{2}$$

$$m_B\ddot{x}_1 + c\dot{x}_1 + kx_1 + W_x = m_B \cdot g \tag{3}$$

$$m_B\ddot{y}_1 + c\dot{y}_1 + ky_1 + Wy = 0 \tag{4}$$

For conical whirl of the system the equation of motion are:

$$I_R(\ddot{\phi}+\ddot{\alpha}) - J_R\omega(\dot{\psi}+\dot{\beta}) - M_y = 0 \tag{5}$$

$$I_R(\ddot{\psi}+\ddot{\beta}) + J_R\omega(\dot{\phi}+\dot{\alpha}) - M_x = 0 \tag{6}$$

$$I_B\ddot{\alpha} + \eta\dot{\alpha} + T\alpha + M_y = 0 \tag{7}$$

$$I_B\ddot{\beta} + \eta\dot{\beta} + T\beta + M_x = 0 \tag{8}$$

Ausman expresses the equations for the fluid film force components, W_x and W_y, neglecting the transient portions, as follows:

$$\frac{W_x}{\pi DL\,p_a} = -\left[\frac{\epsilon_x}{E(1+E)} + A\,\frac{\epsilon_x^2+E\epsilon_y^2}{E(1+E)\epsilon^2} + B\,\frac{(1-E)\epsilon_x\epsilon_y}{E(1+E)\epsilon^2}\right] \tag{9}$$

$$\frac{W_y}{\pi DL\,p_a} = -\left[\frac{\epsilon_y}{E(1+E)} + A\,\frac{(1-E)\epsilon_x\epsilon_y}{E(1+E)\epsilon^2} + B\,\frac{\epsilon_y^2+E\epsilon_x^2}{E(1+E)\epsilon^2}\right] \tag{10}$$

where $E=\sqrt{(1-\epsilon^2)}$ and the eccentricity ratio components ϵ_x and ϵ_y are related to the time dependent functions of eccentricity ratio A and B through

$$\epsilon_x = -A - \frac{2H}{\omega}\dot{A} - HB \tag{11}$$

$$\epsilon_y = -B - \frac{2H}{\omega}\dot{B} + HA \tag{12}$$

Substituting equations (9) and (10) into equations (1) to (4) and putting $x_2 = C\epsilon_x$ and $y_2 = C\epsilon_y$ gives

$$\frac{m_R\ddot{x}_1}{\pi DL p_a} + \frac{m_R C\ddot{\epsilon}_x}{\pi DL p_a} + \frac{\epsilon_x}{E(1+E)} + A\,\frac{\epsilon_x^2+E\epsilon_y^2}{E(1+E)\epsilon^2} + B\,\frac{(1-E)\epsilon_x\epsilon_y}{E(1+E)\epsilon^2} = \frac{m_R\cdot g}{\pi DL p_a} \tag{13}$$

$$\frac{m_R\ddot{y}_1}{\pi DL p_a} + \frac{m_R C\ddot{\epsilon}_y}{\pi DL p_a} + \frac{\epsilon_y}{E(1+E)} + A\,\frac{(1-E)\epsilon_x\epsilon_y}{E(1+E)\epsilon^2} + B\,\frac{\epsilon_y^2+E\epsilon_x^2}{E(1+E)\epsilon^2} = 0 \tag{14}$$

$$\frac{m_B \ddot{x}_1}{\pi DLp_a} + \frac{c\dot{x}_1}{\pi DLp_a} + \frac{kx_1}{\pi DLp_a} - \frac{\epsilon_x}{E(1+E)} - \frac{A\epsilon_x^2 + E\epsilon_y^2}{E(1+E)\epsilon^2} - \frac{B(1-E)\epsilon_x\epsilon_y}{E(1+E)\epsilon^2} = \frac{m_B \cdot g}{\pi DLp_a} \quad (15)$$

$$\frac{m_B \ddot{y}_1}{\pi DLp_a} + \frac{c\dot{y}_1}{\pi DLp_a} + \frac{ky_1}{\pi DLp_a} - \frac{\epsilon_y}{E(1+E)} - \frac{A(1-E)\epsilon_x\epsilon_y}{E(1+E)\epsilon^2} - \frac{B\epsilon_y^2 + E\epsilon_x^2}{E(1+E)\epsilon^2} = 0 \quad (16)$$

To investigate the stability of the equilibrium positions of the journal and bearing for the nonlinear set of equations (13) to (16), the time varying quantities can be expressed in terms of constant and time varying portions thus

$$\epsilon_x = \epsilon_{xo} + \epsilon_{xt} \quad (17)$$

$$\epsilon_y = \epsilon_{yo} + \epsilon_{yt} \quad (18)$$

$$A = A_o + A_t \quad (19)$$

$$B = B_o + B_t \quad (20)$$

From equations (11) and (12) and (17) to (20)

$$\epsilon_{xo} = -A_o - HB_o \quad (21)$$

$$\epsilon_{yo} = -B_o + HA_o \quad (22)$$

$$\epsilon_{xt} = -A_t - \frac{2H}{\omega}\dot{A}_t - HB_t \quad (23)$$

$$\epsilon_{yt} = -B_t - \frac{2H}{\omega}\dot{B}_t + HA_t \quad (24)$$

Substituting equations (21) to (24) into (13) and (14) and separating out the constant terms

$$\frac{\epsilon_{xo}}{E_o(1+E_o)} + \frac{\epsilon_{xo}^2 + E_o\epsilon_{yo}^2}{E_o(1+E_o)\epsilon_o^2} \cdot A_o + \frac{\epsilon_{xo}\epsilon_{yo}}{E_o(1+E_o)^2} \cdot B_o = \frac{m_R \cdot g}{\pi DLp_a} \quad (25)$$

$$\frac{\epsilon_{yo}}{E_o(1+E_o)} + \frac{\epsilon_{xo}\epsilon_{yo}}{E_o(1+E_o)^2} \cdot A_o + \frac{\epsilon_{yo}^2 + E_o\epsilon_{xo}^2}{E_o(1+E_o)\epsilon_o^2} \cdot B_o = 0 \quad (26)$$

Equations (25) and (26) are used to obtain the steady state locus of the journal centre, which is shown plotted in Figure 3 for various values of the loading parameter F_o'.

The remaining time varying terms resulting from the substitution of equations (21) to (24) into (13) to (16), neglecting second and higher order terms in A_t and B_t and writing $x_1 = CC_t$ and $y_1 = CD_t$, yield the following equations:

$$\frac{2H\Omega}{\omega^3}\dddot{A}_t + \frac{\Omega}{\omega^2}\ddot{A}_t + \frac{G_1}{\omega}\dot{A}_t + G_3 A_t + \frac{H\Omega}{\omega^2}\ddot{B}_t + \frac{G_5}{\omega}\dot{B}_t + G_6 B_t - \frac{\Omega}{\omega^2}\ddot{C}_t = 0 \tag{27}$$

$$\Omega\frac{2H}{\omega^3}\dddot{B}_t + \frac{\Omega}{\omega^2}\ddot{B}_t + \frac{G_2}{\omega}\dot{B}_t + G_4 B_t - \frac{H\Omega}{\omega^2}\ddot{A}_t + \frac{G_5}{\omega}\dot{A}_t - G_7 A_t - \frac{\Omega}{\omega^2}\ddot{D}_t = 0 \tag{28}$$

$$\frac{G_1}{\omega}\dot{A}_t + G_3 A_t + \frac{G_5}{\omega}\dot{B}_t + G_6 B_t + \frac{m'\Omega}{\omega^2}\ddot{C}_t + \frac{c'H}{\omega}\dot{C}_t + k'C_t = 0 \tag{29}$$

$$\frac{G_2}{\omega}\dot{B}_t + G_4 B_t + \frac{G_5}{\omega}\dot{A}_t - G_7 A_t + \frac{m'\Omega}{\omega^2}\ddot{D}_t + \frac{c'H}{\omega}\dot{D}_t + k'D_t = 0 \tag{30}$$

where $\Omega = \frac{m_R C\omega^2}{\pi DLp_a}$; $m' = \frac{m_B}{m_R}$; $c' = \frac{c}{12\pi L\mu (R/C)^3}$; $k' = \frac{Ck}{\pi DLp_a}$.

and the constant coefficients, given by Ausman, are:

$$G_1 = \frac{2H}{E_o(1+E_o)}\left[1 + \frac{H^2(1+2E_o)\epsilon_{xo}^2 + 2E_o^2 H\epsilon_{xo}\epsilon_{yo} - E_o^2\epsilon_{yo}^2}{E_o^2(1+E_o)(1+H^2)}\right]$$

$$G_2 = \frac{2H}{E_o(1+E_o)}\left[1 + \frac{H^2(1+2E_o)\epsilon_{yo}^2 - 2E_o^2 H\epsilon_{xo}\epsilon_{yo} - E_o^2\epsilon_{xo}^2}{E_o^2(1+E_o)(1+H^2)}\right]$$

$$G_3 = \frac{H}{E_o(1+E_o)}\left[\frac{H(1+E_o)^2\epsilon_{xo}^2 + [E_o^2 - (1+2E_o)H^2]\epsilon_{xo}\epsilon_{yo}}{E_o^2(1+E_o)(1+H^2)}\right]$$

$$G_4 = \frac{H}{E_o(1+E_o)}\left[\frac{H(1+E_o)^2\epsilon_{yo}^2 - [E_o^2 - (1+2E_o)H^2]\epsilon_{xo}\epsilon_{yo}}{E_o^2(1+E_o)(1+H^2)}\right]$$

$$G_5 = \frac{2H}{E_o(1+E_o)}\left[\frac{HE_o^2(-\epsilon_{xo}^2 + \epsilon_{yo}^2) + [E_o^2 + (1+2E_o)H^2]\epsilon_{xo}\epsilon_{yo}}{E_o^2(1+E_o)(1+H^2)}\right]$$

$$G_6 = \frac{H}{E_o(1+E_o)}\left[1 - \frac{[E_o^2-(1+2E_o)H^2]\epsilon_{xo}^2 - H(1+E_o)^2\epsilon_{xo}\epsilon_{yo}}{E_o^2(1+E_o)(1+H^2)}\right]$$

$$G_7 = \frac{H}{E_o(1+E_o)}\left[1 - \frac{[E_o^2-(1+2E_o)H^2]\epsilon_{yo}^2 + H(1+E_o)^2\epsilon_{xo}\epsilon_{yo}}{E_o^2(1+E_o)(1+H^2)}\right]$$

The stability of the system can now be investigated by examining the solutions to the set of linear equations (27) to (30). Let these solutions have the form

$$A_t = A_i e^{\lambda t} \tag{31}$$

$$B_t = B_i e^{\lambda t} \tag{32}$$

$$C_t = C_i e^{\lambda t} \tag{33}$$

$$D_t = D_i e^{\lambda t} \tag{34}$$

Substituting equations (31) to (34) into equations (27) to (30) gives:

$$[2ZH^3(\sigma)^3 + ZH^2(\sigma)^2 + G_1(\sigma) + G_3]A_i + [ZH^3(\sigma)^2 + G_5(\sigma) + G_6]B_i - [ZH^2(\sigma)^2]C_i = 0 \tag{35}$$

$$-[ZH^3(\sigma)^2 - G_5(\sigma) + G_7]A_i + [2ZH^3(\sigma)^3 + ZH^2(\sigma)^2 + G_2(\sigma) + G_4]B_i - [ZH^2(\sigma)^2]D_i = 0 \tag{36}$$

$$[G_1(\sigma) + G_3]A_i + [G_5(\sigma) + G_6]B_i + [m'ZH^2(\sigma)^2 + c'H(\sigma) + k']C_i = 0 \tag{37}$$

$$[G_5(\sigma) - G_7]A_i + [G_2(\sigma) + G_4]B_i + [m'ZH^2(\sigma)^2 + c'H(\sigma) + k']D_i = 0 \tag{38}$$

where $\sigma = \frac{\lambda}{\omega}$ and is generally complex.

For non-trivial solutions the determinant of the coefficients of A_i, B_i, C_i and D_i in equations (35) to (38) must be zero. The resulting characteristic equation is a tenth order polynomial in σ. It is now necessary to obtain the roots of this equation, looking for those roots having positive real parts, which indicates a growth of amplitude or instability.

Consider now the conical mode of whirl given by the equations of motion (5) to (8). For the small linear time dependent displacements, the corresponding angular displacements may be written as:

$$\phi = \frac{2C\epsilon_{xt}}{L} \tag{39}$$

$$\psi = -\frac{2C\epsilon_{yt}}{L} \tag{40}$$

$$\alpha = \frac{2x_1}{L} \tag{41}$$

$$\beta = -\frac{2y_1}{L} \tag{42}$$

If it is assumed, as an approximation, that the dynamic fluid film force components W_{xt} and W_{yt} vary linearly with eccentricity, then the restoring couples M_x and M_y are given by

$$M_y = \frac{W_{xt} \cdot L}{6} \tag{43}$$

$$M_x = \frac{W_{yt} \cdot L}{6} \tag{44}$$

Rewriting equations (5) to (8) in terms of the linear time dependent displacements, using equations (39) to (42), and the dynamic fluid force components from equations (43) and (44), the set of linear equations for conical whirl becomes:

$$\frac{2H\gamma}{\omega^3}\dddot{A}_t + \frac{\gamma}{\omega^2}\ddot{A}_t + \frac{H\gamma}{\omega^2}\ddot{B}_t - \frac{\gamma\ddot{C}_t}{\omega^2} - Q\left[\frac{H\gamma}{\omega}\dot{A}_t - \frac{2H\gamma}{\omega^2}\ddot{B}_t - \frac{\gamma\dot{B}_t}{\omega} + \frac{\gamma\dot{D}_t}{\omega}\right] + \frac{1}{12}\left[\frac{G_1}{\omega}\dot{A}_t + G_3 A_t + \frac{G_5}{\omega}\dot{B}_t + G_6 B_t\right] = 0 \quad (45)$$

$$\frac{2H\gamma}{\omega^3}\dddot{B}_t + \frac{\gamma}{\omega^2}\ddot{B}_t - \frac{H\gamma}{\omega^2}\ddot{A}_t - \frac{\gamma}{\omega^2}\ddot{D}_t - Q\left[\frac{2H\gamma}{\omega^2}\ddot{A}_t + \frac{\gamma}{\omega}\dot{A}_t + \frac{H\gamma}{\omega}\dot{B}_t - \frac{\gamma\dot{C}_t}{\omega}\right] + \frac{1}{12}\left[\frac{G_5}{\omega}\dot{A}_t - G_7 A_t + \frac{G_2}{\omega}\dot{B}_t + G_4 B_t\right] = 0 \quad (46)$$

$$\frac{I'\gamma}{\omega^2}\ddot{C}_t + \eta' H\dot{C}_t + \tau' C_t + \frac{1}{12}\left[\frac{G_1}{\omega}\dot{A}_t + G_3 A_t + \frac{G_5}{\omega}\dot{B}_t + G_6 B_t\right] = 0 \quad (47)$$

$$\frac{I'\gamma}{\omega^2}\ddot{D}_t + \eta' H\dot{D}_t + \tau' D_t + \frac{1}{12}\left[\frac{G_5}{\omega}\dot{A}_t - G_7 A_t + \frac{G_2}{\omega}\dot{B}_t + G_4 B_t\right] = 0 \quad (48)$$

where $\gamma = \dfrac{I_R \omega^2 C}{\pi D L^3 p_a}$; $Q = \dfrac{J_R}{I_R}$; $I' = \dfrac{I_B}{I_R}$.

$$\tau' = \frac{\tau C}{\pi D L^3 p_a} \quad ; \quad \eta' = \frac{\eta}{12\pi L^3 \mu (R/C)^3} \; .$$

Substitution of equations (31) to (34) into (45) to (48) again leads to a tenth order polynomial in σ for the characteristic equation.

RESULTS

A computer programme has been written which enables the stability of the bearing system to be examined for a wide variety of design parameters. For the purposes of this investigation the effects of bearing support stiffness and damping and the mass and inertia ratios of the bearing/rotor have been considered. The gyroscopic terms have been neglected, except in the particular case (Fig. 8) where it was desired to study the effect of these terms.

For a selected set of bearing parameters the loading parameter F_o' is first used to obtain the steady state locus of the journal centre.

From a point on the locus, the corresponding values of eccentricity ratio, attitude angle and compressibility number are read off and used to compile the coefficients G_1 to G_7. The coefficients of A_i, B_i, C_i and D_i in equations (35) to (38) are then formed, for given values of stiffness, damping and mass ratios, and their determinant expanded to give the characteristic equation in σ, which is solved by Bairstow's method. For a positive real part in a root of σ the system is unstable and the imaginary part gives the ratio of the orbital speed of the motion to the rotor speed.

Computer solutions have been obtained for a single bearing, having bearing parameters as follows, while varying H (speed only), k', c', τ' and η'.

$$F_o' = 0.2$$
$$\Omega/H^2 = 0.454$$
$$\gamma/H^2 = 0.095$$
$$m' = 0.1$$
$$I' = 0.1$$
$$Q = 0$$

Additional solutions have been obtained for the following ranges of m', I' and Q.

$$m' = 0.02 - 0.50$$
$$I' = 0.02 - 0.50$$
$$Q = 0 - 1.0$$

DISCUSSION OF RESULTS

Figure 4 shows typical stability curves for the bearing system, in conical whirl, in which the torsional stiffness ratio and compressibility number are varied and the torsional damping ratio held constant.

This shows the existence of two quite distinct whirl zones which partly overlap in this example. Suppose, for example, that the stiffness ratio is 10^{-1}. The first onset of whirl occurs at H = 0.53 and cessation from the lower zone would occur at H = 6.0. A second whirl onset is shown to occur at H = 3.7, thus the system is actually unstable until whirl cessation takes place from the upper whirl zone at just above H = 10.0. This compares with a single onset speed at approximately H = 0.6, beyond which the bearing is always unstable, when the support is rigid.

An important difference exists here with Marsh's theoretical treatment, which does not appear to predict a cessation to the upper whirl zone.

At onset to both lower and upper zones, the whirl or orbital speed is generally found to be just less than half the rotor speed, as indicated by the last plot of σ, in the Argand diagram of Figure 5. Where the zones of instability overlap, they are clearly identified by this means. Cessation from the lower zone is not very clearly defined, as indicated by the slope of the curve as it crosses over the imaginary axis. Here the orbital speed reduces to about one tenth of the rotor speed, the pattern of behaviour being the same as that found experimentally by Kerr.

A general stability map, for conical whirl, covering a wide range of damping and stiffness ratios is shown in Figure 6. The lower portions of the dashed lines for small value of η' are very close to the dashed $\eta' = 0$. The interesting feature of these results is that they show it is theoretically possible, given the necessary values of stiffness and damping ratio, to have a bearing system which is stable at all speeds.

The effect of varying the inertia ratio is given in Figure 7. The boundary of the lower whirl zone is not significantly affected, whereas the whirl onset speed of the upper zone shows a marked increase with decrease in inertia ratio. The conclusion is, therefore, drawn that the lower zone is mainly associated with an instability of the rotor and the upper zone with the bearing.

The effect of the gyroscopic forces is a destabilising one as shown by the changes in the lower whirl boundary in Figure 8.

The general pattern of behaviour of the system in the cylindrical mode of whirl, given in Figures 9 and 10, is similar to that of the conical mode.

In Figure 11, a comparison is made between the theory and some of Marsh's experimental results. The whirl onset speeds are shown to be theoretically predictable to within quite close limits but there is some discrepancy between the cessation speeds of the lower whirl zone. It was previously mentioned that this cessation is rather ill-defined and it is interesting that some difficulty was found in ascertaining it in the above experiments, due to the presence of a small synchronous whirl amplitude.

CONCLUSIONS

1. A purely analytical theory, based on the work of Ausman, has been developed, which will predict the instabilities of a long bearing, having a flexible damped support, for a wide variety of design parameters.

2. The theory shows the presence of two quite distinct whirl zones, a lower one associated mainly with an instability of the rotor and an upper one with the bearing.

3. It is shown to be theoretically possible, given the necessary values of damping and stiffness of the bearing support, to have a bearing system which is stable at all speeds.

4. The prediction of whirl onset compares well with the theory and experimental work of Marsh. However, an important difference exists between the present theory and that due to Marsh, in that the former shows there to be a definite cessation to the upper whirl zone.

ACKNOWLEDGEMENTS

The work discussed in this paper is part of a research programme which is being supported by a grant from the Science Research Council.

The author would particularly like to thank Dr. A.D.S. Barr for his guidance and encouragement, and also Dr. G.T.S. Done for his considerable help with the computation.

REFERENCES

1. REYNOLDS, D.B. and GROSS, W.A. "Experimental Investigation of Whirl in Self-acting Air-lubricated Journal Bearings". Trans. A.S.L.E. Vol. 5, 1962.

2. AUSMAN, J.S. "Linearized ph Stability Theory for Translatory Half-speed Whirl for Long, Self-acting Gas Lubricated Journal Bearings". Journal of Basic Engineering, Trans. A.S.M.E. Vol. 85, 1963.

3. PAN, C.H.T. and STERNLICHT, B. "Comparison between Theories and Experiments for the Threshold Instabilities of Rigid Rotors in Self-acting Plain cylindrical Journal Bearings". Journal of Basic Engineering, Trans. A.S.M.E. Vol. 86, 1964.

4. MARSH, H. "The Stability of Aerodynamic Gas Bearings". Mechanical Engineering Science Monograph No. 2, Inst. of Mech. Engs., London, 1965.

5. CASTELLI, V. and ELROD, H.G. "Solution of the Stability Problem for 360° Self-acting Gas-lubricated Bearings". Journal of Basic Engineering, Trans. A.S.M.E. Vol. 87, 1965.

6. ELROD, H.G. McCABE, J.T. and CHU, T.Y. "Determination of Gas Bearing Stability by Response to Step-jump". Journal of Lubrication Technology, Trans. A.S.M.E. Vol. 89, 1967.

7. MARSH, H. "The Stability of Aerodynamic Gas Bearings. Part 2: Non-circular Bearings". Report for Ministry of Aviation, 1964.

8. KERR, J. "The Onset and Cessation of Half-speed Whirl in Air-lubricated Self-pressurised Journal Bearings", Proc. Inst. Mech. Engs. Vol. 180, 1966. (4th Convention of Lubrication and Wear Group, Paper No. 22).

NOMENCLATURE

A, B	time dependent functions of journal eccentricity ratio components
A_i, B_i	initial values of A_t and B_t
A_o, B_o	constant portion of A and B
A_t, B_t	time varying portions of A and B
C	average radial clearance in bearing
c	damping coefficient for bearing support
c'	damping ratio = $\frac{c}{12\pi L\mu(R/C)^3}$
C_i, D_i	initial values of C_t and D_t
C_t, D_t	non-dimensional form of time varying bearing displacements = x_1/C and y_1/C
D	diameter of journal bearing

E	$\sqrt{(1-\epsilon^2)}$
E_o	$\sqrt{(1-\epsilon_o^2)}$
F_o'	loading parameter $\dfrac{m_R \cdot g}{\pi D L p_a}$
G_{1-7}	constant coefficients of the linear time dependent terms in the equations of motion
g	gravitational constant
H	non-dimensional bearing compressibility number $= \dfrac{6\mu\omega R^2}{p_a C^2}$
I_B	transverse moment of inertia of bearing sleeve
I_R	transverse moment of inertia of rotor
I'	inertia ratio $= I_B/I_R$
J_R	polar moment of inertia of rotor
k	stiffness coefficient of bearing support
k'	stiffness ratio $= \dfrac{C k}{\pi D L p_a}$
L	bearing length
Mx, My	fluid film restoring couples
m_B	mass of bearing sleeve
m_R	mass of rotor
m'	mass ratio $= m_B/m_R$
p_a	ambient pressure
Q	J_R/I_R
R	radius of journal bearing
t	time
Wx, Wy	fluid film restoring force components
x_1, y_1	time varying displacements of bearing centre
x_2, y_2	time dependent displacements of journal centre relative to bearing centre
Z	non-dimensional bearing parameter $= Q/H^2$
α, β	time varying angular displacements of the bearing axis

γ	non-dimensional conical stability parameter $\frac{I_R \omega^2 C}{\pi D L^3 p_a}$
$\epsilon, \epsilon_x, \epsilon_y$	eccentricity ratio and its components
$\epsilon_o, \epsilon_{xo}, \epsilon_{yo}$	constant portions of ϵ, ϵ_x and ϵ_y
$\epsilon_{xt}, \epsilon_{yt}$	time varying portions of ϵ_x and ϵ_y
η	angular damping coefficient
η'	angular damping ratio = $\frac{\eta}{12\pi\mu L^3 (R/C)^3}$
λ	exponential constant coefficient of time
μ	absolute viscosity of fluid
σ	λ/ω
τ	angular stiffness coefficient of bearing support
τ'	angular stiffness ratio = $\frac{\tau C}{\pi D L^3 p_a}$
ϕ, ψ	time varying angular displacements of the rotor axis relative to the bearing axis
Ω	non-dimensional cylindrical stability parameter $\frac{m_r C \omega^2}{\pi D L p_a}$
ω	angular velocity of rotor about its axis

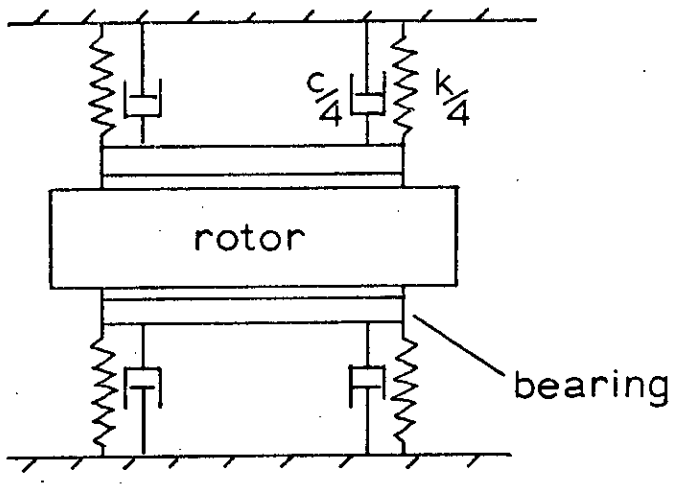

FIG.1. BEARING SYSTEM

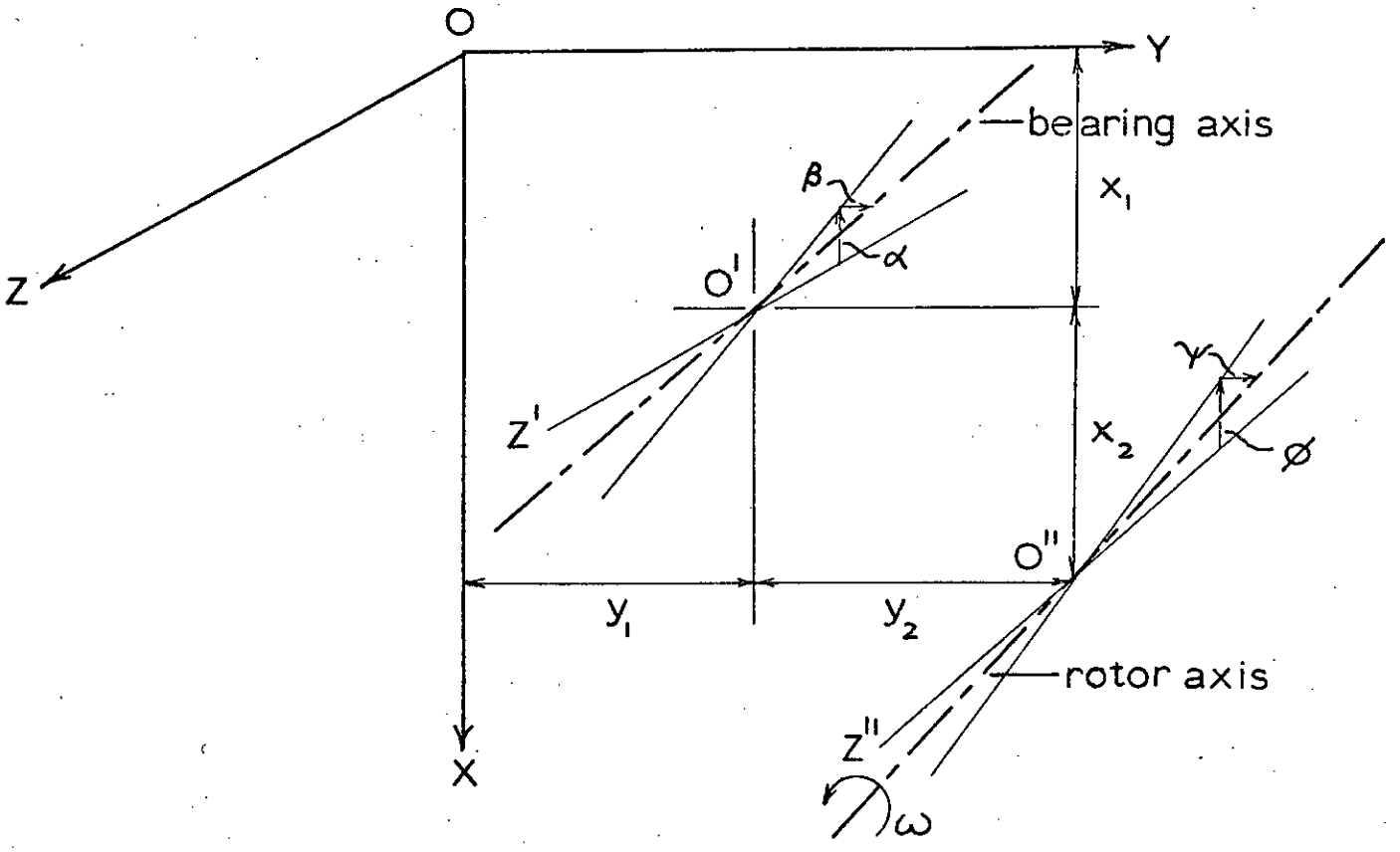

FIG.2. CO-ORDINATE SYSTEM FOR JOURNAL AND BEARING

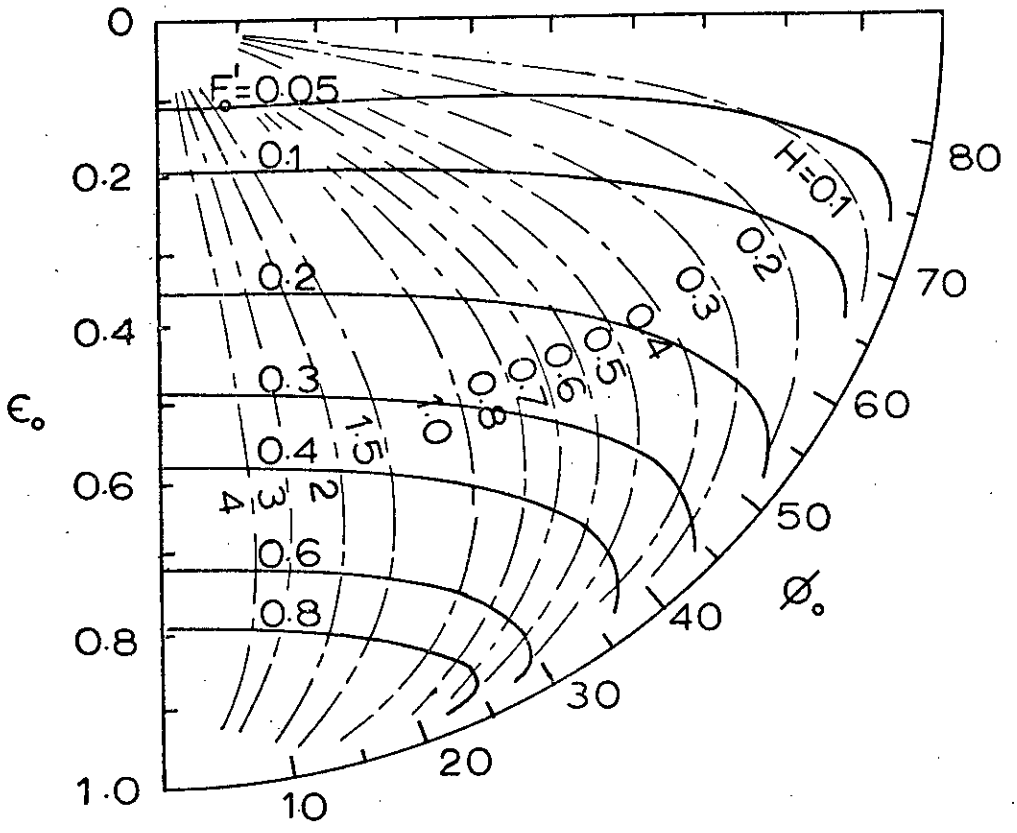

FIG.3. STEADY STATE LOCI OF JOURNAL CENTRE

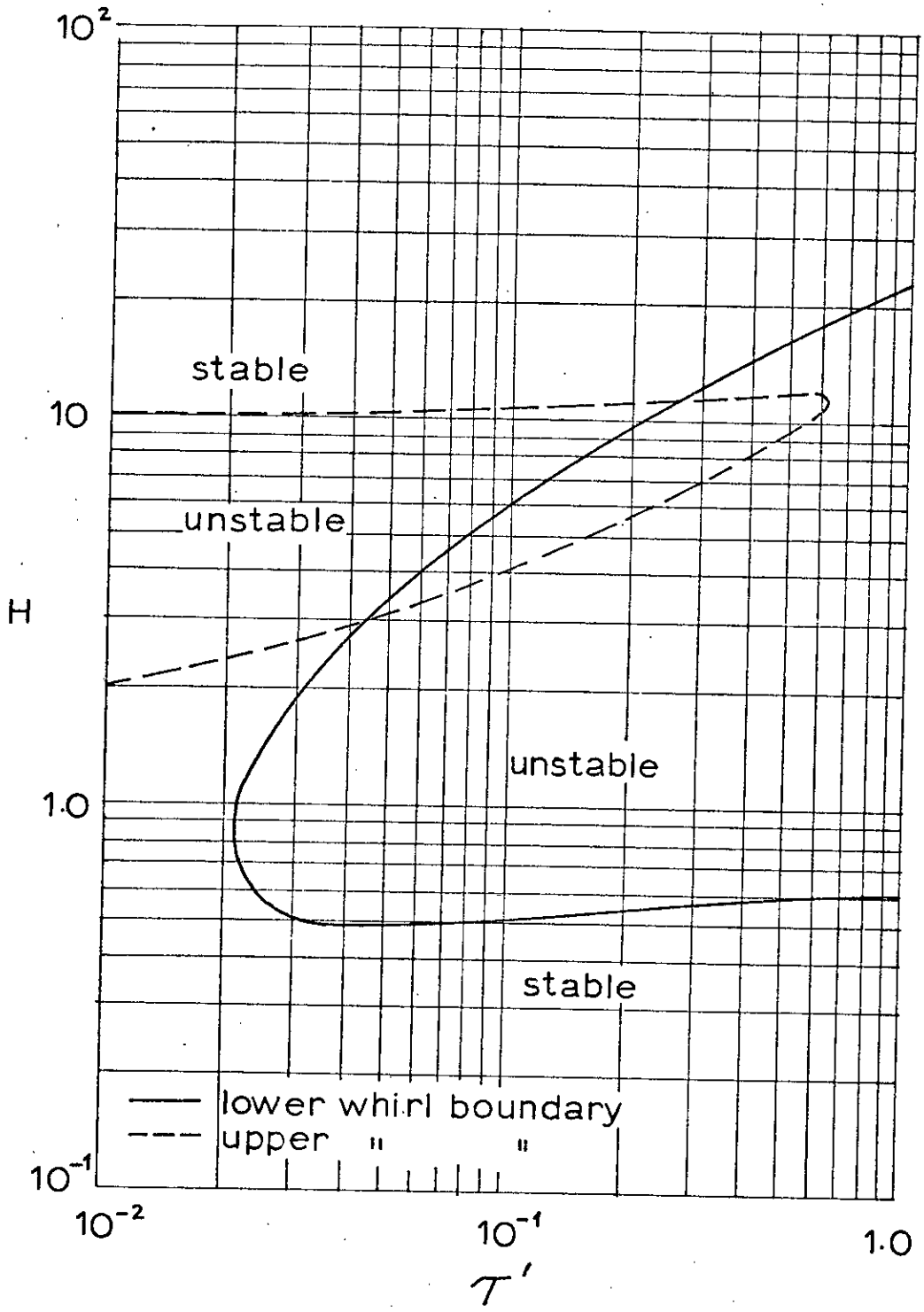

FIG.4. TYPICAL STABILITY CURVES FOR CONICAL WHIRL

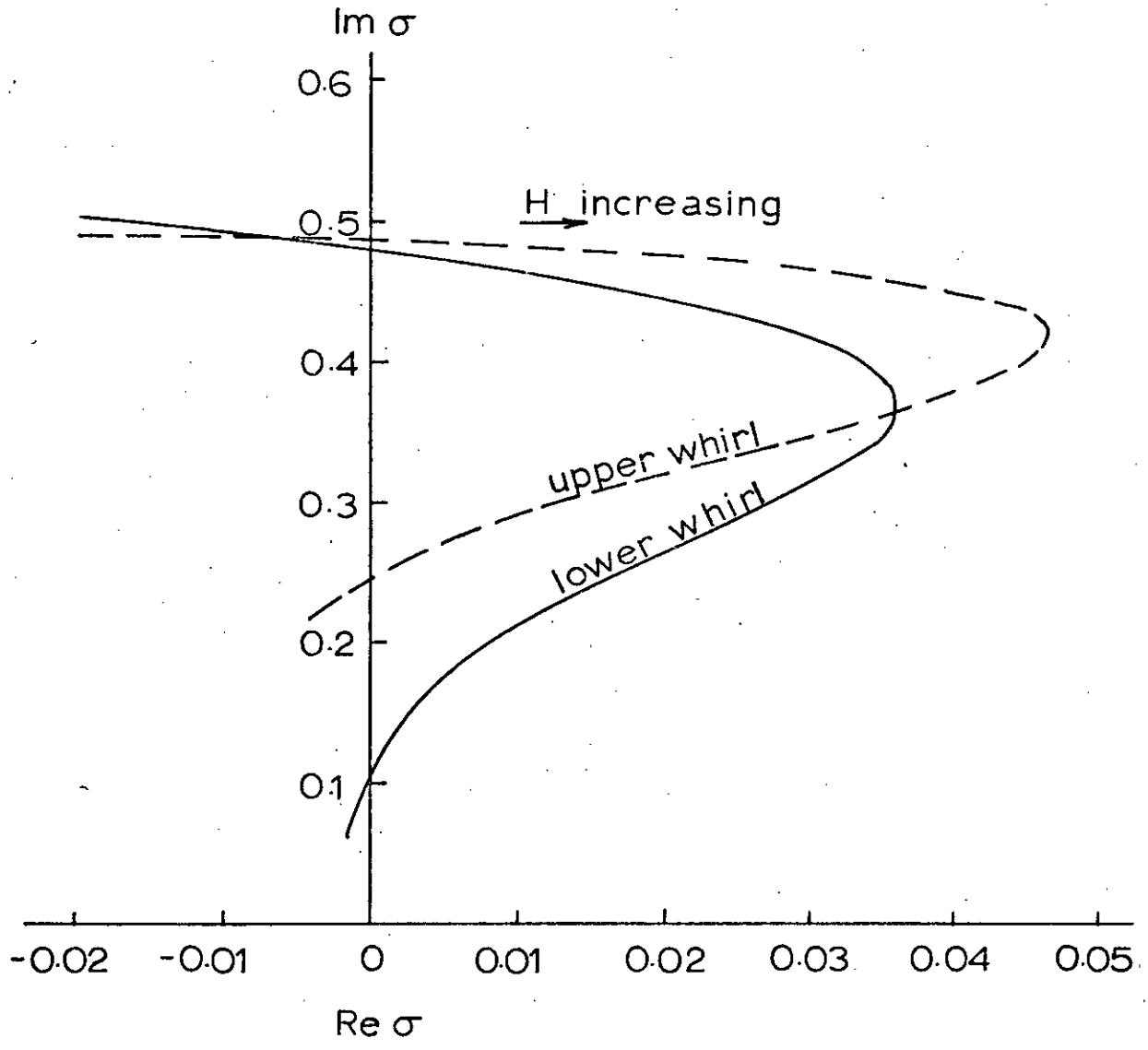

FIG.5. GROWTH FACTOR AND FREQUENCY RATIO

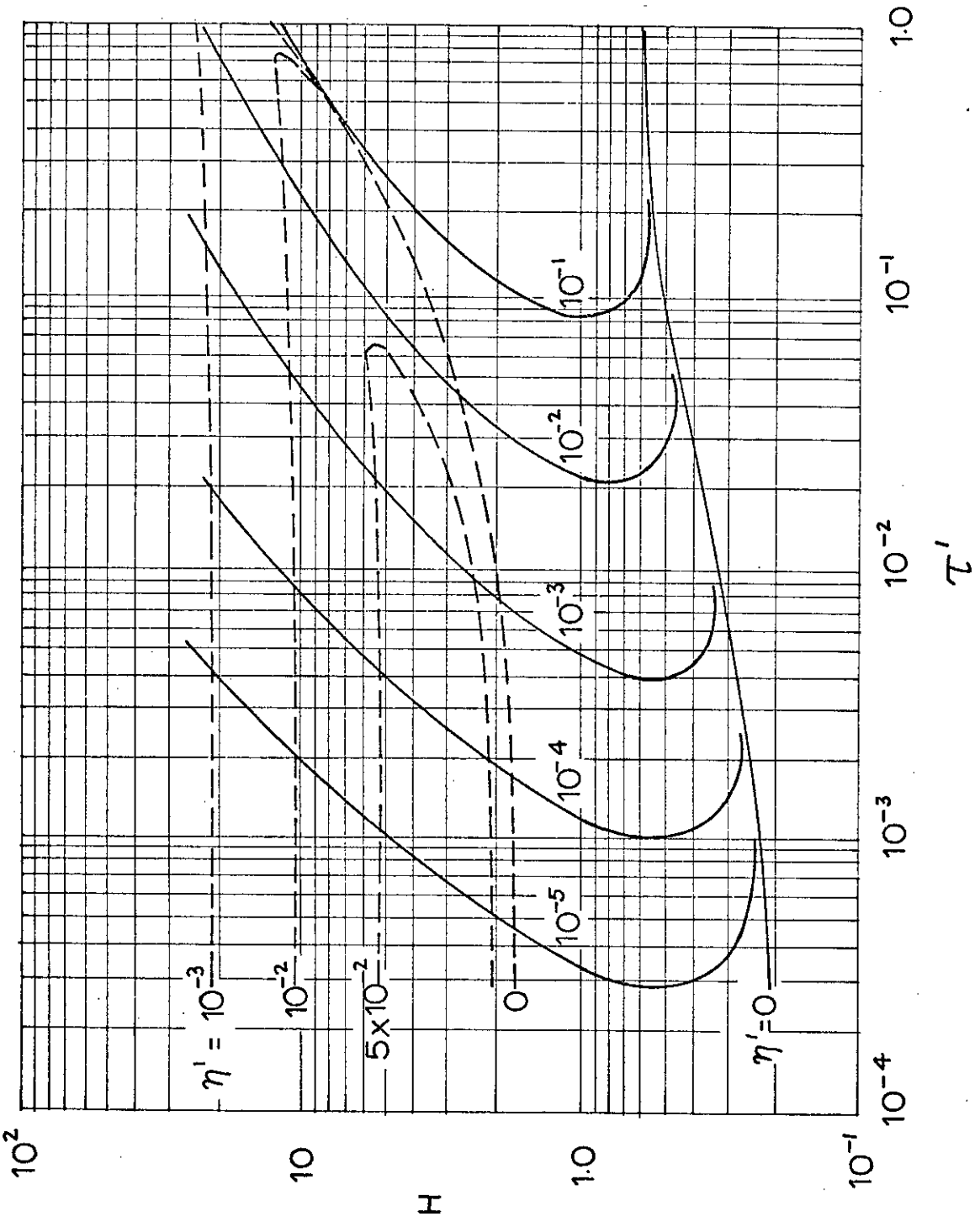

FIG.6. THE EFFECT ON THE CONICAL WHIRL BOUNDARIES OF SUPPORT STIFFNESS AND DAMPING. $\gamma/H^2 = 0.095$: $I' = 0.1$: $Q = 0$.

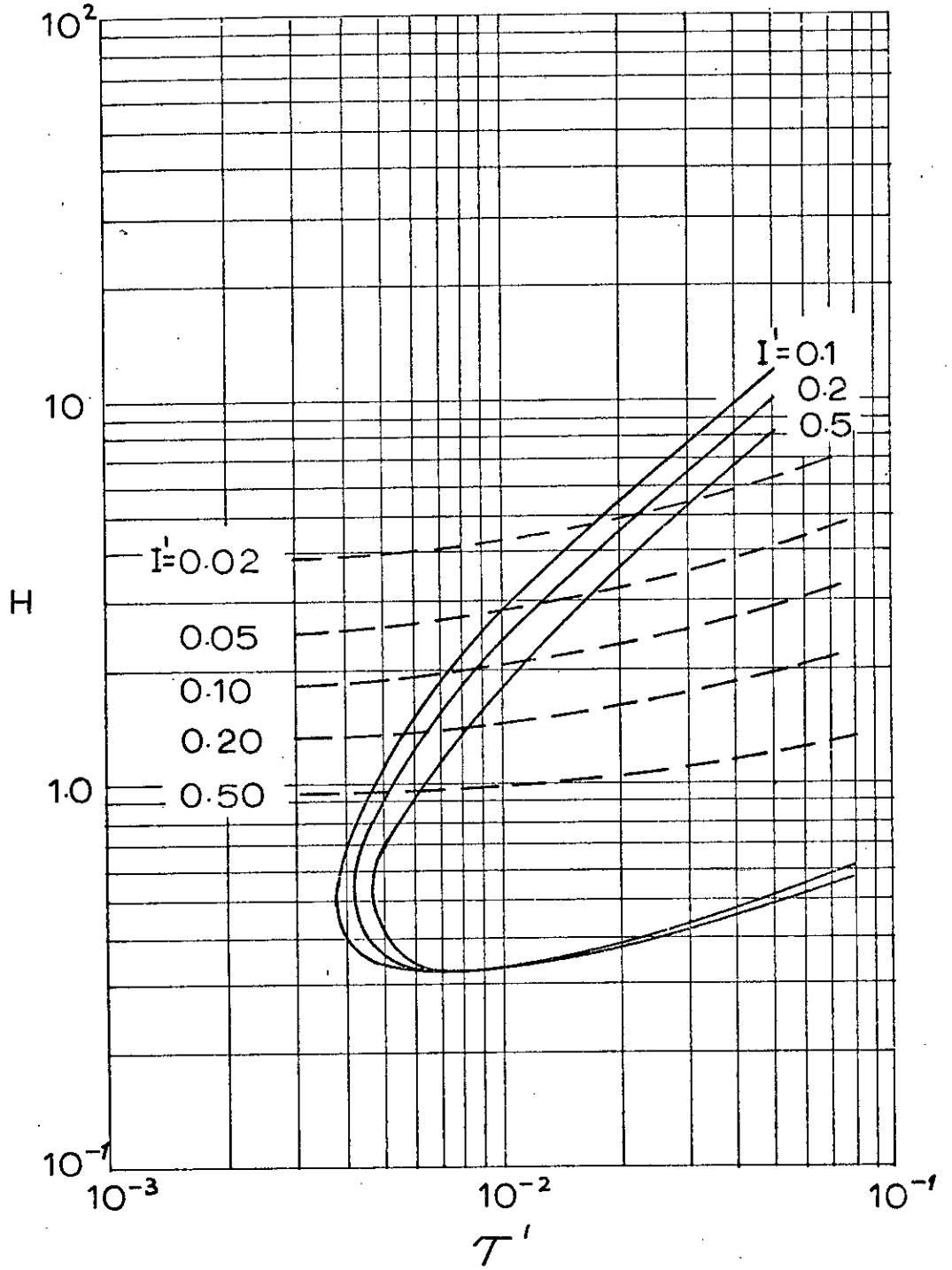

FIG. 7 THE EFFECT ON THE CONICAL WHIRL BOUNDARIES OF INERTIA RATIO. $\gamma/H^2 = 0.095 : Q = 0 : \eta' = 10^{-3}$.

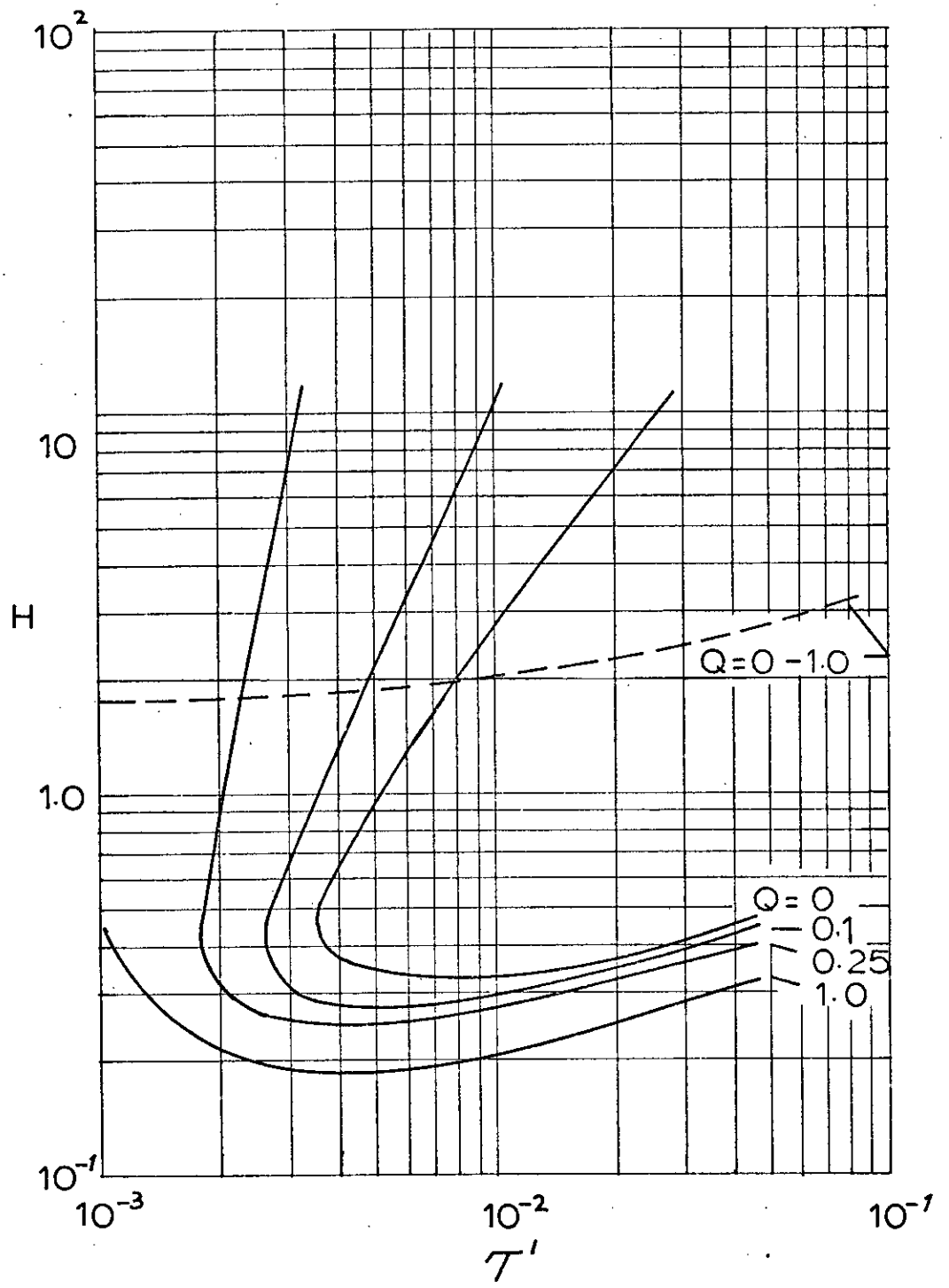

FIG. 8. THE EFFECT ON THE CONICAL WHIRL BOUNDARIES OF THE GYROSCOPIC TERMS.

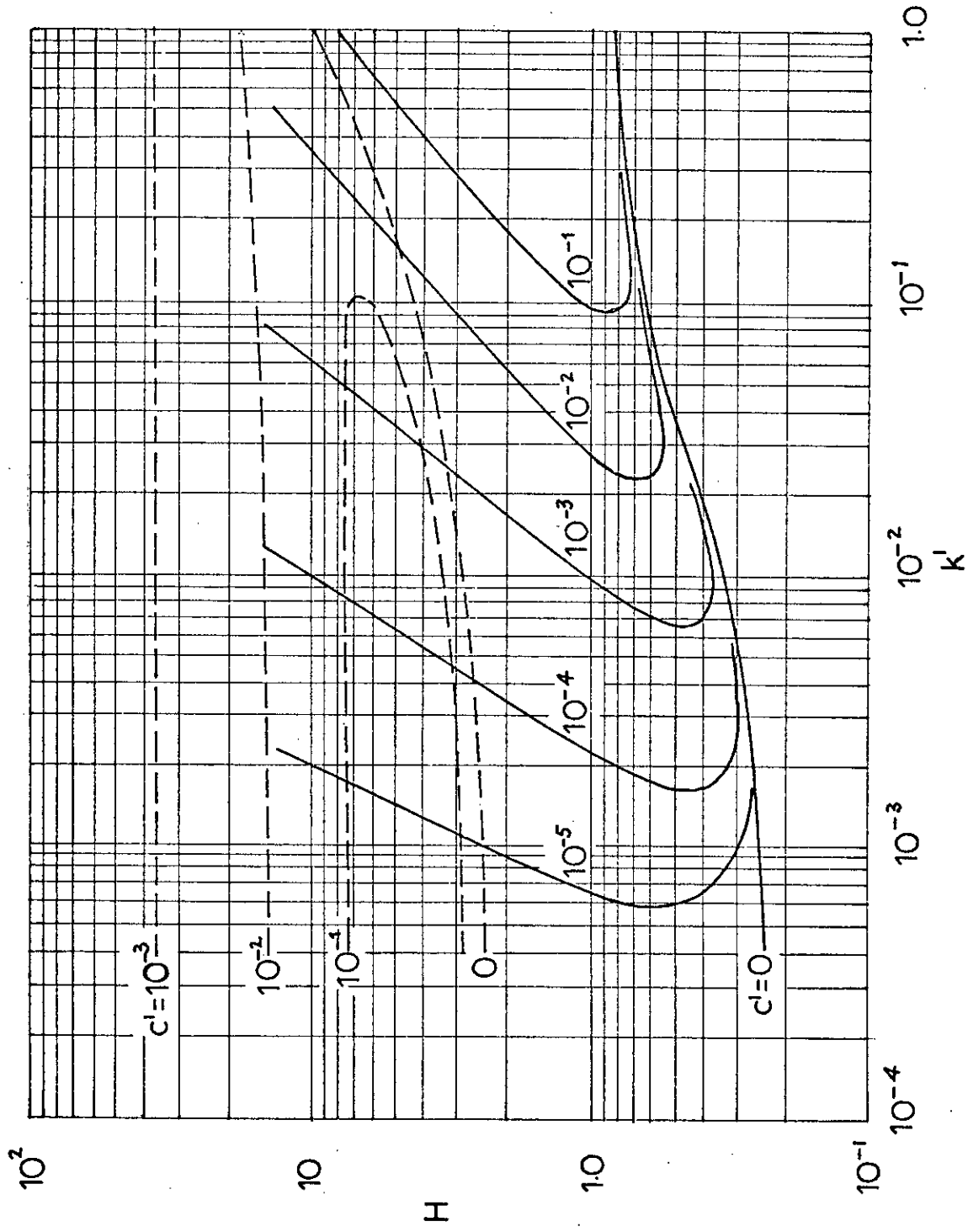

FIG.9. THE EFFECT ON THE CYLINDRICAL WHIRL BOUNDARIES OF SUPPORT STIFFNESS AND DAMPING. $\Omega/H^2=0.454$: $m^1=0.1$.

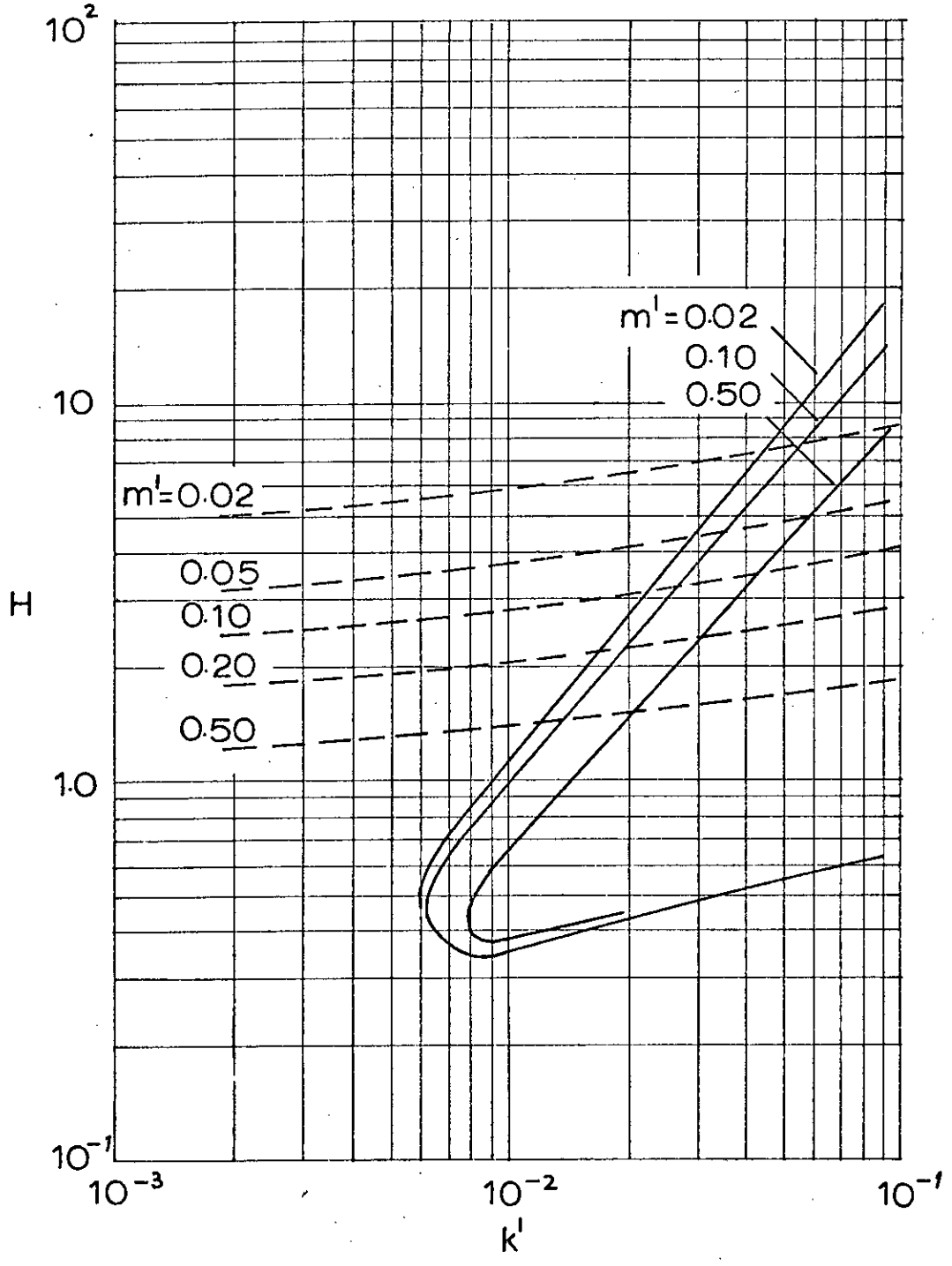

FIG.10 THE EFFECT ON THE CYLINDRICAL WHIRL BOUNDARIES OF MASS RATIO. $\Omega_H^2=0.454 : c'=10^{-3}$.

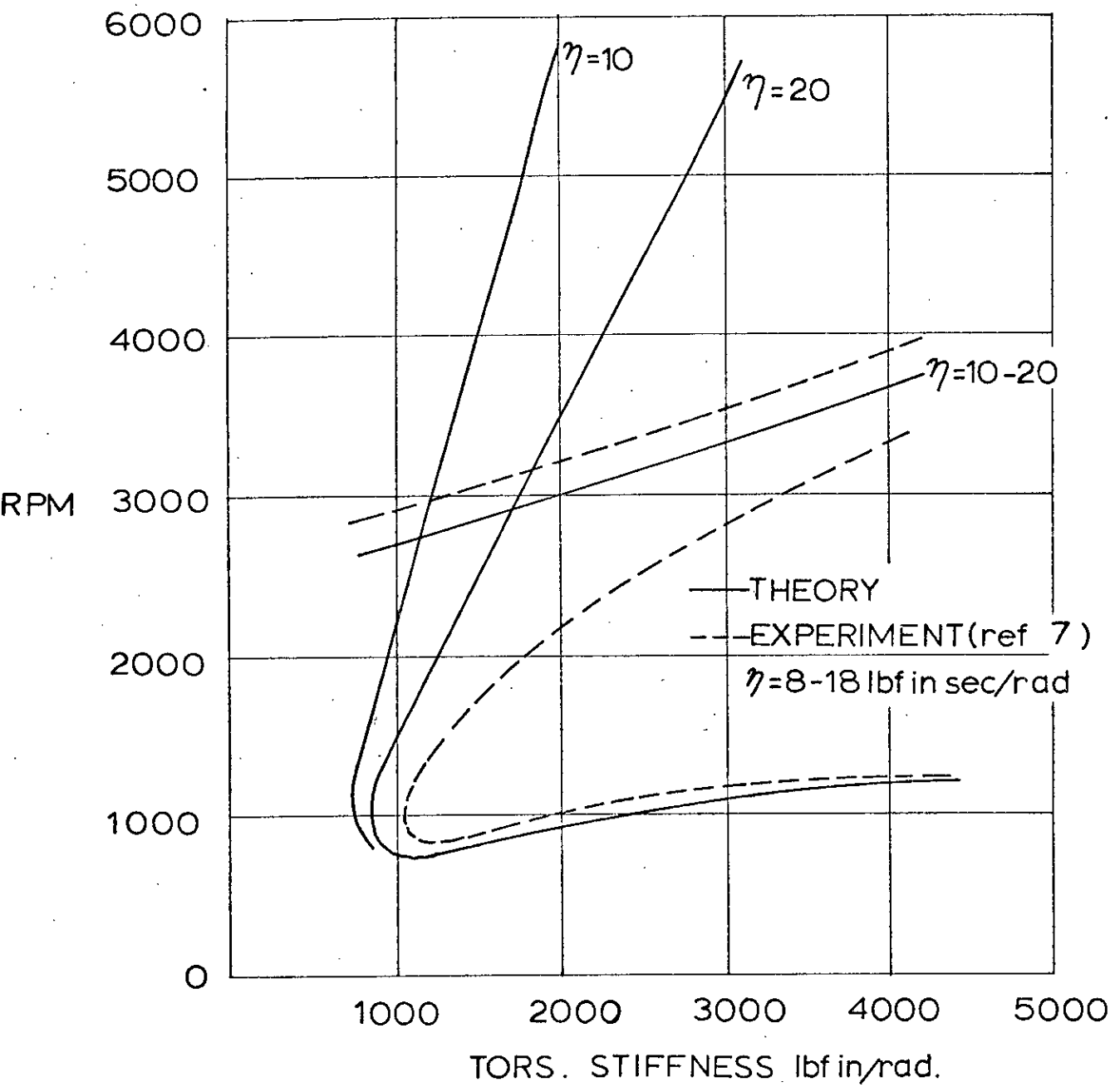

FIG.11 COMPARISON OF THEORY WITH EXPERIMENT

r/H^2=0.0019 : I'=0.532 : Q=0.0415.